UCLouvain

epl

École polytechnique de Louvain

Towards electro-chemical characterisation of paper-based sensors and usage perspectives

Responsible water quality sensor design

Author: **Margo Hauwaert**
Supervisor: **Jean-Pierre Raskin**
Readers: **Ignace Adant, Marc Debliquy, Grégoire Le Brun**
Academic year 2019–2020
Master [120] in Electro-mechanical Engineering

Acknowledgements

The accomplishment of this master thesis has been an enriching experience. I would like to thank several people for making this possible:

Gregoire Le Brun for his impressive energy, availability and enthusiasm. It was both productive and pleasant to collaborate with him. I wish him all the best for his future projects and endeavours.
Prof. Jean-Pierre Raskin for his trust, genuine benevolence and guidance. For always asking the right questions and for feeling so involved that ideas pop right up at 3 a.m.

Prof. Ignace Adant who is inspiringly passionate about his study field and made it possible to add a multidisciplinary touch to this paper. Adrian Agbon from the ARES-BIMWAM who provided precious perceptions about water management in the Philippines.

Prof. Marc Debliquy for his time spent, his critical yet beneficial view and his insights. Hugues Charlier for his tips and tricks in ZView.

Pascal Simon and Souley Djandjandi from the WELCOME platform, Sebastien Faniel and Christian Renaud from the WINFAB platform , Audrey Leprince and Martin Rack for their patience, advice and help.

Roselien Vercauteren, Romain Hanus and Rafael Puyol for granting me asylum in their office, product-placing Galler chocolates and sharing fan wind.
Odile Crahay for the interesting interactions, advice and the mutual "lockdownsupport".

My parents, whose support is so valuable. My fantastic brother. Oma, Mamy and Papet for the uncountable calls and lit candles ever since I started school. A tender thought for Opa who would have been so eager to discuss this thesis together.

Aurélia and Miguel for being the glass of milk to the brownie of my university journey. Arthur, Lucie, Rodolphe, Corentin, Charles, Otje, Paolo, All-In, and Lise for the precious big and little things.
Les Alterépotes, my roommates, for the colorful vibes they provided me all year long.

My fellow scoutsleaders for every single sunday afternoon, unforgettable summer camps, laughter and surprises. A special load of gratitude for Bij, Sint-Bernard and Staart-mees who really had my back during the past few weeks and did a fantastic job, as always.

Abstract

Point-of-care biosensors have the potential to revolutionize health care and disease prevention in both developing and developed countries. Indeed, rapid and relatively inexpensive disposable tests are powerful tools for accessible and adequate health control on the one hand and for environmental quality monitoring on the other hand.

The project that led to this master's thesis aims to create a point-of-care paper-based electrical screening device suitable for detection of bacteria in water. This affordable, portable and sensitive biosensor creates opportunities in applications that need frequent and rapid pathogen detection, such as the detection of E. Coli in drinking water or Legionella in cooled industrial water. Through appropriate modification, our sensor could meet the need for detection of various viruses as well, which may prove particularly useful in the light of the recent COVID-19 pandemic.

This work focuses on the electro-chemical detection of bacteria with interdigital electrodes (IDE) through impedance spectroscopy. These bacteria are captured in a nitrocellulose membrane through bio-functionalisation, thus altering the permittivity and conductivity of the sensed medium. The conducted study adds two innovations to the field of impedimetric sensing with IDE, which already has a wide variety applications. First, the electrodes are directly deposited on nitrocellulose. Second, we aim at sensing the whole nitrocellulose membrane volume rather than the IDE surface, which is commonly targeted.
In the present thesis, the whole system is characterised from scratch. An analytical model is established and validated at different frequency ranges. A proof of concept is substantiated: 10^8 CFU/ml of Bacillus thuringiensis are detected in DI water. Phage endolysin is used for specific capture of these bacteria on the nitrocellulose membrane.

The protoyping of our biosensor is framed by a responsible design approach. In this work, an innovative study evaluates the societal impacts of the information generated by the sensor, using a relevant water economy approach as developed in academic research. It proposes a configuration of an information system focusing on tap water, which relies on citizens and anticipates the problems associated with their inclusion in a water quality monitoring system. Two case studies, in Belgium and in the Philipines, are established to validate the approach.

Acronyms

AgNP Silver Nanoparticles.

AuNP Gold Nanoparticles.

BNC Bayonet Neill Concelman connector.

CBD Cell Binding Domain.

CFU Colony Forming Unit per ml.

CNT Carbon Nanotubes.

CPE Constant Phase Element.

CVD Chemical Vapor Deposition.

DI desionised water.

DNA Deoxyribonucleic Acid.

DUT Device Under Test.

EDL electrical Double Layer.

EF Evanescent Field.

EIS Electrical Impedance Spectroscopy.

ELISA Enzyme Linked Immunosorbent Assay.

FSO Full Scale Output.

GFP Green Fluorescent Protein.

HDL Highest detectable level.

IDE Interdigitated Electrodes.

LAMP Loop-mediated isothermal amplification.

LCA Life Cycle Assessment.

LFA Lateral Flow Assay.

LoD Limit of detection.

LTI Linear Time Invariant.

MALDI-TOF MS Matrix Assisted Laser Desorption ionization time-of-flight mass spectroscopy.

NC Nitro-Cellulose.

PBS Phosphate buffered solution.

PCR Polymerase Chain Reaction.

PoC Point of Care.

PQC Piezoelectric quartz crystal.

PtNP Platinum Nanoparticles.

PVD Physical Vapor Deposition.

RBP Receptor Binding Protein.

RNA Ribonucleic Acid.

SPE Screen printed electrodes.

SUT Sample Under Test.

TF Transfer Function.

TLBMC Triple Layer Business Model Canvas.

TSB Tryptic soy broth.

UI User Interface.

VNA Vector Network Analyser.

YPL Yeast peptone lactose broth.

Contents

Introduction

Water is at the very origin of life on earth. Due to its remarkable chemical and physical characteristics, it allowed for complex living organisms to develop almost 4 billion years ago and it has thenceforth been indispensible. [1] Since up to 60% of adult human bodies are made from water, it is essential for our survival: our water consumption has a direct and profound impact on our health.

In addition to being a primary biological need, water also plays a fundamental societal role. It has the power to be an economic catalyst across a vast array of global sectors ranging from food and health to energy and transport. Nevertheless, this growth accelerator can only be leveraged if the **water security** is strong.

Regrettably, access to safe water is far from being a given: 30% of the global population lacks access to safely managed drinking water services and 60% lacks access to safely managed sanitation services. [2]. Addressing this problem is complex, since there is a close link between the access to water and economic growth of a country. Lack of qualitative water is a barrier to sturdy socio-economic development, while lack of development is a barrier to solving water problems.

One of the key elements to contribute to water security, is water quality testing: "Will we be sick if we drink this water?". The PhD project [3] that led to this master thesis aims to prototype a **Point of Care (PoC) bacterial biosensor**, adapted to developing countries, that can detect the presence of pathogen bacteria in drinking water.

Over the last few years, the interest for PoC sensing devices has increased tremendously. There has been a global effort to make healthcare more accessible and patient oriented. PoC sensors make it possible to detect pathogens at the "point of care", both in human and environmental analytes. This is especially interesting in contexts where visiting a doctor or centralised laboratory is no sinecure, mainly in developing countries. The World Health Organization outlined the ASSURED guidelines to frame the research and development of such PoC devices: *Affordable, Sensitive, Specific, User-friendly, Rapid and robust, Equipment-free and Deliverable to end-users.*[4]

In the light of recent emergence of the COVID-19 pandemic, caused by the infectious SARS-CoV-2 virus, the field of action of PoC devices has widened. Indeed, the most effective way to contain the spread of this virus is to trace its hotbeds. Since many carriers are assymptomatic, this implies mass screening and thus in increased need for rapid, cheap and simple testing devices [5]. This has broadened the scope for PoC bacterial sensing application: its main focus is no longer limited to developing countries.

The general idea of the sensor is schematised in figure 1. The fluid, potentially containing
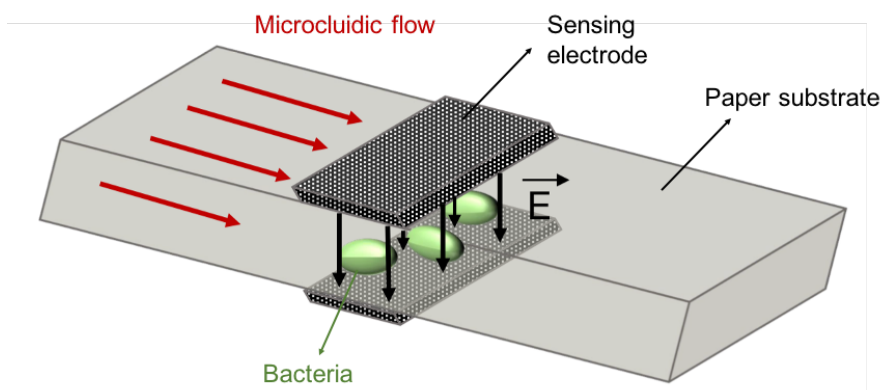
Figure 1: Conceptual schema of an impedimetric microfluidic paper-based biosensor [6]

target bacteria, is applied on a paper strip. Due to capilarity, this analyte is conducted to electrodes, that sense and quantify the presence of bacteria. This design is a hybridation of classical paper-based Lateral Flow Assay (LFA) (such as pregnancy strips) and electrochemical sensing. The former offers the advantage of interesting microfluidic and biofunctionalisation properties, while the latter offers the advantage of generating a precise and quantifiable signal.

This master thesis is complementary to the master thesis of Odile Crahay [7] and contributes to the PhD thesis of Grégoire Le Brun [3]. Odile's master thesis mainly focusses on the microfluidic flow aspects. Future research will be dedidacted to the immobilization of bacteria. In this work, we focus on the electrical sensing: we analyse the possibilities for impedimetric sensing on paper with printed **Interdigitated Electrodes (IDE)**. An electrical sensing model is established and compared to the results of some practical experiments.

In addition to being a point of care, our sensor is subject to a **responsible design** approach. Design choices are made considering their environmental, societal and economical impact. This implies that different assessments are made throughout different contributions to the PhD project, and integrated in the research and development process.
Paper was chosen as main substrate for the device, given its low-impact manufacturing, low-cost and degradability. Odile and Gregoire made up a Life Cycle Assessment (LCA) that justified the choice of paper from the point of view of energy consumption. [7]

In this work, we introduce a **societal impact assessment** in which we elaborate the opportunities and pitfalls for the use of an accessible and cheap sensor. If these are used at large scale, a large amount of results will be generated. How can this flux information input influence the functioning of a community? What are the opportunities and pitfalls? These are then challenged with a case study in Belgium and in the Philippines.

We begin with a state of the art, that sets a context for the two main research domains that converge in this paper: point-of-care impedimetric sensors and the fabrication of

paper-based electronics. We also introduce two projects implying large-scale usage of sensors for environmental quality monitoring. Based on the elaborated state of the art, we refine the research objectives in chapter 2.

Next, we go through the different steps of the used materials and methods: the main models, simulations, measuring protocols and measuring equipment are presented.

Afterwards, the most important results are presented and discussed.

Subsequently, a chapter is dedicated to the usage perspectives of this sensor.

All this is completed with a conclusion in which the main findings are summarized.

Chapter 1

State of the Art

In this master thesis, we introduce a point of care, micro-fluidic, impedimetric, paper-based biosensor. This state of the art overview focuses on the aforementioned characteristics and is structured as follows:

1. General introduction to bacteria detection: we present traditional methods and elaborate why point of care devices are needed.

2. Transducers and biosensors: we go over the main biosensing techniques and introduce paper as a microfluidic support for biosensors.

3. Impedance spectroscopy: we explain the method of impedimetric sensing through impedance spectroscopy and present the design of interdigitated electrodes which are used on our sensor of interest.

4. Electrode deposition: we give a non-exhaustive overview of fabrication techniques for micro- and nano-electronics. We then focus on current techniques for electrode deposition on paper.

Since this project is framed in a responsible design approach, a socio-economic impact assessment of the sensor of interest will be made at the end of this master-thesis. In the final section of this state of the art, we introduce several examples of study projects that targeted the quality of human health-affecting parameters and that involved a large scale citizen participation.

1   Bacteria detection

1.1   Bacteria specifications
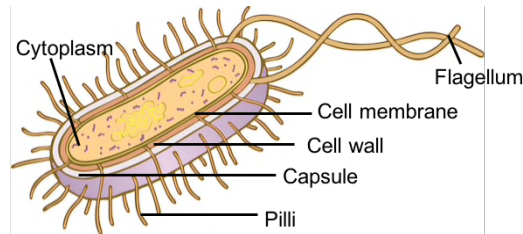
Figure 1.1: Schematic representation of a bacterial cell [8]

Bacteria are prokaryotic[1] mirco-organisms that typically measure a few μm in length and can have lots of different shapes. They first appeared on Earth about 4 billion years ago [9]. The human body is estimated to contain 10^{13} bacterial cells [10]. A large majority of those are beneficial to human life, but some of them cause diseases and infections. The latter are qualified as pathogenic.

As can be seen on figure 1.1, the main component of the bacterial cell is the cytoplasm. It is surrounded by a plasma membrane.

The conventional unit to express the concentration of bacteria is Colony Forming Unit per ml (CFU).

1.2   Traditional detection methods

In this section, 4 tranditional bacterial detection techniques are presented:
- Colony counting

- Polymerase Chain Reaction (PCR)

- Enzyme Linked Immunosorbent Assay (ELISA)

- Matrix Assisted Laser Desorption ionization time-of-flight mass spectroscopy (MALDI-TOF MS)

These methods are commonly used for at least 15 years. [11, 12]

Three characteristics are evaluated and summarized in table 1.1
1. **Limit of detection (LoD)**: the smallest amount of target substance that can be distinguished from the absence of that substance.
2. **Analysis time**: necessary time lapse to obtain results that can be interpreted.
3. **Selectivity**: the ability of the method to discriminate the response from adjacent substances from the response of the target substance [13].

---

[1]Prokaryotes are organisms made up of cells that lack a cell nucleus or any membrane-encased organelles. On the other hand, eukaryotes are organisms made up of cells that possess a membrane-bound nucleus that holds genetic material as well as membrane-bound organelles. Human cells are eukaryotic cells.

	Colony counting	PCR	ELISA	MALDI-TOF
LoD [CFU/ml]	1	10^{1-2}	10^{1-6}	10^{5-6}
Analysis time	>2 days	1-2h	5-30h	10min
Selectivity	Very high	Very High	high	High

Table 1.1: Conventional methods for the detection of bacterial cells (adapted from [12] and [14])

Colony counting

This method, which was used since the 19th century, estimates the number of bacterial cells present based on their ability to give rise to colonies under specific conditions of nutrition, temperature, pH and oxygen. The analyte is transferred to a medium that favorites their growth and kept under optimal circumstances from 1 to 10 days [15].
Theoretically, one viable cell can give rise to a colony through replication. This makes it possible to detect a single bacterial cell (given that it grows under test conditions) [11]. However, this method often underestimates the number of living cells present in a sample. Indeed, single cells are rare: they often occur in clumps or chains. It is thus hard to determine how many bacterial cells are at the origin of a colony. Furthermore, since this method consists in counting the formed colonies, these should be distinguishable. That causes an upper limit of the countable range: if the colonies are too numerous, they can't be differentiated from one another [12].
The growth media can be both selective or non-selective. For the latter, additional optical screening such as colorimetry is required to identify target bacteria colonies [16].

Polymerase Chain Reaction (PCR)

PCR exponentially multiplies target DNA samples. Apart from bacteria detection, other application fields are genotyping, forensic medecine, cloning,... The method was introduced in 1988 at the university of California by Kary Mullis, who won the Nobel Prize in chemistry in 1993.
A PCR cycle consists of three mains steps, which are visualized on figure 1.2:

1. Denaturation (at 95° C): double-stranded DNA breaks down to two single-stranded DNA molecules.
2. Annealing (55-65° C): attachment of the primers to each of the single-stranded DNA templates.
3. Extension (72°C): synthesising DNA, constituted of the free nucleotides.

The DNA amplification is exponential: for S_{in} intial DNA samples, the number of final samples S_{fin} after C cycles is:

$$S_{fin} = (2S_{in})^C \tag{1.1}$$

Usually, 25 to 30 cycles are performed [17]. This lasts between 2 to 4 hours.
The amplified DNA sequences can thereafter be detected by gel electrophoresis. Other detection methods based on nucleic acid amplification, such as LCR (ligase chain reaction) and SDA (strand displacement amplification) are also used [12].
This method has the advantage of being ultra sensitive and being able to detect a low number of bacterial cells (minimum 10 to 100) within hours.
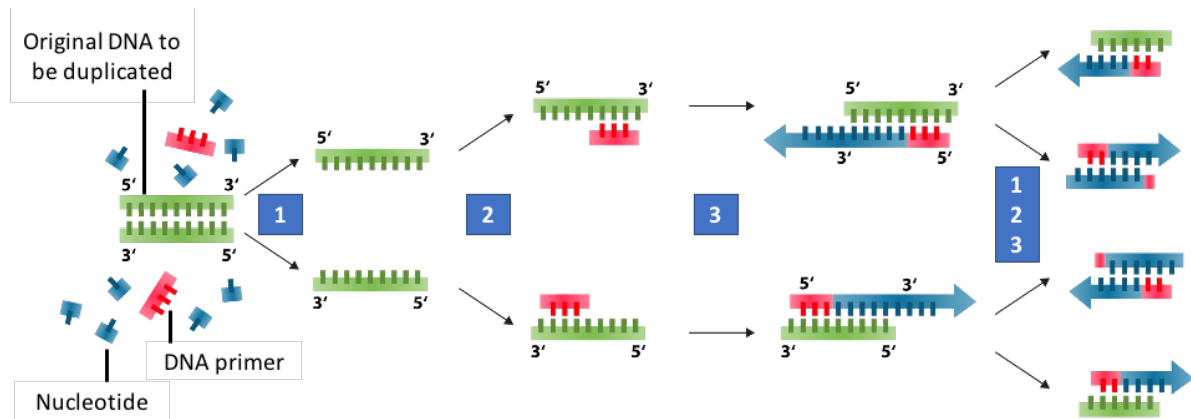
Figure 1.2: Main steps of PCR

However, it has some drawbacks:

- Prior isolation of the bacterial DNA is needed. This is a laborious and time-consuming process, for which qualified personnel is required.
- It is relatively expensive: a PCR machine costs over €10 000.
- This technique can't differentiate living cells from dead cells, as DNA is present in both.[18] Real-Time-PCR was developed in order to solve this problem: it relies on several genes which are only present during the growth of a bacteria. This can last up to 24 hours. [12]

Enzyme Linked Immunosorbent Assay (ELISA)

In this method, various antigen-antibody combinations are used, always including an enzyme-labeled antigen or antibody, and enzyme activity is measured colorimetrically. It was first introduced by two Swedish scientists form the university of Stockholm, Eva Engvall and Peter Perlman, in 1971. [19]
Depending on the antigen-antibody combination, different configurations are used: direct ELISA, indirect ELISA, competitive ELISA, sandwich ELISA, etc.

The main steps of sandwich ELISA are illustrated on figure 1.3. Between every step, washing (e.g. with PBS) is needed, in order to remove non-attached elements and avoid contamination.

1. An antibody to a target protein ("capture antibody") is immobilized on the surface of microtiter wells, through hydrophobic and electrostatic interactions.
2. The analyte is added. If the target bacteria is present in the analyte, the capture antibodies bind to it.
3. Another target antibody solution is added. These are labeled with an enzyme.
4. The enzyme activity is measured using a substrate giving a coloured, fluorescent or luminescent reaction to the enzyme. Light absorption of the product formed after substrate addition is measured and converted to numeric values.

This method makes it possible to detect concentrations down to an LoD of 10^5 CFU per ml. However, a one-day pre-enrichment treatment may be required. [11].

Figure 1.3: Main steps of sandwich-ELISA. (figure adapted from [20])
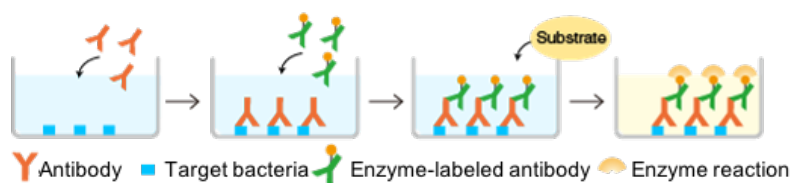
MALDI-TOF MS

First introduced by the team of Michael Karas [21] (Bonn University, Germany) and Koichi Tanaka [22] (Tohoku University, Japan) in 1988, Matrix Assisted Laser Desorption ionization time-of-flight mass spectroscopy (MALDI-TOF MS) was commercialized in the early 1990s. Mister Tanaka won the Nobel Prize in Chemistry in 2002 for his works on mass spectroscopy.
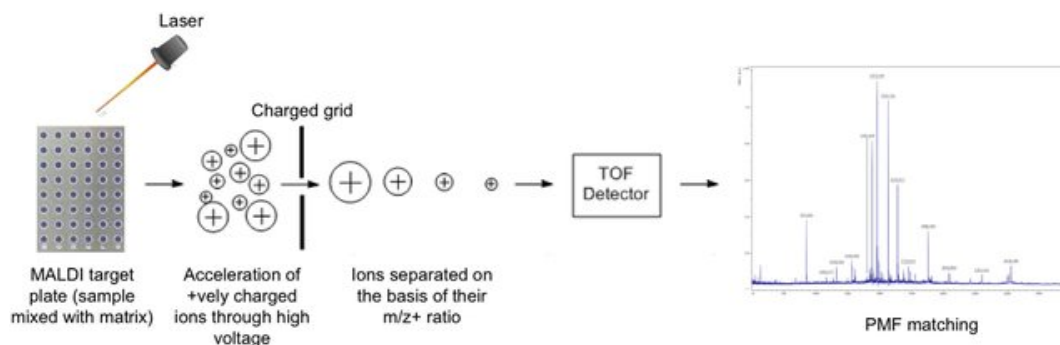
Figure 1.4: Main steps of the MALDI-TOF MS process [23]

The sample for analysis is prepared by mixing or coating it with asolution of an energy-absorbent, organic compound called matrix. When the matrix crystallizes on drying, the sample entrapped within the matrix also co-crystallizes. Then, the sample within the matrix is ionized with a laserbeam. The protonated[2] ions are then accelerated at a fixed potential, where these separate from each-other on the basis of their mass-to-charge ratio m/z. The charged analytes are then measured by a time of flight (TOF) analyzer. The m/z ratio is of an ion is determined by the time it needs to travel the flight tube. Based on the TOF information, a characteristic spectrum called peptide mass fingerprint(PMF) is generated for analytes in the sample. [23] This process is summarized on figure 1.4.

With MALDI-TOF MS, colonies growing in culture are accurately identified in minutes, without a priori knowledge of micro-organism type; users do not need to know whether a bacterium or a yeast is being tested. [24]
It is possible to test 16 to 384 samples simultaneously. [11]
This method can detect concentration of 10^4 CFU per ml or more. It has the drawback that it cannot always differentiate Gram-positive[3] bacteria, for instance *Streptococci* and

---

[2]Protonation is the addition of a proton an atom, molecule, or ion.

[3]Gram-positive bacteria are bacteria that give a positive result in the Gram stain test. Gram-positive bacteria take up the crystal violet stain used in the test, and then appear to be purple-coloured when seen through an optical microscope. This is because the thick peptidoglycan layer in their bacterial cell

Staphylococci.

1.3 Interest for point-of-care devices

Even though the aforementioned methods are widely used today, they have some major usage restrictions due to their bulkiness, relatively high-cost, time constraints and requirements for well-equipped laboratory facilities and trained staff. Globally, there's an increasing need for low-cost, simple, small and faster devices for the detection of harmful bacteria. [3]
This is especially true in developing countries, that lack the basic resources and well-equipped laboratory facilities needed for the traditional diagnostic methods. However, even in developed countries, there are several application areas where large-scale, cheap and instantaneous biological tests are needed.

Criteria for point-of-care detection devices have been listed by the World Health Organization. These are gathered under the acronym "ASSURED": Affordable, Sensitive, Specific, User-friendly, Rapid and robust, Equipment-free and Deliverable to end-users.

To better understand the pathway towards the implementation of such detection devices, it is important to have a general overview of the existing biosensors and transduction principles. This is presented in the next section.

2 Transducers and biosensors

The term sensor should be distinguished from transducer. The latter is a converter of one type of energy into another, whereas the former converts any type of energy into electrical. [25] Thus, every sensor is a transducer, but the opposite is not true.

2.1 Sensor principles

In section 1.2, we already introduced LoD, selectivity and detection time. In this section, we introduce a few more characteristics of transduction and sensing mechanisms.

Transfer Function (TF)
An ideal (theoretical) output–stimulus relationship exists for every sensor. This can be characterised by the so-called Transfer Function.
It is often considered unidimensional (under the condition that ambient factors, like temperature and humidity, are constant) : electrical signal S produced by the sensor as a function of the stimulus s : $S = f(s)$.

The TF can be any kind of function. A linear transfer function has the following form:

$$S = as + b \qquad (1.2)$$

---

wall.

With a the slope, which is also called the **sensitivity** (cfr figure 1.5) and b the intercept, i.e. the output signal at zero input signal.

For a nonlinear transfer function, the sensitivity a is not constant. At any particular input value, s_0, it can be defined as:

$$a = \frac{dS_0}{ds} \tag{1.3}$$

Even though transfer functions are often non-linear (exponential, power function, logarithmic,...), it is common to approach them by a linear TF over a limited range. Over the extended range, a nonlinear TF may be modeled by several straight lines. This is called a **piecewise approximation**.

Span

A dynamic range of stimuli which may be converted by a sensor is called a span. As can be seen in figure 1.5, it ranges from the LoD to the HDL.

For the sensors with a very broad and nonlinear response characteristic, the span may be expressed in decibels. It should be emphasized that decibels do not measure absolute values, but a ratio of values only. When we transform energy or power, decibels are defined as

$$1dB = 10log(\frac{X_{lin}}{X_{ref}}) \tag{1.4}$$

When we transform a quantity that relates to amplitudes (force, voltage, current,...) decibels are defined as

$$1dB = 20log(\frac{X_{lin}}{X_{ref}}) \tag{1.5}$$

with X_{lin} the target quantity and X_{ref} the reference quantity (often, $X_{ref} = 1$ in the case of amplitudes).

Full Scale Output (FSO)

FSO is the algebraic difference between the electrical output signals measured with maximum input stimulus and the lowest input stimulus applied. As can be seen in figure 1.5, this must include all deviations from the ideal transfer function.

Saturation

Every sensor has its operating limits. At some levels of the input stimuli, its output signal no longer will be responsive. A further increase in stimulus does not produce a desirable output.

Accuracy

By accuracy, we actually mean inaccuracy: it measures the highest deviation between the input value which is computed from the output voltage and the actual input value.

A real TF rarely coincides with the ideal. However, all runs of the real transfer functions must fall within the limits of a specified accuracy. These permissive limits differ from the ide al transfer function line by $\pm\Delta$. The real functions deviate from the ideal by $\pm\delta$,
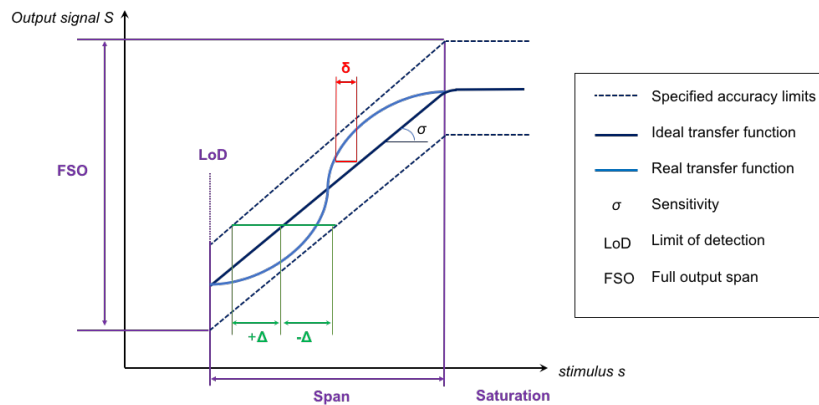
Figure 1.5: Overview of sensor characteristics

where $\delta \leq \Delta$. This is illustrated in figure 1.5.

Calibration

The causes for Transfer Function (TF) variations can be devided in three cathegories:

- Systematic for all sensors: when the TF is approximated

- Stochastic from one sensor device to another (device-to-device variations). Manufacturing tolerances are one of the causes for this.

- Stochastic in time with a single sensor. This is expressed in terms of **repeatability**. A repeatability error is caused by the inability of a sensor to represent the same value under identical conditions. Possible sources of the repeatability error may be thermal noise, buildup charge (hysteresis), material plasticity,...

When the variations in TF are higher than the required accuracy, calibration is needed.

From a mathematical point of view, calibration can be seen as "finding the parameters" of the TF. Let us consider a simple linear transfer function. Because a minimum of two points are required to define a straight line, at least a two-point calibration is required. This then allows us to find the parameters a and b from equation 1.2.
For nonlinear functions, more than two points may be required, depending on a mathematical model of the transfer function and the required accuracy. Since calibration may be a slow and/or expensive process, a trade-off between has to be made.

Resolution

Resolution describes the smallest increments of stimulus which can be sensed. When a stimulus continuously varies over the range, the output signals of some sensors will not be perfectly smooth. Moreover, any signal which is converted into a digital format is broken into small steps.
Resolution should not be confused with accuracy. In figure 1.6, the difference between these two characteristics is explained [26].
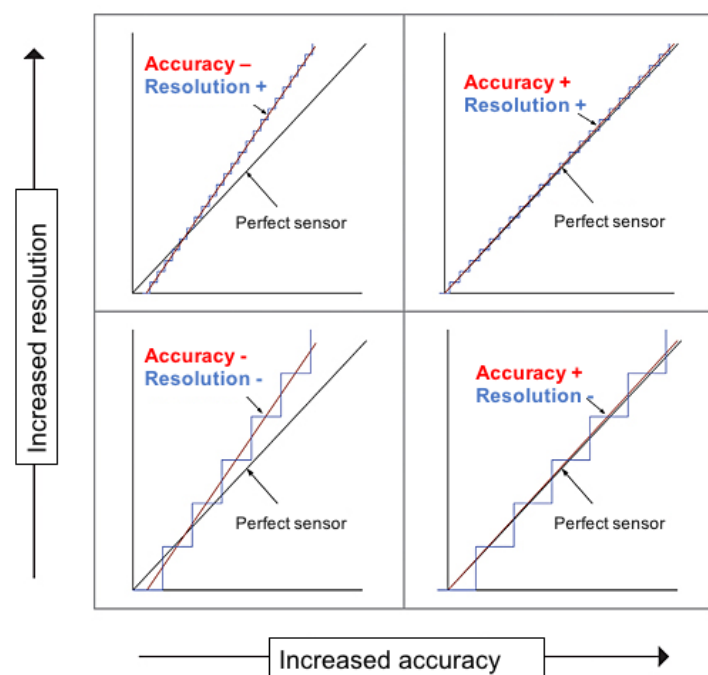
Figure 1.6: Resolution and accuracy: illustration

2.2 Biosensors

Biosensors are analytical devices that convert a biological response into a quantifiable and processable signal. The main components of a typical biosensor are the bioreceptors, which specifically interacts with the target analyte, and the transducer, which converts this interaction into an electronic signal [27].

The transduction chain of a typical biosensor is represented in figure 1.7. According to the type of transducer, biosensors can be classified as electro-chemical biosensors, calorimetric biosensors, optical biosensors, piezoelectric biosensors,...

The main types of bioreceptors are proteins, enzymes, nucleic acids, antibodies and whole cells. [28]

Some bacterial sensors use **labeling** to improve the sensor sensitivity and selectivity. This is done by nanoparticles, fluorophores, magnetic beads, enzymes... [11]

In the next sections, we introduce the main bioreceptors and transduction mechanisms.

2.3 Bioreceptors and selectivity

Based on the type of bio-recognition event that they monitor, biosensors can be either catalytic or based on affinity.

2.3.1 Catalytic biosensors

Catalytic biosensors incorporate enzymes, whole cells or tissues as the biosensing element and detect the presence of analytes by producing electro-active signals.
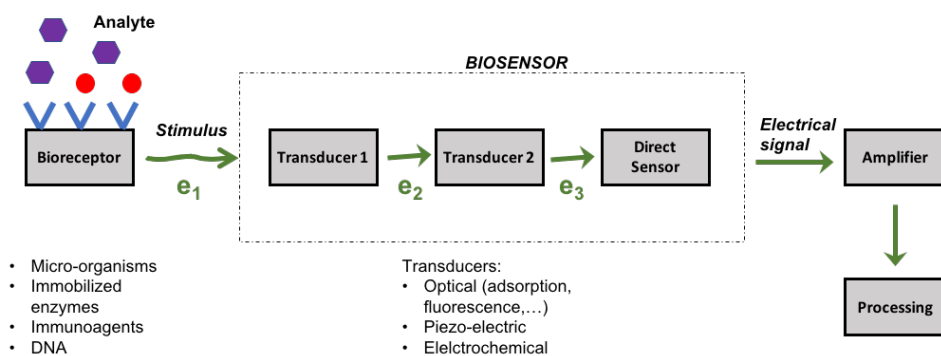
Figure 1.7: A biosensor may incorporate several transducers which transform the detected signal in several types of energy e_1, e_2,... The final tranducer block is a direct sensor: it converts the intermediate singal into an electrical signal. [25, 27]

Usually, the target analyte is either oxidised or reduced in presence of an enzyme. Owing to their complex molecular structure, enzymes can selectively detect very small concentrations of analyte even in complex mixtures like urine and blood.[29]

The most common commercial biosensors, personal glucose monitoring devices, rely on the enzyme "glucose oxidase" to detect glucose concentration in whole blood, as is explained in section 2.4.4. Despite their inherent selectivity and high biocatalytic activity, enzymes have the drawback that they are unable to detect analytes of interest which cannot be catalyzed by a specific enzyme or are not commonly found in living systems.

2.3.2 Affinity biosensors

Affinity biosensors monitor the binding of a target to immobilized recognition elements on transducer surfaces. They take advantage of the selective binding properties of certain biomolecules, most often antibodies, receptors or nucleic acids. The molecular recognition in affinity biosensors is mostly determined by the complementary shape and size of the binding site to the analyte of interest. [28]

Most often, affinity biosensors take advantage of **antibodies** that are raised against targets such as viruses, bacteria, drugs or other chemicals. These biosensors are called immunosensors.

Nucleic acids are used to detect complementary nucleic acids.

Affinity biosensing can be performed either in a single step (binding of the target analyte to produce a measurable signal) or more commonly in multiple steps, using **amplification techniques** (enzymes or nanoparticle labeling) to improve sensitivity.

Currently, the **immobilization** of affinity bioreceptors on solid surfaces while still retaining their stability and activity is one of the major challenges facing affinity biosensors in general. Selectivity of affinity sensors is also a challenge: since detection of analytes is often performed in complex fluids, the sensor surface must be highly selective towards the target analyte so that non-specific interactions due to presence of interferences can be minimized.
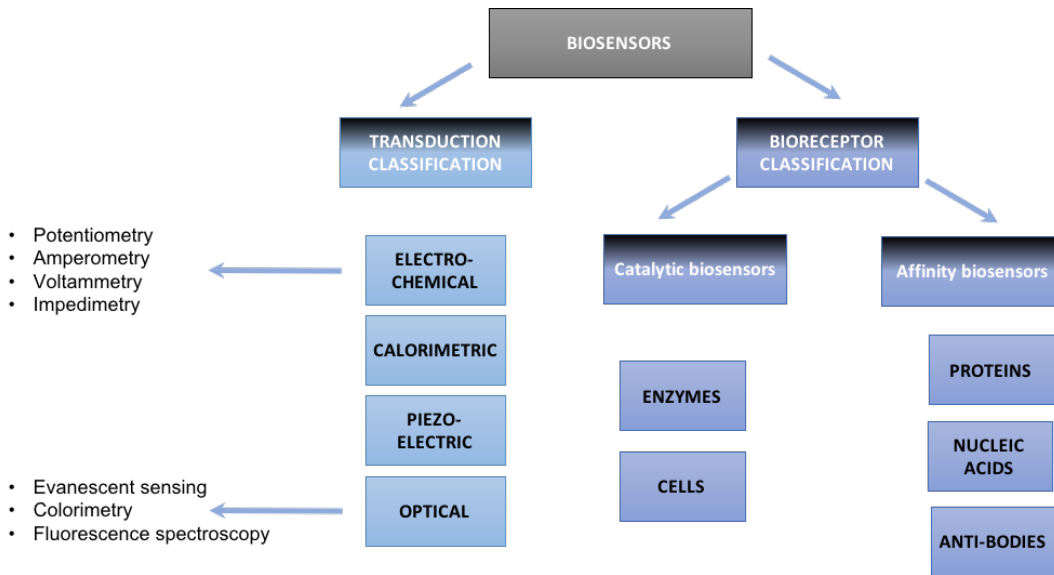
Figure 1.8: Classification of biosensors according to the transduction mechanism and biosensing mechanism.

2.4 Transduction mechanisms of biosensors

2.4.1 Optical biosensors

Optical biosensors are the most widespread biosensors.[30] They measure the light spectrum emitted from the labels or bacteria themselves. They exist in different forms, detecting variations in four main optical phenomena: absorbance, fluorescence, luminescence and reflectance. The advantages of optical sensors include: sensitivity, remote sensing, immunity to electromagnetic interference, non-conductivity and safety for personnel. [31]
An overview of the different optical sensing principles is given in this section. [11]

Evanescent sensing

According to Snell's Law, total internal reflection occurs when waves in one medium reach the boundary with another medium (with a higher refractive index) at an incident angle θ_i which is larger than the critical angle θ_c (cfr figure 1.9). However, since electrical and magnetic waves cannot be discontinuous at the interface between the two materials, an Evanescent Field (EF) appears.
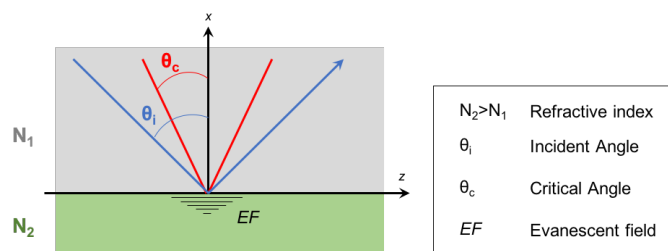
Figure 1.9: Evanescent field creation

The EF does not propagate as an electromagnetic wave. Its energy is spatially concentrated in the vicinity of the source, thus at the boundary between the 2 materials. It should thus be noted that the EF does not cause a net energy flow.
The amplitude of the evanescent[4] wave decays exponentially with respect to the depth of its penetration in the material.

This phenomenon is used for evanescent sensing: according to the composition of the analyte, the evanescent wave will be absorbed differently. The mechanisms used in evanescent sensing depend on the analytes and the application of the sensor. Hollow core fibers and tapered optical fibers are common structures for optical sensors. For biosensing applications, it is common since the 1980's to use Surface Plasmon Resonance (SPR) [32] and Evanescent field absorption Tapered Optic-Fiber biosensor (TOFBS).[33, 34]

Colorimetry

Colorimetric biosensors can be used to detect a particular analyte through color changes by naked eyes or simple portable optical detectors for quantitative measurement.
From the point of view of the ASSURED guidelines, colorimetric detection has several advantages: the human eye easily identifies a change in color to determine whether a specific virus is present, so as to prevent its spread. Meanwhile, color change is also easy to be detected using a simple camera or intensity based optical detector, with relatively simple algorithms to quantify test results in an inexpensive and instant way.

An important subcathegory of colorimetric biosensors, are based on **pH variation** of the analyte. For example, Loop-mediated isothermal amplification (LAMP) was developed for DNA detection in 2000 [35]. LAMP is a detection method that amplifies DNA using DNA-polymerase, being carried out in isothermal conditions, at a constant temperature of 60–65 °C. The amplified sequence is made up of several inverted repeats and multiple loops formed by annealing between alternately inverted repeats of the original DNA strand. DNA can be amplified up to 10^{39} times.[36]
During this process, byproducts including a pyrophosphate moiety and hydrogen ions cause a pH change. This change can be observed by a color indicator, for instance containing phenol red and cresol red. With this indicator, the color of a positive reaction changes from purple-red to yellow, but the negative reaction tube remains the original color.[37]
It should be noted that in other contexts, the amplification can also be detected via photometry, measuring the turbidity caused by magnesium pyrophosphate precipitate, another byproduct.[38]
Other physical parameters related to the bacterial concentration can cause a pH-shift. For instance, colorimetric pH indicator slightly changes its colour when CO_2 is released during the growth of bacterial cells. [11]

Unmodified Gold Nanoparticles (AuNP) have been reported to detect RNA of several viruses in **Nanoparticle-based colorimetric biosensors**. [36] This is because the presence of the virus RNA causes coagulation of AuNP. When the AuNP aggregate, the

---

[4]Etymologically, "evanescent" has the same root as the french verb "s'évanouir": this wave literally fades away in the z-direction of figure 1.9
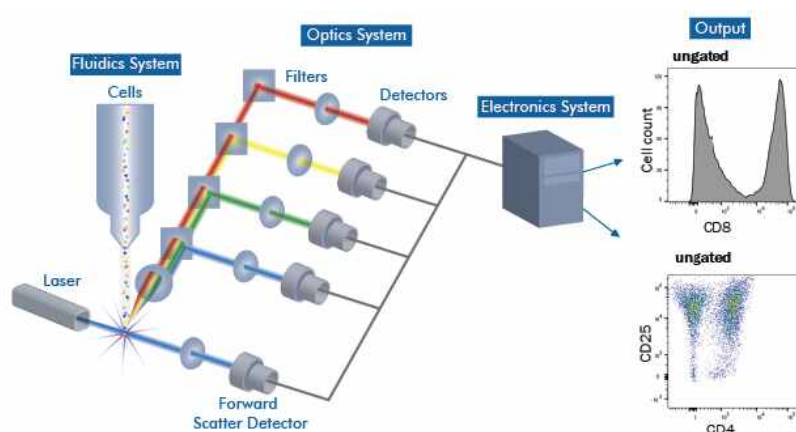
Figure 1.10: Flow Cytometry schema

absorption and scattering peaks shift.

In the absence of virus RNA, the single strand DNA (ssDNA) primers added into the bioassay uncoil and expose their nitrogenous bases to form attractive electrostatic forces between the bases and AuNP. Subsequently, the ssDNA primers attach to the AuNP, where these primers coat the AuNP to stabilize them, causing dispersed AuNP to remain red.

On the other hand, in the presence of virus RNAs, the ssDNA primer attaches to the RNA to form double strands. Since there are no primers to stabilize the AuNP, the AuNP aggregate and the bioassay solution turns from red to blue, as the absorption and scattering peaks shift. [36]

The AuNP can also be *functionalized*, for instance with antibodies or peptides. They can also be used in combination with aforementioned thecniques, such as PCR [11], ELISA and LAMP. [36]. Other nanoparticles such as Gold Nanorods (AuNR), Silver Nanoparticles (AgNP) and Quantum Dots (QD) are also used. [27]

Various other colorimetric methods exist, such as polymerized polydiacetylene [39, 40] and gene expression reaction. [41, 42]

Fluorescence spectroscopy

Fluorescence is the excitation of a valence electron from its ground state to a singlet state excited by an external light source. After excitation, the electron immediately returns to its initial position by emitting a lower energy photon which gives the fluorescent light. To observe this phenomenon, fluorescent markers must be added to the sample, which can be costly but also time-consuming because these compounds must be conjugated with the detection elements. [7] Fluorescence spectroscopy consists in measuring the light intensity emitted from fluorescent labels bound to target bacteria.

Flow cytometry is a fluorescence spectroscopy based bacterial sensing technique which is being used by FARYS[5] for drinkwater monitoring. [43, 44] Figure 1.10 summarizes its working principle. A sample containing cells or particles is suspended in a fluid

---

[5]FARYS is a drinking water society that operates in the east of Flanders.

and injected into the flow cytometer instrument. The sample is focused to ideally flow one cell at a time through a laser beam. After interaction with the particle, this beam is scattered in a particular way, making it recognizable. Cells are often labeled with fluorescent markers so light is absorbed and then emitted in a band of wavelengths. Tens of thousands of cells can be quickly examined and the data gathered are processed by a computer.

This principle was first introduced by Wallace H. Coulter, in 1953, for cell-sorting purposes. [45]

2.4.2 Piezo-electric biosensors
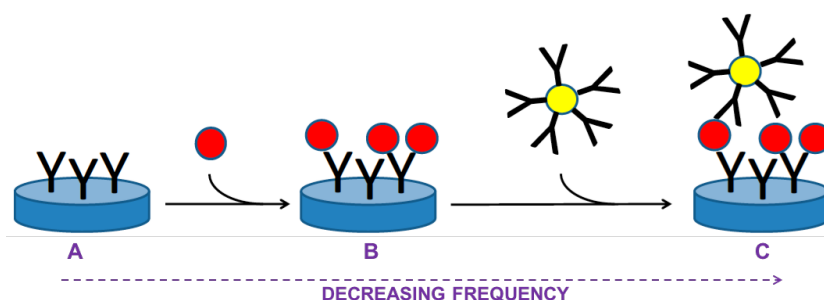
Figure 1.11: Piezoelectric immunosensors for the determination of an antigen (red granule) and increase of oscillations by application of a nanoparticle (yellow granule) covered with immunoglobulins (Y shaped). The blue disc represents a piezoelectric crystal. [46]

Piezoelectricity is a physical phenomenon which refers to an ability of a material to produce voltage when mechanically stressed. The effect works in the opposite situation as well. Alternating voltage applied to the surface of a piezoelectric material causes mechanical oscillations. Anisotropic crystals (crystals without center of symmetry) are typical materials exerting piezo-electricity. A Piezoelectric quartz crystal (PQC) is often used to build up a piezoelectric biosensor.[46]

The first investigation on piezo-electricity was performed in 1880 by Jacques and Pierre Curie, who observed that a mechanical stress applied to the surfaces of various crystals caused a corresponding electrical potential across the crystals, the magnitude of which was proportional to the applied stress.[47]

In 1959, Sauerbrey made the first quantitative investigation [48] on the piezo-electric effect and derived the relationship for change in frequency (in Hz) caused by the added mass:

$$\Delta f = \frac{-2f_0^2}{A\sqrt{\rho_q \mu_q}} \Delta m \tag{1.6}$$

with f_0 the resonant frequency of the fundamental mode, Δf the normalized frequency change, Δm the mass change, A the active crystal area, ρ_q the density of quartz, μ_q the shear modulus of quartz.

In a general way, a piezoelectric biosensor or "acoustic wave biosensor" can be constructed by immobilising a receptor (antibody, nucleic acid...) onto the surface of a PQC and

	Year	LoD	Bacteria	NP
Pohanka et al. [50]	2007	10^5	Francisella Tularensis	/
Olsen et al. [51]	2006	10^2	Salmonella Typhimurium	/
Salam et al. [52]	2013	10-20	Salmonella Typhimurium	AuNP
Guo et al. [53]	2012	10	Escherechia Coli O157:H7	AuNP

Table 1.2: Examples of piezo-electric bacterial detectors, the year in which the article was published, their limit of detection [CFU/ml], the target bacteria and the type of nanoparticles.

monitoring the changes of resonant frequency due to the mass variation caused binding of the target particle (antigen, nucleic acid,...). This is shown on the steps A and B of figure 1.11. The very first paper dealing with the development of a piezoelectric immunosensor was published in 1972 [49].

The major difficulty for bacteria detection is that microbial cells don't act like ideal mass points and only in the proximity of receptor captured by an immobilized antibody is involved in change of oscillations. [46] As can be seen in table 1.2, the LoD can be improved by an application of nanoparticles to the target biomolecule which increases mass on the sensor surface and crosslink the particular bacteria into a firm layer. The principle of adding nanoparticles is shown in step C of figure 1.11.

2.4.3 Calorimetric biosensors

Many enzyme catalysed reactions are exothermic, generating heat which may be used as a basis for measuring the rate of reaction and, hence, the analyte concentration. This shift in temperature can be measured by a thermistor or by a quartz resonator. [54, 55] Calorimetric sensors have the advantage of offering a relatively fast measurement and being generically applicable as almost all enzymatic reactions and biological interactions will produce or consume heat. This unique attribute allows the development of a single sensor platform in which a remotely coupled, disposable cartridge containing the enzyme(s) of interest permits a selective detection of a wide variety of biomolecules. [56] However, in some cases, the transfer function varies a lot.

In 2007, Yoon et al. [57] developed a sensor for Neisseria meningitidis which had an accuracy and LoD comparable to ELISA. However, this was under clinical conditions.

2.4.4 Electrochemical biosensors

These devices are mainly based on the observation of current or potential changes due to interactions occurring at the sensor-sample interface. Techniques are generally classified according to the observed parameter: current (amperometric, active sensing), potential (potentiometric, passive sensing) or impedance (impedimetric).

Potentiometry

Potentiometry passively measures the open-circuit DC potential of a solution between two electrodes. One electrode is called the reference electrode and has a constant

potential, while the other one is an indicator electrode whose potential changes with the composition of the sample. Therefore, the difference of potential between the two electrodes gives an assessment of the composition of the sample. [58].

Ion-selective electrodes convert the activity of a specific ion dissolved in a solution into an electrical potential. The voltage is theoretically dependent on the logarithm of the ionic activity, according to the Nernst equation:

$$E = E_0 - \frac{RT}{nF} ln(a_i)$$

with E the measured potential, E_0 the standard cell potential (for a reference ion concentration), R the gas constant, F the Faraday constant, T the absolute temperature and a_i the ion activity.

A common example is the glass electrode pH meter. [59] The glass electrode has a glass bulb specifically designed to be selective to hydrogen-ion concentration. Hydrogen ions in the test solution exchange for other positively charged ions on the glass bulb, creating an electrochemical potential across the bulb. According to Nernst law, this voltage difference is logarithmic with $H+$ concentration and linear with pH variation.

For bio-sensing purposes, enzyme catalysed reactions are used to consume or produce substances which are detected by the ion-selective electrode. Since potentiometry yields a logarithmic concentration response, the technique enables the detection of extremely small concentration changes. [60]

Coated wire electrodes (CWES), and ion-selective field-effect transistors (ISFETs) offer other, more recent transduction mechanisms for potentiometric biosensors. [61, 62].

Amperometry and voltammetry

Amperometric biosensors measure the quantity of current produced at a constant potential between a working electrode and a reference electrode. This current is caused by an electro-chemically active analyte that can be oxidized or reduced at the working electrode. Note that in this technique, the measurement is done with a shorted circuit whereas potentiometry works with an open circuit measurement.

As can be seen in figure 1.12.A, it is common to add a counter electrode in order to obtain a three-cell electrode for amperometric measurements. Indeed, if one uses the reference as the current carrying electrode, then its potential changes and the reference would vary. [63] Thanks to the counter electrode, the potential difference between the working electrode and the reference electrode is constant.

When the current is measured at a constant potential, the process is called amperometry. In contrast, voltammetry is the technique that measures current during controlled variations of the potential or over a set potential range [64, 65, 66].

Amperometric biosensors often rely on enzyme systems that catalytically convert the analyte into a product that can be oxidized or reduced at the working electrode. Therefore, amperometry is often used for **catalytic biosensors** which are described in section 2.3.
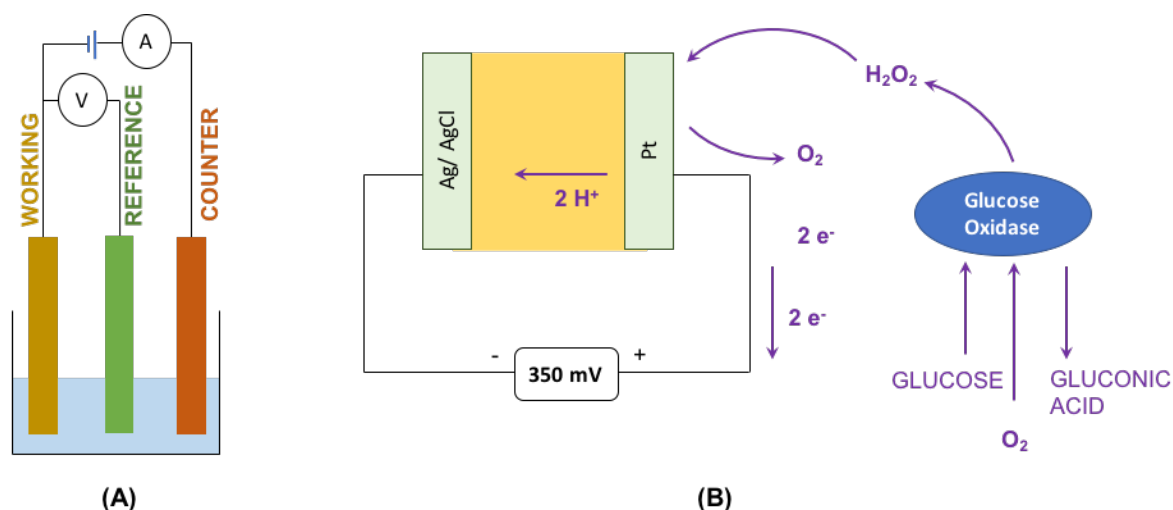
Figure 1.12: (A) A typical three-cell setup for amperometry. (B) Simplified illustration of glucose detection through amperometry. Hydrogen peroxide is formed due to catalytic reaction of the enzyme glucose oxidase. This H_2O_2 is then oxidised at the working electrode (Pt). This causes electrons to flow to the counter electrode (Ag). [67]

Typical enzymes are **oxidases** that catalyze the following class of reactions:

$$\text{Substrate} + O_2 \longrightarrow \text{Product} + H_2O_2$$
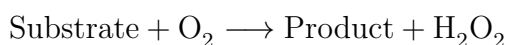
A widely used example is a glucose meter for blood.[67] Due to the enzyme "glucose oxidase", the following reaction occurs:

$$\text{Glucose} + O_2 \longrightarrow \text{Gluconic acid} + H_2O_2$$

In 1962, L.Clark introduced the first biosensor based on this principle: he trapped glucose oxidase over an electrode using a semi-permeable membrane. [68] Thanks to an applied voltage (around 0.3V), the oxidation potential of the working electrode (platinum) increases. [67] This makes it easy for the hydrogen peroxide H_2O_2 to oxidize at the working electrode, which is here the anode:

$$H_2O_2 \longrightarrow O_2 + 2H^+ + 2e^- \tag{1.7}$$
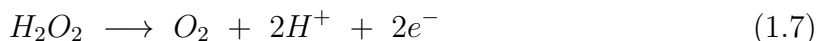
Every oxidized H_2O_2 molecule causes two electrons to flow to the counter electrode. This is illustrated in figure 1.12.B.

Since there are lots of electrons on the working electrode, the backward reaction of 1.7 occurs at the analyte-electrode interface: O_2 and H^+ may recombine to H_2O_2. Thus, the net current flow is proportional to the difference between the number of liberated electrons and the number of recombined electrons. This is modelled by the Butler-Volmer equation:

$$I = A_e q(k_f \rho_{H_2O_2} - k_b \rho_{O_2})$$

with A_e the area of the working electrode, k_f and k_b the forward and backward reaction rates determined by the applied potential, ρ_x the concentration of x.

It can be shown that when a voltage of 350 mV is applied, the backward reaction is negligible compared to the forward reaction. [67] In other words, the current is **directly proportional** to the hydrogen peroxide concentration, and thus to the glucose concentration. Note that for potentiometric measurements, the voltage signal was dependent on the logarithm of ion concentration.

Thus, in general, the voltage range must be chosen carefully to guarantee a (quasi)-linear relation between the current and the concentration of the electro-active product -given that there is no saturation in the enzymatic reaction.[66, 69]

Although amperometric devices are the most commonly reported class of biosensors, they tend to have a small dynamic range due to saturation kinetics of the enzyme. Furthermore, a large over-potential is required for oxidation of the analyte: this may lead to oxidation of interfering compounds as well, causing contamination. [70] These effects can be eliminated through the use of selective membranes, which carefully control the molecular weight or the charge of compounds which have access to the electrode. An interesting example is found in [71], where E. coli is detected using a flow-through immunofiltration method coupled to amperometry. The resulting detection range was from $4.7 \cdot 10^6$ to $2.4 \cdot 10^9$ CFU/mL in cultivation medium, and the detection time was 30 min. [72]

Impedimetry

Impedimetric biosensors use Electrical Impedance Spectroscopy (EIS), which is explained in section 3. In this technique, a cyclic function of small amplitude and variable frequency is applied to a transducer, and the resulting current is used to calculate the impedance over a range of applied voltage or current frequencies. The amplitude of the current and potential signals and the resulting phase difference between voltage and current, which depends on the nature of the system under study, dictates the system impedance. [62, 69] Based on the obtained impedance, the resistive and capacitive components of impedance are determined.

Impedance detection can target suspended bacterial cells in the electrolyte (volume-based) or captured bacterial cells at the sensor surface (surface-based). [11]
A common **volume-based** method is called impedance flow cytometry (IFC), which enables an accurate counting and statistical size analysis of a large number of cells (> 10:000 in less than 2 min [11, 73]). Its main disadvantage is the inability to selectively distinguish one bacteria from another, despite some promising works that show slight differences of the dielectric footprints [74, 75].
The **surface-based** method uses planar electrodes designed atop a solid substrate, in order to detect bacterial cells that progressively adhere the sensor surface thanks to the microfluidic flow [76]. The main disadvantage of this method is that many cells flowing atop the sensor are lost. However, selectivity can be easily obtained by functionalizing the sensor surface with affinity bio-receptors like antibodies.
Planar impedance microbiology has been developed as a rapid method that can detect bacteria in food samples (e.g. Salmonella in milk) within 2 to 10h. [77, 78]

This technique is not the most common among electro-chemical biosensors, but it has been attracting more and more attention over the last few years. [79] This is due especially to the possibility of label-free performance, the use of miniaturized systems and the relative low cost. [80]

Note that EIS is better suited for affinity biosensors (cfr section 2.3) than amperometry and voltammetry. Indeed, the latter often require redox active labels to achieve sensitive and specific detection. Furthermore, EIS requires smaller voltages (approx. 20mV [81]) than voltammetry and amperometry (approx 300mV [67]). Thus, if performed correctly, EIS has the capability to sensitively monitor interfacial changes without damaging or even disturbing the affinity binding event. [82]

2.5   Paper as a support for microfluidic biosensors

Microfluidic devices exploit the physical and chemical properties of liquids and gases at a microscale. They offer several benefits over conventionally sized systems. Indeed, they enable the analysis and use of less volume of samples, chemicals and reagents; typically femto to microliter and can therefore lead to lower costs and less environmental impact. Furthermore, the precision and selectivity of these devices can reach a high level. [7] Working with very small volumes helps to improve the sensitivity of the impedimetric measurement. [12]

Many operations can be executed at the same time thanks to their compact size, shortening the time of experiment.

Poly-dimethyl siloxane (PDMS) is widely used for microfluidic devices for biological applications. This elastomer is transparent, bio-compatible, permeable to gas and can be transformed into microfluidic devices through simple molding procedures. [83]

Paper is a cellulosic material characterized by a porous structure giving it a high surface/volume ratio. It has several important features that make it interesting for point of care biosensors.

- Paper has an excellent **capillarity**, which offers the possibility to integrate microfluidics.

- Paper is **biocompatible**, which means that bioreceptors can be immobilized. This can be done by physical absorption, chemical coupling, deposition on a support or sol-gel treatment. [84] Most of the techniques used to immobilize biomolecules are based on physical adsorption between the biomolecule and reactive functional groups in the paper structure, mainly hydroxyl. [7]

- Paper is excellent for point of care devices due to its **low cost, portability and ease of operation**. [5]

- Due to their **recyclability**, paper-based biosensors can reduce electronic waste.

- It is possible to integrate **electronics** on paper. This is further elaborated in section 4.4.

The main drawback in using paper-based microfluidic devices is that it is very complex to exactly pattern the channels, due to its rough surface and its high capillarity. [85] From
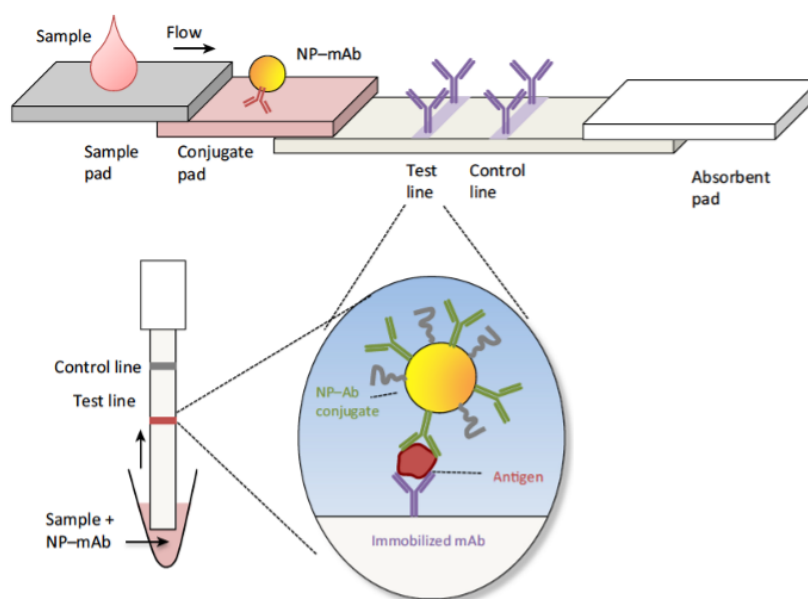
Figure 1.13: Basic Structure of a Lateral Flow Assay (LFA) [87] (mAb, monoclonal antibody; NP, nanoparticle)

an environmental point of view, paper has the drawback that its production process is very water-consuming because of the pulp-washing stage: it consumes up to 1790 liters of water per kilogram of paper. [86]

Currently, some paper-based sensors are already widely spread over the market. They are **Lateral Flow Assay (LFA)** which rely on optical detection (colorimetric and fluorescence).
LFA comprise single or multiple layers of paper substrates with hydrophilic paper channels patterned by hydrophobic materials, and can transport fluids autonomously for performing single- or multi-step analytical assays and detecting various analytes in human fluids (e.g. urine, serum and blood). [88] The patterning of channels using hydrophobic materials can be done by photolithography, plasma treatment, inkjet printing, screenprinting and wax printing. [89]
The latter procedure is widely used due to its simplicity, non-toxicity, and low cost compared to the other techniques. The wax patterns are directly printed on the paper, which are then used to control the flow of the fluid that includes the samples and the reagents.
A pregnancy strips that utilize gold nanoparticles, which is a common LFA, is illustrated in figure 1.13. The sample pad's main purpose is to ensure uniform and controlled distribution of the sample onto the conjugate pad. The conjugate pad contains antibody-conjugated microspheres. When wetted with the sample, these detector reagents solubilize and if the bacteria are present in the sample, their antigenic sites bind to them. The main function of the absorbent pad is to increase the volume of sample entering the strip.

However, these colorimetric LFA only provide qualitative or semi-quantitative yes/no responses, limiting its range of application. Currently, there is a huge amount of research

ongoing in order to solve these issues. This is reflected in the peer-reviewed literature with 693 articles on paper biosensors published in 2017. [90]

Several methods exist to increase the sensitivity of LFA and make the results quantitative. The most common and investigated one is electrochemical detection. The idea is to apply electrodes on the paper substrate (cfr section 4.4) and detect the presence of analyte through amperometry or impedimetry. In addition to optical and electrochemical methods, two other detection methods exist. The thermal detection method exploits the thermal response of tracing nanoparticles under external stimulation. The result is an increase in temperature that can be related to the amount of tracer particles. Similarly, the magnetic method exploits the magnetic response of magnetic nanoparticles under the application of an external magnetic field. [7]

3   Impedance spectroscopy

Electrical Impedance Spectroscopy (EIS) is a powerful technique to investigate the electrical properties of materials and electro-chemical cells. It has gained great attention as an analytical tool for a broad range of analytes, mainly because it can be performed as a non-destructive method and it enables *in situ* measurements. Moreover, EIS is suitable for label-free applications, which significantly diminishes its cost in relation to other techniques and can make it easier to perform. [80]
The measured impedance spectrum, usually fitted with an equivalent electrical model, represents an electrical fingerprint of the sample, thus providing an insight into its properties and behavior.
EIS dates back to 1894 when W.Nerst measured the dielectric constant of aqueous electrolytes. [91] However, it was only in the 1980's that the interest in EIS grew substantially, thanks to computer-controlled digital instruments allowing quicker and easier frequency sweeps and data analyses.

Two versions of EIS exist: *potentiostat* and *galvanostat* EIS. In the former, a sinusoidal test voltage is applied to the SUT and the induced current in measured while in the latter, it's the opposite. In most cases, both versions are equivalent. However, due to application-specific conditions, one of them may be more suitable. For example, in the case of corrosion analysis, galvanostat EIS assures that the measurements are carried out at true corrosion potential.[92]

In general, impedance can be defined as:

$$\mathbf{Z}(\omega, t) = \frac{\mathbf{V}(\omega, t)}{\mathbf{I}(\omega, t)}$$

where $\mathbf{Z}, \mathbf{V}, \mathbf{I}$ are complex values. To simplify the analysis, impedance can be defined as a Linear Time Invariant (LTI) system [93], exhibiting 3 conditions:

- Linearity: the response is first order

- Stability: the system does not change with time, nor does it continue oscillating after the perturbation is removed.

- Causality: the response only comes from the applied perturbation.

Since both solid and liquid electrochemical systems tend to show strong non-linear behavior, the applied stimulus should be very small. It can be shown that the basic differential equations which govern the response of the system become linear to an acceptable approximation when the potential difference is less than the **thermal voltage** U_T, about 25 mV at 25 °C. [81] Furthermore, applying a voltage in the range of 25 mV ensures non-destructive probing of the bio-molecular layer. [94]

If the system is non-linear, the current response will contain harmonics of the excitation frequency. [81, 95] Thus, considering that the system is linear, implies that the frequency of the output current should be equal to that of the input voltage.

In the aforementioned case, the impedance $Z(\omega)$ is defined as

$$Z(\omega) \triangleq \frac{V_0 \cdot e^{j\omega}}{I_0(\omega) \cdot e^{j\omega t + \theta(\omega)}} = \frac{V_0}{I_0(\omega)} \cdot e^{-j\theta(\omega)} \tag{1.8}$$

with

- $\omega \triangleq 2\pi f$ the angular frequency

- V_0 the amplitude of the applied voltage

- I_0 the amplitude of the measured voltage, θ the phase of the measured voltage

There are three different types of electrical stimuli which are used in EIS. Usually, the time-varying results are Laplace- or Fourier-transformed into the frequency domain. [81]

1. Step function of voltage: $V(t) = 0$ when $t < 0$ and $V(t) = V_0$ when t>0. This signal is very easy to generate but the stimulus does not excite all the frequencies with the same power, introducing potential issues of non-uniform sampling in frequency.

2. Random (white) noise, which allows for very uniform stimulation in frequency. This offers the advantage of fast data collection because only one signal is applied to the interface over a short time. The main disadvantage is that it requires "true" white noise. Using a sum of well-defined sine waves as excitation instead of white noise offers the advantage of a better signal-to-noise ratio for each desired frequency.

3. Applying single-frequency sinusoids and measuring the phase shift and amplitude of the resulting output. This is the most commonly used technique since it is implemented in a lot of commercial instruments which easily swipe from $1mHz$ to $1MHz$. However, sweeping the frequency requires a longer time interval.

Depending on the presence or absence of redox species in the electrode or in the electrolyte, two types of EIS exist: faradaic[6] or non-faradaic EIS respectively.

---

[6]Faraday's laws of electrolysis are quantitative relationships based on the electrochemical research published by Michael Faraday in 1833 [96]. They state that the amount of material produced at an electrode (or liberated from it) during an electrochemical reaction is directly proportional to the total conducted charge.

Non-faradaic EIS sensors use an electrolyte that does not contain a redox reagent. It predominantly depends on the capacitance change at the interface between the electrodes and the electrolyte.

Faradaic EIS sensors use the charge transfer process between the electrodes and the redox reagent. By controlling the charge transfer process using a bio-reaction, the faradaic EIS can achieve a higher sensitivity than non-faradaic EIS. However, the incorporation of a redox reagent makes it difficult to detect specific biomolecules. [11, 80, 97]

3.1 Impedance representation

Prior to the availability of modern EIS instrumentation, analysis of Lissajous[7] figures on oscilloscope screens was the accepted method. [81, 98] As can be seen on figure 1.14, the sinusoidal voltage and current are represented respectively on the x-axis and on the y-axis. Given that the variations are small enough so that the impedance can be considered as an LTI system -which implies that the input frequency equals the output frequency, as already explained-, the resulting figure can vary from a circle ($\Delta\{\phi_{voltage}, \phi_{current}\} \in \{90°, 270°\}$) to an inclined line ($\Delta\{\phi_{voltage}, \phi_{current}\} \in \{0°, 180°, 360°\}$). [99]
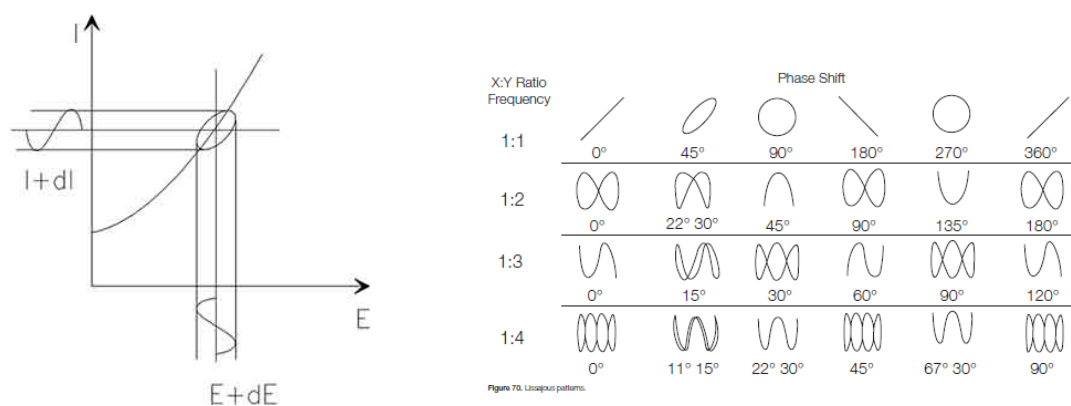
Figure 1.14: Origin of the Lissajous figure and Reference Lissajous figures [98, 99]

In 1748, Leonard Euler published *"On transcending quantities arising from the circle"*, evoking an equation which would turn out to be fundamental for both mathematics and physics:

$$e^{j\theta} = cos(\theta) + jsin(\theta) \tag{1.9}$$

Combining equations 1.9 and 1.8, it is possible to decompose $Z(\omega)$ in two different ways:

$$Z(\omega) = \|Z(\omega)\| \cdot e^{j\ \theta(\omega)} \tag{1.10}$$

$$= \|Z(\omega)\| \cdot [cos\ \theta(\omega) + j \cdot sin\ \theta(\omega)] \tag{1.11}$$

Nowadays, thanks to modern instrumentation and Euler's groundbreading work, two graphical representations are common: the Bode plot based on eq. 1.10, and the Nyquist

---

[7]Jules Antoine Lissajous published several works on waves in the second half of the 19th century. On his birth house in Versailles is a commemorative plaque which refers to him as "the man who made sound visible".

plot based on eq. 1.11.

The Bode[8] plot represents the impedance modulus and phase in function of the frequency f (logarithmic scale).
The Nyquist[9] plot represents the opposite imaginary part $-Im(Z) = -\|Z(\omega)\| \cdot sin\,\theta(\omega)$ as a function of the real part $Re(Z) = \|Z(\omega)\| \cdot cos\,\theta(\omega)$.

To illustrate both plotting techniques, we consider a parallel RC circuit. The impedance of a parallel RC circuit is

$$Z(\omega) = \frac{R}{1 + j\omega RC} \tag{1.12}$$

$$\|Z(\omega)\| = \sqrt{\frac{R^2}{1 + \omega^2 R^2 C^2}} \tag{1.13}$$

$$\Phi(Z(\omega)) = atan(-\omega CR) \tag{1.14}$$

Observing equation 1.12, we see that when $\omega \longrightarrow \infty$, the total impedance of a parallel RC-circuit tends towards a closed circuit, which means that the circuit behaves more and more like a capacitor at infinite frequency. On the other hand, when $\omega \longrightarrow 0$, the total impedance tends towards R.
The impedance phase corresponding to a resistive behavior is 0° while the phase corresponding to a capacitive behavior is -90°. In equation 1.14, we observe that $\Phi(Z(\omega)) = -\frac{\pi}{4}$ when $\omega = \frac{1}{RC}$, which lies exactly in between the two asymptotic values of the phase.
All these trends are confirmed on the Bode and Nyquist plots in figure 1.15 which represents the complex impedance $Z(\omega)$ for a resistor R = 1kΩ, a capacitance C=10nF and the parallel association of both.

In the Nyquist plot, the spectral information is not explicit. However, since we know the asymptotic values for $\omega \longrightarrow 0$ and $\omega \longrightarrow \infty$, it is obvious that the semicircle is swept through in counterclockwise direction as the frequency increases.
The derivative of $Z(\omega)$ is:

$$\frac{\partial Z(\omega)}{\partial \omega} = \frac{2C^2 R^3 \omega}{(C^2 R^2 \omega^2 + 1)^2} + j \cdot \frac{CR^2(C^2 R^2 \omega^2 - 1)}{(C^2 R^2 \omega^2 + 1)^2} \tag{1.15}$$

Based on this, we can determine that the maximum absolute value of $Im(Z)$ is -unsurprisingly- reached at $\omega = \frac{1}{RC}$. This crucial value is called the **relaxation angular frequency** [100], i.e the frequency at which the dielectric loss factor reaches a maximum. Intuitively, this can be explained as follows: when the impedance tends towards purely resistive behavior with decreasing frequency, its imaginary part is obviously small. When the impedance tends towards purely capacitive behavior, the modulus of the impedance becomes smaller with increasing frequency, and so does the imaginary part. The maximum of the imaginary part occurs at the transition between both behaviors, when the

---

[8]Hendrik Wade Bode started working for the Bell Laboratories in the 1920's. In 1938 he developed his Bode Plots in the context of his works on feedback control systems.

[9]Harry Nyquist worked at the American Telephone and Telegraph Company as well as at the Bell Laboratories, in the first half of the 20th century. Among other things, he worked on the stability of feedback amplifiers using Nyquist plots.
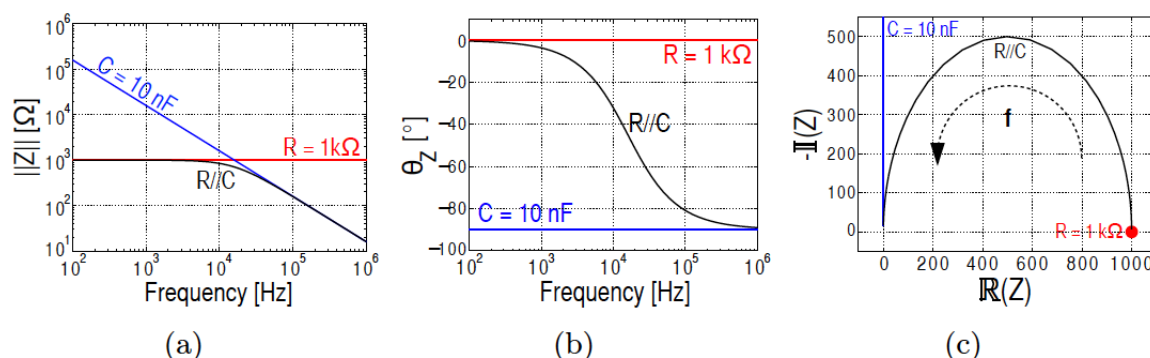
Figure 1.15: (a) (b) Bode plots, (c) Nyquist plot of a resistor, a capacitance and the parallel combination of both. [11]

frequency is "not small enough for the impedance to be purely resistive" yet "not quite high enough for the capacitance to tend towards a closed circuit".

We define $\tau = RC$ the time constant of the parallel RC circuit. It quantifies at what rate the capacitance is charged through the resistor and is thus an important indication for the timescale at which different processes are occurring.

From this example, we conclude that both graphs offer valuable information for understanding the spectral behavior of a measured sample. Although the spectral information provided by Bode plots is more consistent, Nyquist plots represent time constants better and are suitable for frequency-independent parameters (such as the charge transfer resistance in faradaic EIS). [11]

3.2 Equivalent circuit

3.2.1 The electrical double layer

When a metal is partly immersed in an electrolyte, a potential is set up across the two phases, i.e., at the electrode/electrolyte interface. The phases may be solids (metals or alloys, semiconductors, insulators), liquids (ionic liquids, molten salts, neutral solutions), or gases (polar or non polar). [101] The more common terminology in electro-chemistry is that an electrical Double Layer (EDL) is set up at the interface. The EDL refers to two parallel layers of charge surrounding the object.

In 1853 Hermann von Helmotz showed that an electrical double layer is essentially a molecular dielectric and stores charge electrostatically.[101] As can be seen in figure 1.16, this theory states that the surface charge is neutralized by opposite sign counter-ions, separated by the radius of the counter-ions (which are considered finite). The surface charge potential is linearly dissipated from the surface to the counter-ions. [102] Since rigid layers of opposite charges are considered, it does not consider important factors such as ion diffusion in solution, thermal motion or the possibility of adsorption onto the surface.

Louis Georges Gouy in 1910 and David Leonard Chapman in 1913 both observed that
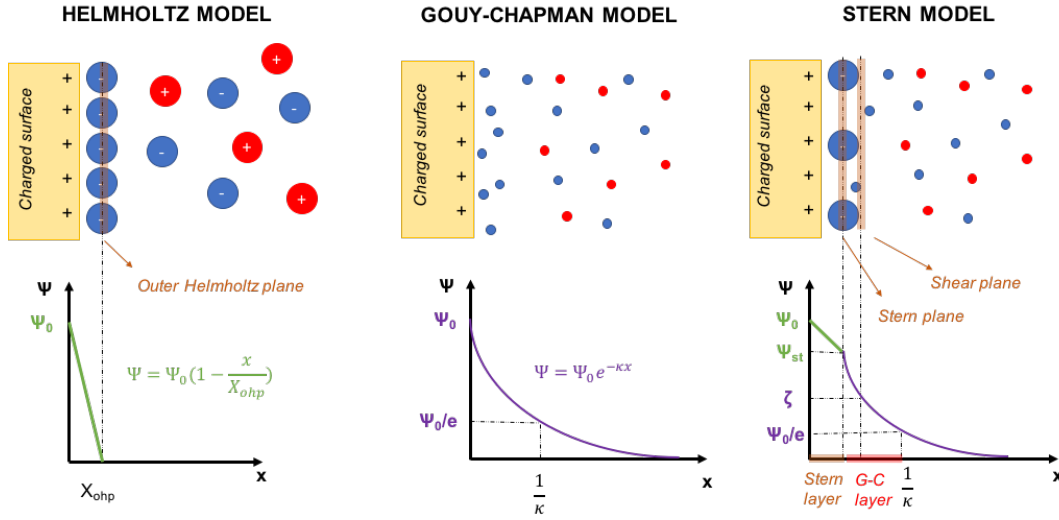
Figure 1.16: Helmholtz, Gouy-Chapman and Stern model of the EDL, with Ψ the local potential and κ^{-1} the Debye length.

capacitance was not a constant and that it depended on the applied potential and the ionic concentration. [103] According to Gouy and Chapman, ions in the EDL are subjected to electrical and thermal fields. This allows the Maxwell-Boltzmann statistics [10] to be applied to the charge distribution of ions as a function of distance away from the electrode surface. [102]

The Gouy-Chapman theory describes a rigid charged surface with a cloud of oppositely charged ions in the solution, which are considered as point charges. The concentration of the oppositely charged ions decreases with distance from the surface. This is the so-called diffuse double layer. The thickness of this layer is defined as the **Debye length** $\frac{1}{\kappa}$. It corresponds to the distance from the surface where the decreasing local potential has reached $\frac{1}{e}$ of its initial value.

$$\kappa^{-1} \cong \sqrt{\frac{\epsilon_{r,sol}\epsilon_0 U_t}{2FC_{ions} \cdot 10^3}} \tag{1.16}$$

With $\epsilon_{r,sol}$ the relative electrolyte permittivity, U_t the thermal voltage, F the Faraday constant, C_{ions} the ionic strength expressed in Molar concentration and κ^{-1} the Debye lenght. [11] The given expression of κ^{-1} holds only when local potentials are smaller than the thermal voltage U_t, because only in this case the Poisson-Boltzmann equation[11] can be linearized. [104]

This model neglects ion-ion interactions which become increasingly important at higher concentrations and it assumes a constant value of the dielectric constant in the region between the electrode and electrolyte. [101]

In 1924 Otto Stern suggested combining the Helmholtz model with the Gouy-Chapman

---

[10]the Maxwell-Boltzmann statistics describe the average distribution of non-interacting material particles over various energy states in thermal equilibrium

[11]The Poisson-Boltzmann equation describes the distribution of the electric potential in solution in the direction normal to a charged surface
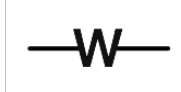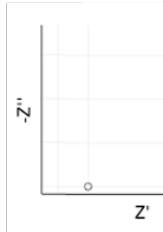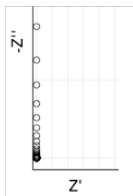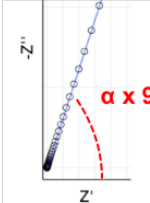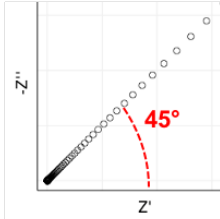
	Resistance	**Capacitance**	**Constant phase element**	**Warburg impedance**
Definition	$Z = R$	$Z = \dfrac{1}{j\,\omega\,C}$	$Z = \dfrac{1}{Q\,j\,\omega^\alpha}$	$Z = \dfrac{\sigma}{\sqrt{\omega}}(1-j)$
Phase angle	0°	90°	0-90°	45°
Symbol				
Nyquist Plot			α x 90°	45°

Figure 1.17: Definitions and phase shift of the impedance elements used to describe biosensor systems. [82, 108]

model. The stern layer is a first layer of ions of finite size, tightly adsorbed onto the surface, as suggested by Helmholtz. In the subsequent Gouy-Chapman layer, ions -now considered as point charges- diffusely spread out. There is a linear variation of local potential across the first layer and a semi-exponential variation in the Gouy-Chapman layer, until it reaches neutral equilibrium in the bulk electrolyte. At the boundary of the diffuse layer there's the slipping (shear) plane, where the potential is the electrokinetic potential or ζ-potential, as can be seen in figure 1.16.

In the 1960's and 1970's, refinement of Stern's model were published by among others Esin-Markov, Grahame-Devanathan and Bockhs-Devanathan-Muller. [105]

3.2.2 The Randles circuit as general models for EIS

For analysis purposes, it is useful to determine the equivalent electrical circuit(s)[12] corresponding to the EIS data.

To check the validity of the experimental data with respect conditions of impedance system (i.e the system should be linear, causal, stable and finite), the Kramers-Kronig transforms are used. [106, 107]

Indeed, if the system is LTI and stable, it is possible to use this transform to calculate the imaginary part of results given the change in the real part as a function of the frequency, and vice versa. Comparing the calculated imaginary parts with the experimental, thus validating the aforementioned conditions, is highly before trying to fit a model to the experimental data.

In figure 1.17, we summarize the four basic circuit elements that are commonly used to describe impedance behavior. The simplest and actually most common used equivalent

---

[12]Several distinct configuration may result in the same impedance. It should be considered that the equivalent circuit needs to make physical sense.

circuit is the **Randles model** [80], which is shown in figure 1.18.
Three main phenomena are embodied in this model: ohmic resistance of the solution, formation of the double layer and redox-related mass- and charge transfer.

First, R_s is the **ohmic resistance of the solution**. Since all the current flows through the resistance of the electrolyte solution, R_s is put in series.

Next, the total current in the electrode is either a contribution of the interfacial charging or of the charge transfer. Thus, both phenomena are in parallel.

The behavior of the double layer is mainly capacitive. However, it was observed that a pure capacitance does not fit the experimental data very well. This is mainly due to surface roughness and chemical inhomogeneities. [109] In order to represent the real phenomena better, the **Constant Phase Element (CPE)** was introduced. The CPE is a funky capacitor: its effective capacitance and 'real' resistance both increase as the frequency degrease. Since $Z = \frac{1}{Qj\omega^\alpha}$, its phase is constant and equal to $\alpha \cdot (-90°)$. Theoretically, α is between 0 and 1. However, in practice, it is observed that often $>$ 0.75 [108]. Note that Q has the units $[S \cdot s^n]$, which does not make real physical sense.

Redox reactions result in the charge-transfer resistance at the electrode-solution interface R_{ct} in the presence of a redox probe and the Warburg impedance W resulting form diffusion of ions from bulk electrolyte to the electrode surface. Mathematically, the **Warburg impedance (W)** is similar to a CPE with a 45° phase angle (α=0.5). We define $Z = \frac{\sigma}{\sqrt{\omega}}(1 - j)$. σ has the units $[\Omega\ s^{1/2}]$. It is related to Q through the following equation: $\sigma = \frac{1}{\sqrt{2}Q}$.
Intuitively, the physical meaning of σ can be explained by considering a soluble redox couple in a solution with a reversible electro-chemical reaction which is as follows:

$$\mathrm{O + n\ e^- \leftrightarrow R}$$

In that case, σ is related to the diffusion coefficients and concentrations of those species:

$$\sigma = \frac{RT}{n^2 F^2 A \sqrt{2}} \left(\frac{1}{D_O^{0.5} c_O^\infty} + \frac{1}{D_R^{0.5} c_R^\infty} \right)$$

with

- D_O and D_R the diffusion coefficients

- c_O^∞ and c_O^∞ the bulk concentrations for O- and R-species

- T the temperature [K], F Faraday's constant, A the surface, R the universal gas constant and n the number of transferred ions

A typical Nyquist plot for the Randles model is also given in figure 1.18. The offset of the semicircle to the right is due to R_s. At high frequencies, the impedance follows the semi-circular track which is typical for parallel RC-circuits as was already shown in figure 1.15. Since the double layer phenomenon does not behave like a perfect capacitance but
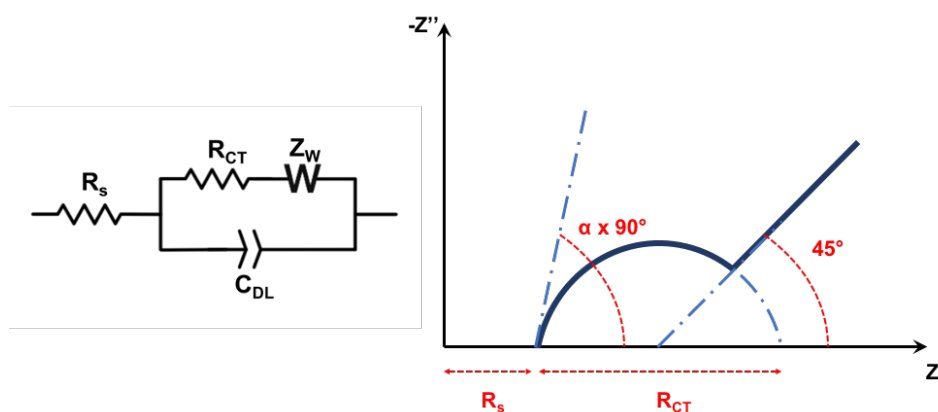
Figure 1.18: General Randles circuit and corresponding Nyquist plot. α is defined in figure 1.17

rather like a constant phase element, the semicircle is somehow "depressed": indeed, the asymptotic behavior at high frequencies is like a constant phase element. As is shown in figure 1.17, this means that the tangent line at the high-frequency extremity is not at 90° but at the angle corresponding to the phase of the CPE.

At low frequencies a straight line is observed. This corresponds to the Warburg impedance, which represents the mass transfer limited process due to delay in diffusion of ions from the electrolyte to the electrode surface.[82]

Note that R_s and W portray bulk properties of the electrolyte solution and the diffusion of redox probes respectively. These are unaffected by the presence of biomolecules on the electrode surface. On the other hand, R_{ct} and C_{dl} depend on the insulating and dielectric features of the biomolecules and are the main parameters used to analyze the response of a surface-sensing impedance biosensor. [97]

3.2.3 Faradaic and non-faradaic model

EIS biosensors can be categorized as either Faradaic or non-Faradaic, depending on whether there is a redox charge transfer at the electrode-solution interface or not.

Faradaic impedimetric sensors use EIS benefiting from electrochemical reactions between bi- ological species and the electrolyte medium, which are often amplified by redox probes, also called electroactive species. In this case, the electron transfer through faradaic electrodes is quantified through the charge transfer resistance Rct.

When no electron transfer occurs at solid-electrolyte interface, the electrodes are called non-faradaic and the sensing information is mainly contained in the dielectric properties of the system. This electrical impedance spectroscopy, also called electrochemical capacitance spectroscopy (ECS), thus involves no electrochemical reactions. [11] Non-Faradaic or capacitive biosensors do not require the addition of any redox probes and are inherently simpler and more amenable for point of care testing. Nonetheless, this methodology will detect any species binding onto the surface, without discriminating between specific and unspecific capture. Because of this, it is of extreme importance that the electrode surface is sufficiently functionalized. This can be guaranteed by performing carefully chosen **negative controls** in parallel.

The complete Randles circuit in figure 1.18 incorporates faradaic phenomena. Assuming that the electrodes have a perfect passivation layer or that they are made of perfectly inert metals, and that no charge transfer occurs in the absence of a redox probe, the equivalent circuit can be simplified to a **non-Faradaic circuit**.

In that case, the impedance response of the biosensor is purely capacitive: capacitive changes can be due to several factors such as variations in dielectric properties, changes in protein conformation originating from the formation of the antigen-antibody complex,... The resulting equivalent consists of the double layer CPE in series with the solution resistance.

In reality however, most electrode-solution interfaces in biosensors often have a combination of Faradaic and Non-Faradaic components. [82] Since the passivation layer is never perfect, charge leakage can occur between the electrode surface and the solution. This effect may reduce the dynamic range and sensitivity of the capacitive immunosensor. When this charge leakage is non-negligible, it might be preferable to add a "leakage resistance" in parallel with the double layer CPE. Obviously, this corresponds to the complete Randles circuit of figure 1.18 without the Warburg impedance.

Table 1.3: Performance comparison of EIS biosensors [11, 115]

Princ	Medium	Bacteria	Selectivity	Electrode type (*)	Electrode OOM	Freq range	LoD	Time
R_{ct} [110]	Milk	Listeria innocua	SAM EL	Gold SPE (3E)	3.6 mm^2	$10^{-1} - 10^5$	10^5	20min
R_{ct} [111]	PBS	Streptococcus pyogenes	Biotin Ab	Gold SPE (3E)	4 cm^2	$10^{-1} - 10^4$	10^4	30min
R_{ct} [112]	Milk	Brucella melitensis	Ab	AuNP SPCE	3 cm^2	$10^{-1} - 10^5$	$4 \cdot 10^5$	1.5h
R_{ct} [113]	PBS	Staphilococcus aureus	Ab	Gold (3E)	0.28 cm^2	$1 - 5 \cdot 10^4$	10^2	10min
C_{DL} [114]	PBS	Eschericia coli	Ab	Gold IDE (2E)	W=50um	$10^2 - 10^5$	$10^4 - 10^5$	40min
C_{DL} [115]	TSB	Staphilococcus epidermis	-	Gold IDE (2E)	W=20um	$10 - 10^5$	$8.5 \cdot 10^5$	10h
Z_{sol} [116]	DI water	Salmonella Typhimurium	Magn Ab	Gold IDE (2E)	W=15μm	$1 - 10^5$	10^6	30min
R_{sol} [117]	YPL	Eschericia coli	-	Gold IDE (2E)	W=15μm	$10 - 10^6$	10^4 (**)	14h
C_{sol} [11]	PBS	Staphilococcus epidermis	Lytic enzymes	Al/AlO_3 (2E)	W=10μm	$10^2 - 10^6$	$5 \cdot 10^6$	20min

(*) for 3E sensors, the working electrode material is given.

(**) before enrichment-process of 13h.

Freq [Hz], LoD [CFU/ml]

OOM = Order of Magnitude of electrode dimensions, **SAM**= Self-Assembled Monolayer, **EL**= endolysin, **Ab**= antibody, **Magn** = magnetic beads, **W**= finger width, **2E**= two electrode configuration, **3E** = three electrode configuration, **SPCE** = Screen printed carbon electrode

3.3 Interdigital electrodes

As can be seen in table 1.3, both 3-electrode configurations and 2-electrode configurations with IDE are common for impedimetric sensors. The former use the Faradaic approach and sense charge transfer R_{ct} at the electrode/solution interface, while the latter use the non-Faradaic approach. Even if three electrode systems reduce background effects and enable sensitive and reliable measurements, Interdigitated Electrodes (IDE) are interesting for impedance-based affinity sensors because of their inherent simplicity. Note that for 2-electrode measurements, the electrodes are either made from an inert metal (e.g gold) or covered with a passivation layer (e.g AlO_3).

Interdigitated Electrodes (IDE) have been studied by many authors since the early 1970s. [118] They are widely used in both integrated circuits and transducers.
They have the advantage of fast measurement process and compatibility for continuous operation. [119] Thanks to their design, they have a low Ohmic drop, a fast attainment of steady-state and an increased signal-to-noise ratio. [82]

The sensitivity of capacitance IDE sensors is directly dependent on the finger width and finger spacing. Reducing the finger spacing increases the sensitivity. However, decreasing the finger spacing increases the risk for short-circuits, which ruins the sensor. Thus, the minimum feasible finger spacing (and thus the sensor sensitivity) depends on the precision of the chosen fabrication technique. Other constraints may occur. For instance, in [120], 100 μm silver nanowires were used. Thus, the finger spacing had to be larger than 200 μm to avoid short-circuiting because of the nanowires.

Other designs have been investigated to exceed the aforementioned advantages of IDE. For example, the serpentine electrode structure (figure 1.19) shows a greater geometrical capacitance factor compared to the interdigitated capacitor, which improves the sensitivity of capacitive sensors.
In [121], both designs were tested for capacitive humidity sensing. For a total electrode area of 11.6 mm^2, the sensitivity was of (5.2 ± 0.2) fF/%RH for serpentine electrode capacitors, whereas for IDE the sensitivity was (4.2 ± 0.2) fF/%RH at 1 MHz.
However, this design has a major drawback: if one finger is interrupted in serpentine electrodes, it leads to sensor failure while interrupted fingers in IDE only result in lower sensor performance. [122]

4 Electrode deposition

For bulky and reliable production of a significant number of sensors, two broad fabrication categories can be distinguished: thick-film and thin-film technologies. [68]

In this work, we present Screen printed electrodes (SPE), which is the main thick film technology. In this technique, the application of the layer and the creation of the desired shape is done simultaneously.
For thin film technologies, it is common to separate these two steps. First, we introduce Physical Vapor Deposition (PVD) and Chemical Vapor Deposition (CVD) which are the
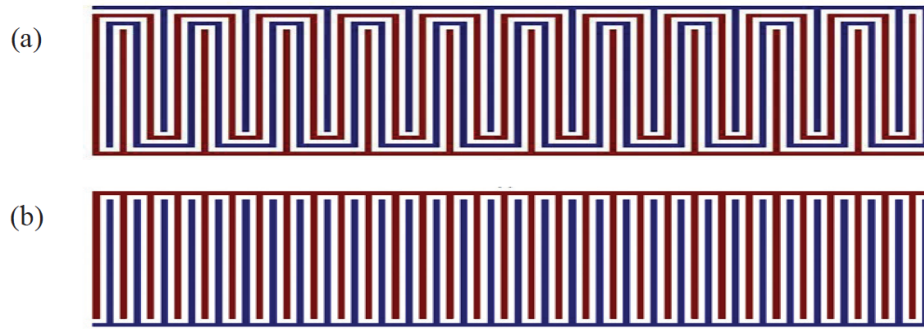
Figure 1.19: (a) serpentine electrode and (b) interdigitated electrode [121]

most common thin film deposition techniques. Then, we introduce litography, which is commonly used to obtain the desired shape out of the thin film.

4.1 Thin film deposition

In general, the fabrication methods for thin films (several nm to a few μm) can be divided in two categories: physical processes and chemical processes. [123]

Physical deposition process encompasses the techniques where the material is released from a source and deposited on substrate by means of electro-chemical, mechanical or thermodynamic processes.
Chemical processes involve specific chemical reactions. It may depend on the thermal effect as in thermal growth and vapor phase deposition but in all of these situations a definite chemical reaction is involved to get the thin film.

4.1.1 Physical Vapor Deposition (PVD)

Physical Vapor Deposition (PVD) covers different vaporisation coating techniques that involve the transfer of material at the atomic level under vacuum or very cautiously controlled environment. The process can be described according to the following sequence of steps: [124]

1. The material to be deposited is physically converted from solid phase to vapor by physical means (high-temperature vacuum or gaseous plasma)

2. The vapor is transported to a region of low pressure from its source to the substrate.

3. The vapor undergoes condensation on the substrate to form a thin film.

The process chambers are highly vacuum ($10^{-4} - 10^{-5}$ Pa) to deposit thin layers of ultra high purity materials ($> 99.999\%$ purity [125]) onto samples and substrates, because air molecules that are present during deposition will become impurities in the deposited films.
To determine the thickness of the deposited layer, a piezo-electric crystal sensor is installed into the vacuum chamber. Depending of the thickness of the deposited layer,
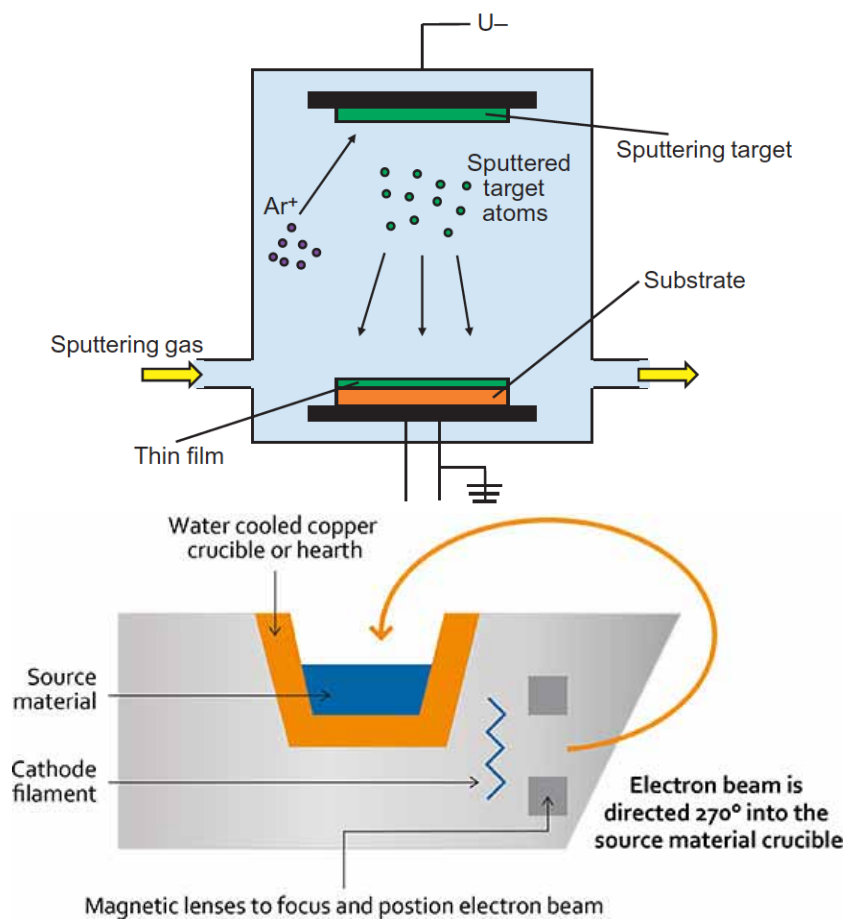
Figure 1.20: Schematic representation of sputtering (above) [124] and PVD through E-gun evaporation (below) [126]

the vibration frequency changes, enabling to calculate the layer thickness in real time. [127]

In general, PVD processes can be divided into two groups: evaporation and sputtering. Evaporation refers to thin films being deposited by thermal means, whereas in the sputtering mode the atoms or molecules are dislodged from the solid target through the impact of gaseous ions (plasma) [123].

In the **Thermal evaporation** process, an electrical current is used to heat a source material (through resistive heating) so that it melts and evaporates. The gas atoms travel to the vacuum and condense when they hit the substrate, forming a thin film. This technique is mostly used for metals [128] since they melt at low temperatures (eg. 660 °*C* for Al and 1064 °*C* for Au) and produce a steady deposition rate [129]. The source material is typically contained in a tungsten reservoir because it has the highest melting point (3422 °*C*) and is electrically conductive [125].

Electron Beam Evaporation is a process in which a source material is bombarded with an electron beam given off by a tungsten filament. The electron beam causes atoms from the source material to evaporate into the gaseous phase. These atoms then precipitate into solid form, coating everything in the vacuum chamber (within line of sight) with a thin layer of the anode material. [128]

As can be seen in figure 1.20, an E-beam evaporator has two main components: the electron gun which produces the beam of electrons and the crucible where the source material that we want to evaporate is contained. The crucible is water-cooled, which prevent the crucible material from melting and mixing with the source material. Contained within the electron gun is a filament (the source of the electrons) and magnets for focusing the electron beam and directing it towards the crucible.

The electron beam is generated by heating the metal filament to the point where it glows bright (2500°*C*). At this temperature, electrons are so energetic that some of them leave the surface of the filament. [125] They are then accelerated by a high voltage electrode and directed towards the crucible using a set of magnets. Adjusting the current allows to adjust the electrons energy in order to adapt is to the source material.

One of the advantages of E-beam evaporation is that different source materials can be rotated into the path of the beam, so that multiple materials can be deposited sequentially without opening the vacuum system. [129]

Sputtering is a deposition technology involving a vapor/gas plasma which is often an inert gas such as argon. As can be seen in figure 1.20, this ionised gas is confined in the same space as the desired deposition material or the evaporation target. The surface of the target negatively charged, causing positively charged argon high-energy ions from the plasma to be attracted and hit it. [125] Individual target atoms are knocked of and travel through the vacuum chamber in order to be deposited onto the substrate, where they form a thin-film. Sputtering is used extensively in the semiconductor industry to deposit thin films of various materials in integrated circuit processing. Because of the low substrate temperatures used, sputtering is an ideal method to deposit metals for thin-film transistors. [130, 131] An important advantage of sputtering is that even materials with very high melting points are easily sputtered while evaporation of these

materials in a thermal evaporator is complicated [127].

4.1.2 Chemical Vapor Deposition (CVD)

CVD involves chemical reaction of vapors near the substrate or on a substrate to form a thin film.

1. The coating materials are converted to gases, for example by heating.

2. Introduction of a control flow of mixed reactant gases into the reaction chamber.

3. Reaction of the reactant gases at the surface of the substrate, forming coating layer on the substrate.

4. Evacuation of the waste gases.

Physical structure and chemical composition of the thin films can be customized by controlling the deposition conditions.
A typical example is a metal being deposited from a metal chloride gas. [125] The metal is combined with chlorine to give a compound that can be maintained as a gas. At the same time, a controlled flow of hydrogen gas is introduced. The flow conditions are such that the reaction occurs when the gas flow comes into contact with the heated substrate surface. After reaction, a waste hydrogen chloride waste-gas is produced while the metal atoms remain bounded to the component.

$$MCl_2 + H_2 \longrightarrow M + 2HCl$$
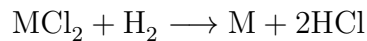
The reaction on the substrate needs a form of activation energy. A common way to do that is to heat the substrate to the desired reaction temperature (between 400 and 2200 °C [132]). This is the case in for instance **Low Pressure chemical vapor deposition (LPCVD)**. This technique is often used in MEMS production since it can deposit on both layers of at least 25 wafers at the same time [130] (see figure 1.21).

Plasma enhanced chemical vapor deposition (PECVD) is a variation on CVD, which is often used for the deposition of Silicon Dioxide (SiO_2) and Silicon Nitride (Si_3N_4). [133] In contrast to CVD, PECVD uses a plasma as the source of activation energy. That means that the deposition can occur at lower temperature (around 300 °C) and that substrates and samples that do not tolerate high temperatures, can be used. As can be seen in figure 1.21, a high voltage radio-frequency (RF) voltage is applied through an electrode at the top of the chamber. This provides the power needed to create the plasma from the mixture of gases. The energized atoms from the plasma are used to perform a chemical reaction on the substrate surface that deposits a thin film on to the substrate.

4.2 Lithography

Lithography is a type of patterning which is used frequency for devices, interconnections and structures. For example, metal interconnect structures on an integrated circuit are very complex and often use over 10 different layers of patterned metal. [125]
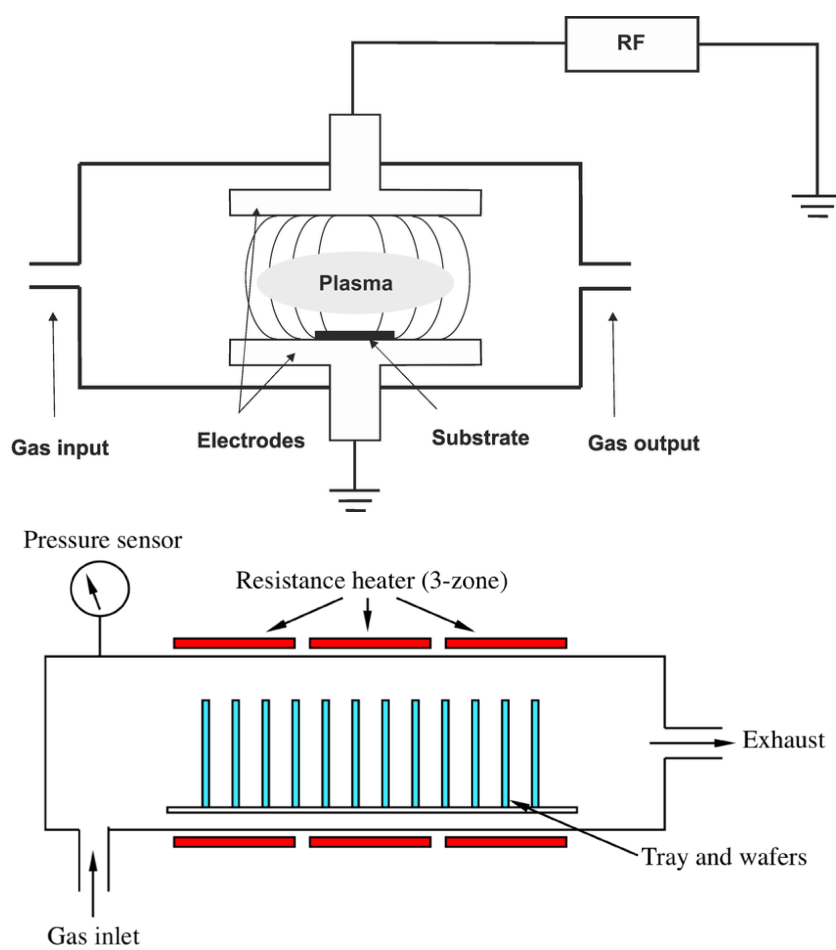
Figure 1.21: Schematic representation of a Plasma Enhanced CVD reactor chamber [133] and a Low Pressure CVD [134]
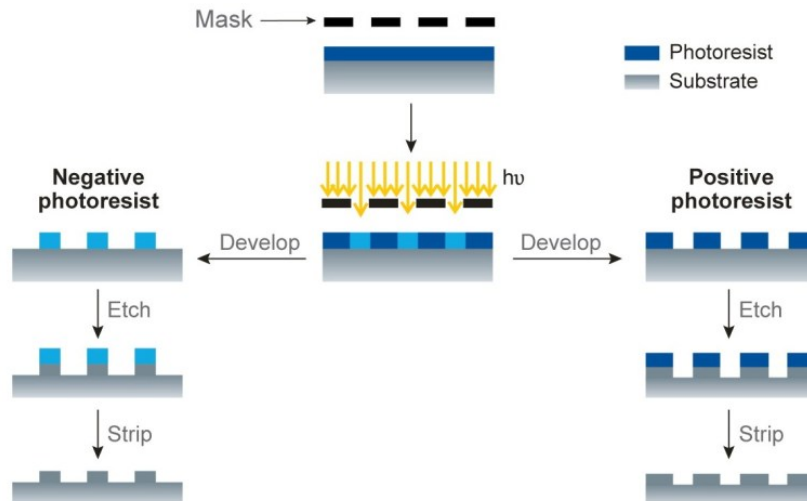
Figure 1.22: Schematic representation of the photolithography process [136]

There are two main types of lithography: photolithography and electron beam lithography.

Photolithography uses light to transfer a pattern to a substrate (e.g. a pattern to connect transistors in a silicon substrate).
The desired pattern is made in metal on a photomask, which is a transparent plate (often glass or quartz). Light can pass through the photomask, unless it is blocked by the metal film pattern. The pattern is transferred on the substrate due to a thin polymer film that is sensitive to light, the **photoresist**. This is applied on the substrate through spin coating: a few milliliters of the polymer are added on the substrate, which is then spinned at high speed, causing the polymer to spread evenly over the surface. The photoresist is fixed by heating.
When the mask and substrate are illuminated by UV-light, the parts of the photoresist that aren't shadowed by the mask undergo a chemical change.
These chemically altered parts of the photoresist are then dissolved in a chemical bath. The photoresist is often only a temporary layer, used to perform some other processing steps in order to make permanent pattern features. [135]

Electron beam lithography the sensitive layer is altered by electrons rather than by UV-light. An electron beam is used to sequentially write each feature in the pattern, in contrast of photolithography where all the pattern is illuminated in one time. Thus, no mask is needed for this technique.
The main advantage of EBL is that the electron beam can be focused very precisely, to spot sizes down to 5nm. [128]

4.3 Printing

Screen-printing

Screen printed electrodes (SPE) fabrication is generally based on the deposition of patterned coatings onto plane surfaces. The paste material is pressed through the screen,
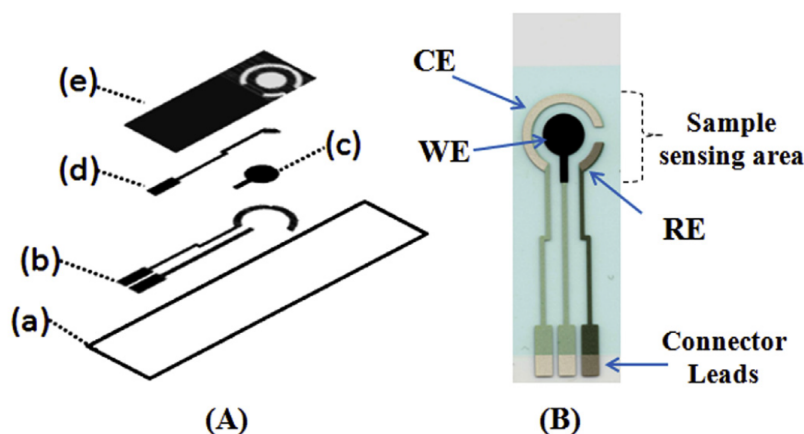
Figure 1.23: Typical screenprinted electrodes for voltammetry [138]. A) Scheme for screen printing of silver/carbon screen-printed electrode (S/C-SPE). (a) polyester substrate, (b) silver track, (c) carbon layer, (d) silver/silver chloride track and (e) insulating layer; B) Counter Electrode (CE), Working Electrode (WE) and Reference Electrode (RE)

forming the desired shape of the electrode. A typical screen-printed sensor, used for voltammetric biosensing (cfr section 2.4.4), is represented in figure 1.23.

The first layer of printing deposits conducting electrodes such as graphite paste. After thermal curing, a different material may be printed with the next layer: for example, the reference electrode can be made of silver-chloride paste. The layers are aligned using a high precision camera. A final passivation layer is applied to protect the sensor and define the area of the working electrode. Finally, the electrodes can be bio-functionalised.[137] Substrate surface pretreatment ensures printing quality.

The screen printing method is a widely used method to make electro-chemical sensors because it can conveniently pattern an electrode with various functional materials of different thicknesses and with over a wide variation of forms, by the applying appropriate designs on a screen. [139]

In [140], SPE are used for capacitive immunosensing for the detection of cardiac biomarker cardiac troponin I (cTnI): anti-cTnI antibodies are attachted to citrate capped gold nanoparticles deposited onto screen printed electrodes. In [141], a DNA-detection made by screenprinting showed the same sensitivity and specificity than standard DNA-chips produced by standard photolithography processes.

Inkjet printing

Inkjet printing recreates a digital image by propelling droplets of ink onto paper and plastic substrates. Most of the inkjet printing patterns as used by the industry are based on drop-on-demand (DOD) method. The most common methods are thermal and piezo-electric DOD inkjet printing. The idea is to force a droplet to fall through a nozzle, either by a thermal excitation or a piezo-electric pressure pulse on the fluid, as illustrated in figure 1.24.
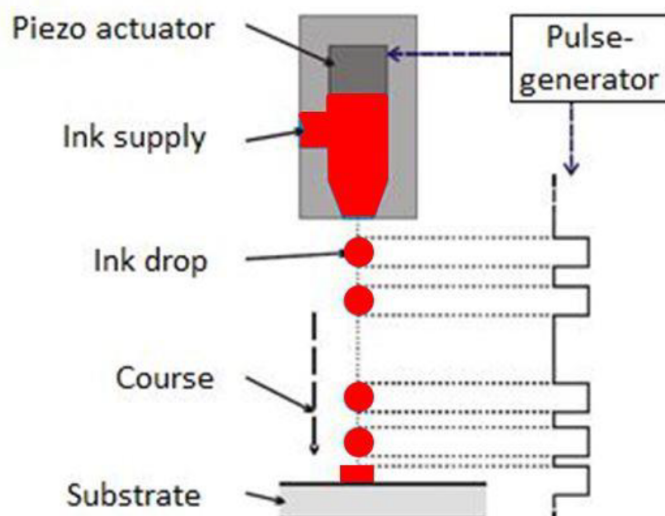
Figure 1.24: Schematic drawing of a piezo-electric "drop on demand" inkjet printing process [142]

This process demands optimum physical properties of the ink for good quality printing. The droplet generation in DOD printers is a complex process which is governed by viscosity, surface tension and density of the printing ink. These properties affect the drop formation process and the drop size at a given injection voltage.

Over the past few years, inkjet printing has gained a lot of interest for electrode printing on flexible substrates. With the development of conducting material's ink, semiconducting material's ink and dielectric material's ink, a complete sensor can now be fabricated by using printing-assisted deposition in extremely short-time scales just by selecting different ink cartridges. [143]

The reported materials for conducting inks are silver, copper, graphene, carbon nanotube (CNT) and conducting polymers.

Some investigations have been carried out for printing of sensors and other associated electronics in substrates like polymers [144], paper [85], metal foils [145], thin glasses [146] and textile fabrics [147].

An interesting example is found in [148], where inkprinted IDE with silver nanoparticle ink on a PET substrate, could detect 10^5 CFU/ml of E. Coli. To do this, an impedance measurement was made by applying a DC voltage sweep ($\pm 2.5V$).

4.4 Fabrication of paper-based electrodes

The matter of electrode deposition on paper goes beyond the scope of point-of-care sensors. Indeed, paper-based electronics are a subset of **flexible electronics**, which is a field that has gained attention in the areas of medicine, energy conversion and wireless sensing. In contrast to conventional electronics, flexible electronics have the advantages of being bendable, easy-to-shape, and lightweight.

Paper based electronics have salient characteristics including disposability, degradability,
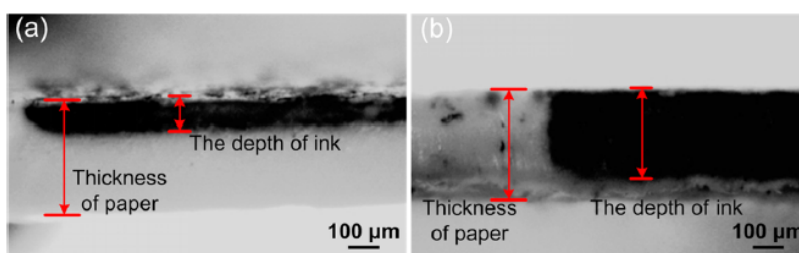
Figure 1.25: (a) Optical image of ink penetration on surface-treated paper. (b) Optical image of ink penetration on paper without any pretreatment. [85]

low cost and simple manufacturing. Environmentally-friendly, paper-based electronic devices may also address long-term issues with electronic waste disposal.[149] This is why research works have been carried out to explore paper as a substrate for flexible and printed electronics for a **wide range of applications**: from displays, energy harvesting and storage capability [150] to point-of care biosensors.

One of the main challenges to overcome is that traditional paper is a rough and absorptive substrate, which provides limitations for manufacturing electronic components on paper substrates.

There are many approaches to fabricate cellulose-based paper electronics. Among them, the most popular technique is printing. In this section, we will give examples of inkjet printed and screen-printed electrodes on paper. An extensive overview of all printing techniques is given in [84, 149].

Demonstrated **inkjet** printable ink solutions on paper include AgNP [149] and bio-ink containing DNA to tailor paper sensors for the detection of bacteria. [151] Inkjet printing has the advantage that no mask is needed and that it is applicable with modified office printers of extremely low cost and high availability. Moreover, ink is used in an economical manner. [7] However, it has an important drawback: **nozzle clogging**. This can be caused by dirt, unadapted operating temperatures, adsorption of polymers in the ink to the nozzle,... Nozzle clogging can damage the precision of the printing process, or the printing process as a whole.

In some cases, a pretreatment of the paper substrate is needed to solve the problem of high ink absorption due to the highly porous characteristics of the paper. This was done in [85] with a stannous chloride colloidal solution. The results are shown in figure 1.25

Screen-printing on paper devices has the advantage that it can print thick layers and that no heat treatment is needed. However, a mask is needed, which makes it less suitable for prototyping than inkjet printing. [153]

Dungchai et al. [152] first demonstrated simultaneous electrochemical detection of glucose, lactate, and uric acid on a $4cm \times 4cm$ patterned paper square, using three screen-printed electrodes as can be seen in figure 1.26. Carbon ink for the working and counter electrodes, and Ag/AgCl ink for the reference electrode and conductive pads. Microfluidic channels were made based on photolithography-based techniques.
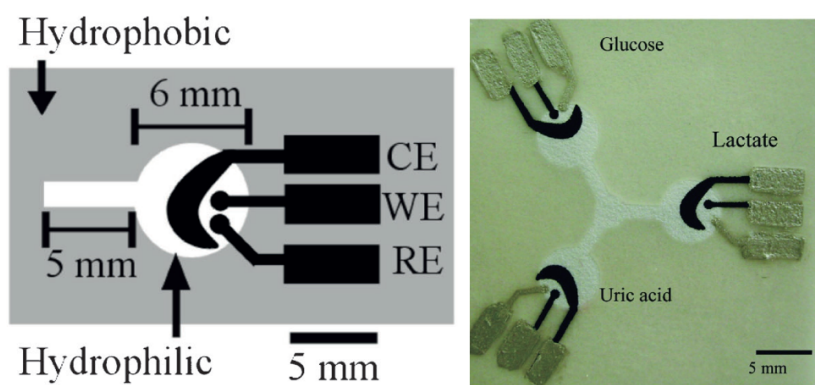
Figure 1.26: Screen-printed electrode layout on a paper-based microfluidic device for simultaneous electrochemical detection of glucose, lactate and uric acid. [152]

Table 1.4, gives an overview of several electrochemical paper-based sensors and their fabrication techniques. Note that, in contrast with table 1.3, these are mostly 3-electrode configurations for amperometric or voltammetric sensing.

Microfluidic fabrication consists in creating microfluidic channels in the paper substrate by patterning a hydrophobic design that fill the cellullose matrix where needed. As mentioned in section 2.5, wax printing is the most common technique. Alternatively, other methods such as wax dipping, photolithography and photolythography with polydimethylsiloxane (PDMS) have been reported. We won't detail the fabrication of microchannels here, but interesting overviews are found in [154, 155].

Several research teams used **laser processing** for patterning metallized paper. This is a powerful technique since it is capable of cutting or engraving complex geometric shape, pattern, and labels on thin worksheet rapidly an accuracy of < 0,1 mm.[149] Mazzeo et al. [162] presented a method for engraving touch pads on metallized paper directly through laser processing. Metallized paper is commercial paper that consists of insulated cellulose layer as the insulated substrate and conductive metal layer on the top of the substrate. Since the laser selectively removes the metal layer, the insulated barriers make it feasible to convert a whole piece of metallized paper into a capacitive sensor. Recent research developments utilize **graphite pencils** as an alternative source for fabrication of electrodes [155], for example on strain gauges. [163]

It is clear that scientific research in paper-based flexible electronics and paper-based electrochemical sensors are closely linked. Nevertheless, it should be noted that for electro-chemical paper-based sensing devices, there are other options than directly deposing electrodes on the paper substrate.

Carvalhal et al. [164] presented an electrochemical detection technique where paper is only used for microfluidic purposes and not as a support for electrodes (figure 1.27). Gold electrodes were fabricated on a polyester film. A narrow strip of chromatographic paper was pressed onto the gold electrode using a glass block. One end of the paper was immersed in the eluent. Capillary action drove the analyte through the paper, which was than analysed by the gold electrodes.

Electrode fabrication	Microfluidic fabrication	Ink	Electrode modification	Target analyte	LoD
Inkjet printing	PDMS casting	Gold	Gluc. oxidase	Glucose	0.1 mM [156]
	Inkjet-printed mineral oil	CNT	-	Dopamine	10 μM [157]
	Mineral oil casting	CNT	AgNP	Hydrogen peroxide	1 μM [158]
Screen-printing	Photo-lithography	Carbon	Sodium dodecyl sulfate	Dopamine	0.37 μM [159]
	Wax printing	Carbon	Graphene Chol. oxidase	Cholesterol	1 μM [160]
	Wax printing Multilayer pap.	Carbon	Gluc. oxidase PtNP	Glucose	9 μM [161]

Table 1.4: Summary of interesting previous works on screen-printed and inkjet printed paper-based electrochemical sensors (based on [89])
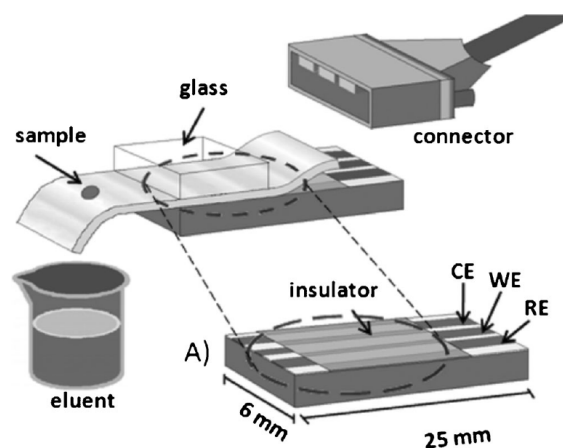
Figure 1.27: Experimental setup for separation and electrochemical detection on a paper-based microfluidic device. [165]

5   Participatory research

In chapter 6, we develop different usage perspectives scenarios for a point-of-care, paper-based pathogen sensor. Given their availability and low price, they offer a good opportunity for large-scale participation of citizens in scientific research.
In this state of the art section, we introduce the concept of citizen science, followed by two example projects that involved the monitoring of environmental quality parameters with citizen participation.

Citizen science is scientific research that is partly or completely conducted by amateur (or non-professional) scientists.[166]
Due to daily life observations, citizens have access to information that scientists do not have or that takes a long time to gather. On the other hand, science and research have great potential to improve the quality of life of citizens. From these two observations sprout the idea of citizen science: involving secular contributions to scientific research has the potential to creating a **win-win situation** in which more information is accessible for the research project and citizens learn by participation.
Participatory monitoring and offers 4 major advantages:

1. It allows for some research projects to be done more quickly, more rapidly and more accurately, given the wider data sampling. They also allow for bigger spatial and temporary scales.

2. It provides citizens with a sense of community and the ability to contribute to science

3. It offers an opportunity of increased learning and a window into the process of science

4. For society at large, it can build a closer connection between scientists and the public

Biodiversity research was one of the first fields to solicit volunteers in projects such as bird counting, from the early 1900's on. [167] For example, the Birdhouse Network (TBN) is a project involving the creation of nesting boxes and reporting on the behavior of cavity-nesting birds. In a very interesting report [168], researchers reported that such a project increases the participants' knowledge on bird biology. However, they were unable to detect a significant change in attitude towards science or the environment, or increases knowledge of scientific methodologies as such. As a result, the authors suggest that "Citizen-science projects that hope to increase understanding of the scientific process should be **framed in a way that makes participants particularly aware of the scientific process in which they are becoming involved**." Other research fields include environmental toxicology, nutrition, astronomy and medicine.
In the vast majority of projects, the citizen observations are added to a **database** (either automatically, semi-automatically or manually), and research teams then analyse these databases and draw conclusions. These are then usually also linked back to the participants.

A first concern arises: are all citizen science measurements equitably valuable to the common database? The answer is succinctly summarized in [169]: **not all citizen science observations are created equal**. This can be explained as follows: if I walk my dog in the park and I spot a bird that was already spotted before, this observation event has a smaller marginal value than if I strand on a desert island and discover the presence of this bird in this geographical zone for the first time. Of course, the exact marginal value of each spotting event is highly dependent on the research objectives. For example, an observation in a project that tends to count as much different species as possible can have a different marginal value than that same observation in a project that aims at counting the population density of some given species of which the presence is already confirmed.

A second concern lays in how citizens create information and transfer it to the scientists. There is a risk of accidental or even intentional bias.

These two concerns lead to two major interests in this work:

- Given the **variation in the marginal value of observations**, how can it be guaranteed that collected information and datapoints are at all useful for the research project?

- How can the **quality of information** gathered by the citizens by guaranteed?

We introduce two different projects that had distinct approaches of to deal with these focal points.

Lead concentration monitoring in drinking water (North-Carolina, USA)

In North-Carolina, a pilot project investigated the concentrations of lead (Pb) in the tap water of 86 childcare centres.[170] The project was a collaboration of the RTI Research Institute and the School of Public health. Due to the life-long impacts of Pb-exposure at young age and due to the fact that federal regulations only require Pb testing every three years, these institutions - all independent from the authorities- decided to perform a series of experiments on their own.

In addition to limited requirements for Pb testing of drinking water in childcare centers and schools, the authors estimate that there are critical gaps in the health-based standards for Pb in drinking water. These are presumably based on the technical feasibility of the majority of the public drinking water utilities rather than on the actual health requirements of young children.

In this project, the "citizens" had close interactions with the "experts" leading the project. Indeed, the scientists involved in the project actually visited the 103 participating childcare centers and gave **training** to the staff to take water samples according to a certain **sampling protocol**. This training was needed since the used sensing devices were rather expensive and complicated to use. While giving the technical training, the experts also took the opportunity to sensitize the day centre staff around lead in tap water.

Both a logistic regression analysis and a Bayesian network analysis were made, highlighting statistical correlations between the excessive presence of lead in water and other parameters such as the type of tap, the age of the building, the distance to the nearest water treatment centre, the water distributor, etc. After drinking water samples were analysed, laboratory results were provided to centres along with specific **recommendations for risk mitigation**.

In summary, the objectives of the project were triple:

1. Raise awareness of the existence of the problem of lead in drinking water, both among citizens and authorities

2. Getting insight in the occurrences of lead in drinking water and the causes of it. Make recommendations for better management of these causes.

3. having unambiguous data to to push for higher standards

The **pertinence** of the collected data was guaranteed by the scientific team who targeted day-care centres that were in areas that were proven at risk for excessive PB in drinking by previous research. The **quality** of the collected data was improved by training the citizens that effectuated the measurements and establishing a very clear and complete protocol.

Air quality monitoring in Aalst (Belgium)

Several German citizen science projects have been bundled under the name "Luftdaten". [171] They created an open-source platform "Sensor.Community" [172] and designed an automated sensor, which can be installed by citizens and sends its collected data directly to the platform without human intervention. This allows for a real-time monitoring overview for air quality in areas where the sensor is installed. An example of the user interface of this platform is given in figure 1.28 In Germany and Flanders, local initiatives sprout to install these sensors in their community.

In Aalst, a local citizen association "Over.Morgen" launched the project "Over.Meten", in order to install several of these sensors all over the city and thus obtaining a clear overview of the air quality per neighbourhood, in real time. [173]

The objectives of the project are double:

1. Raising citizens' awareness of air quality and, subsequently, encouraging citizens to rethink their mobility.

2. Collect reliable data in order to challenge the authorities if necessary.

Around 50 sensors are currently distributed to citizens in Aalst.[173] The sensor being ready-to-use and autonomous, **no training** is required for the participants: the sensor must be hung on the façade and is then completely autonomous in terms of measurement and data transmission. However, the price of the sensor (€40) does provide a threshold.

The participants fit mainly in two kinds of profiles: either middle to high class families with young children commuting to school through the city center every day and retired people. The motivation of participants is mainly **curiosity**: unless certain weather
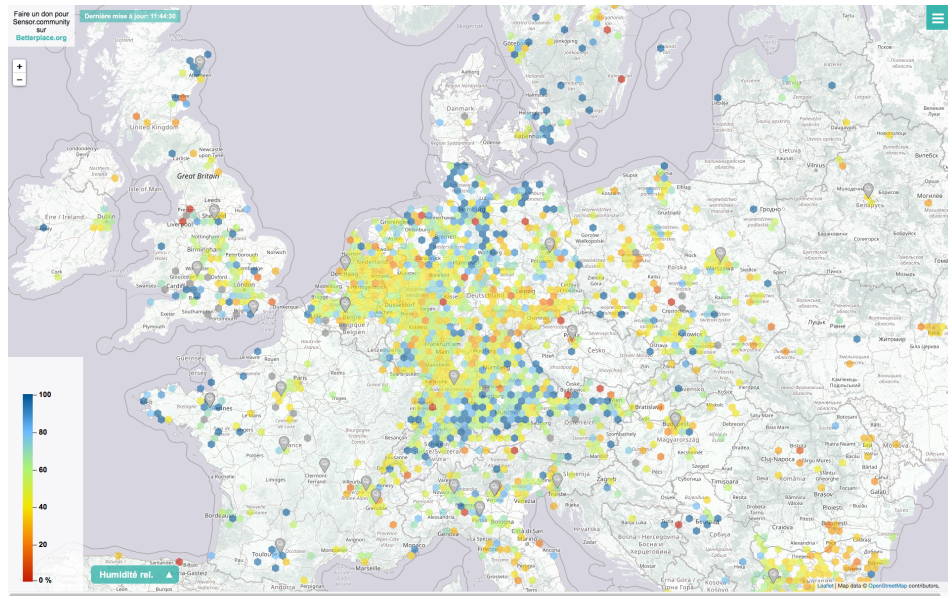
Figure 1.28: User Interface of the Sensor.Community platform [172]. Every coloured dot corresponds to the (average) value of sensor outcomes in that area.

conditions, the air quality is experienced as good on average, thus no real feeling of unsafety exists among citizens in Aalst.
However, measurements of particulate matter occasionally exceed the appropriate amount.

The **pertinence** of the collected data is managed by the citizens organisations themselves: they can either decide to concentrate the sensors in areas where excessive pollution is suspected, or to spread the sensors as evenly over the city as possible. The pertinence of the sample timing is independent of human intervention, since it is automated by the sensor. The **quality** of the collected data is improved by a complete automation of the process: no human intervention is required, thus no bias due to human handling can occur.

Despite the aformentionned precautions, it is difficult to find an unambiguous pattern in the occurrence of threshold exceedances. Three main reasons are acknowledged. First, a bias is observed when the weather conditions are very humid: the sensor is then troubled by suspended droplets in the air. Second, the concentrations of fine particulate matter themselves are very variable with weather conditions. Third, the causes for pollution are very diverse and show significant variations over time: local mobility, neighbouring industry, local combustion for heating, etc.

This has two main consequences on the initial objectives:

1. The interest of participants decreases over time. Although the limit values are exceeded in some conditions, these exceedances are rarely blatant. Therefore a degree of habituation to smaller exceedances grows among citizens, without the general sense of safety being severely affected.

2. The habituation to the slight exceedances and the complexity of causes for occasionally bad air quality, stall local politicians to make better air quality a top priority.

To address these consequences, a parallel project has been launched by Over.Meten: Telraam.[13] This involves the implementation of a traffic counting sensor launched by Mobiel21. Pedestrians, cyclists, cars and heavy vehicles are each counted individually when passing along the traffic count sensor. The resulting traffic data can be used to perform traffic engineering studies. A platform on which these data can be visualised in real time, is under construction.[14] This project monitors a more tangible and easier to tackle phenomenon at the local level: mobility. It is hoped that this project will also provide insights into the influence of mobility on air quality.

---

[13]https://www.tmleuven.be/en/project/telraam
[14]https://telraam.net

Chapter 2

Objectives

The PhD-project that led to this master thesis, aims at prototyping a low-impact, **paper-based bacterial sensor**. The interest for paper as a substrate is twofold. On the one hand, it is low-cost, recyclable and its production has less environmental impact than classical substrates [7]. On the other hand, paper has interesting microfluidic properties and offers the opportunity of biofunctionalisation. These two advantages are already being exploited in current Lateral Flow Assay (LFA) like pregnancy tests.

Current paper-based sensors mostly use optical transduction which require the use of labels (AuNP, fluorescent tags, quantum dots or signal amplification using enzymes) to achieve sensitive and selective detection of analyte. The disadvantages of these devices are twofold. First, there are issues associated with labeling which include additional costs, inherent multi-step nature of analyses and potentially non-specific signals. [82] Second, the resulting information output of these sensors is mostly qualitative or half-quantitative. [84]
We deduced in the state of the art that quantifiable measurements are easily performed by electro-chemical transduction. Furthermore,EIS can be used for real time and direct monitoring of affinity binding events without the use of labeling compounds. [174]

The goal of our project is to **combine the advantages of paper a paper-substrate** (recyclability, microfluidics, bio-functionalisation) **with the advantages of an impedance measurement** (quantifiable, sensitive measurements) [3], thus converging towards a **paper-based, label-free, impedimetric biosensor**.
Impedance based biosensors normally utilize the formation of a recognition complex between a bioreceptor (e.g. antibody) and its corresponding specific analyte (e.g. antigen) on the electrode surface. The bioreceptors are integrated in the functionalised electrodes, thus capturing the analyte near the electrode surface. This formation alters interfacial capacitance and charge transfer resistance at the electrode/electrolyte interface, which can than be sensed through EIS [82]
In order to fully utilise the characteristics of paper, we explore the possibility to functionalise the whole volume of the paper. This implies a divergence from the traditional impedance methods: instead of sensing the electrode surface, we are interested in **sensing the whole volume of the microfluidic channel**.

In this master thesis we focus on the electrical aspects of the sensing mechanism. As
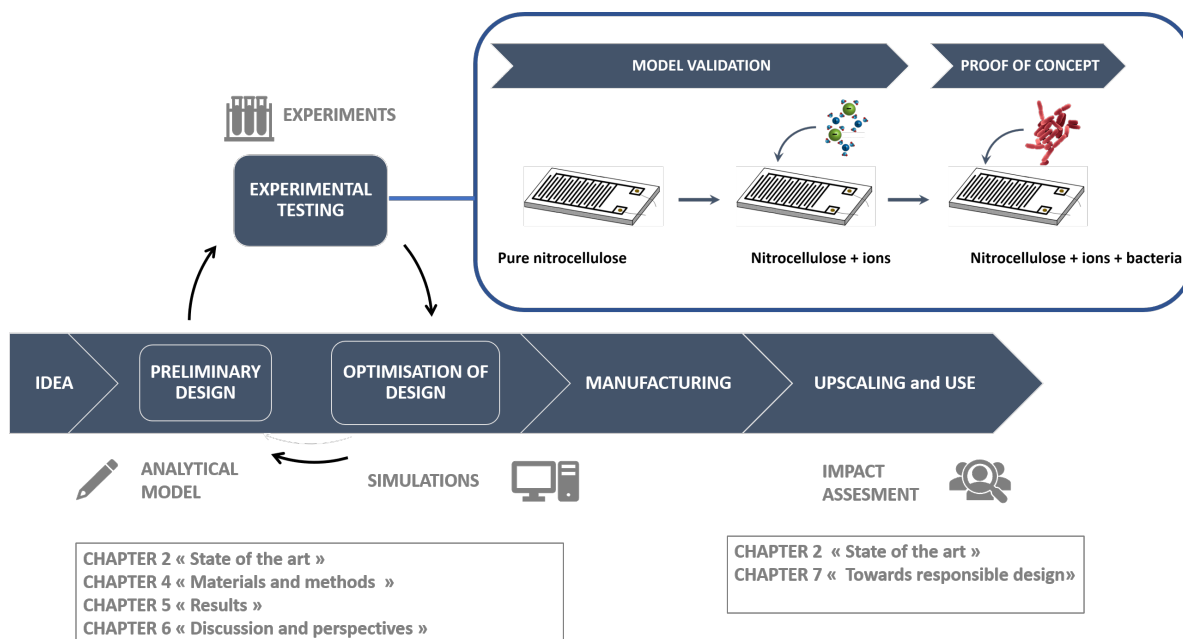
Figure 2.1: General process of development and contributions of this master thesis to the different intermediate steps.

illustrated in figure 2.1, our goal is to **go through the design cycle for the first time**: come up with a first design proposal, carry out rudimentary experimental tests in order to establish a proof of concept and propose a first set of corrections that should be applied to the design in order to improve it. The latter are supported by simulation results.

For the **preliminary design**, we impose a number of constraints:

1. The thickness of the used nitrocellulose paper is modelled on the thickness of commercialy available sheets. We fix the thickness of our samples at 140 μm since this kind of sheets is easily at our disposal.

2. Given the high capillarity and surface roughness of paper, and given that we do not prioritise extra treatment as was done in [152] (cfr figure 1.26), the order of magnitude of the fingerwidth is >100 μm.

3. The highest bacterial concentration that can be used for the proof of concept is 10^8 CFU/ml [175]. Indeed, in a liquid medium, this is a threshold at which the bacterial growth- and perish-rate, reaches its equilibrium.

4. Since the utilisation of labels makes the detection mechanism inherently more complex, we aim at label-free detection. Thus, in the first design round, no labels are used.

5. Given their widely proven advantages and given the favorable results of a research project that was carried out in our faculty until 2012 ([11]), we opt for an IDE design of electrodes.

Based on the preliminary design, an **analytical model** is developed, in order to better understand the main physical phenomena involved in the sensing process.

As schematised in figure 2.1, the objectives of the **experiments** are double. First, we want to validate the analytical model for impedance seen by IDE. Next, we want reach a proof of concept, i.e. sense the mere presence of bacteria without sensitivity constraints nor environmental perturbation. The model validation is done in two steps: a test in which we validate the model that incorporates purely capacitive behavior (i.e when the substrate seen by the IDE is only dry nitorcellulose) and a test in which we validate the model in which conductive phenomena are not neglected (e.g when the paper substrate has absorbed ionised water).
For the proof of concept, the goal is to detect the presence of a bacteria when they are applied in high concentration to the paper substrate. In this sensing process, biochemical interactions adapt both the sensitivity and the conductivity.
In parallel, **simulations** are made in order to validate the experimental results and explore optimisation possibilities through parameter analysis.

In "Chapter 4: Materials and Methods" the analytical model, experimental protocol and simulation environment are presented.
In "Chapter 5: Results" the results of the experiments are presented and compared to the outcomes from the analytical model and the simulations.
In "Chapter 6: discussion and perspectives", the 5 design constraints are challenged and several future research possibilities are presented.

As can be seen in figure 2.1, a chapter is also dedicated to a societal impact assessment. Indeed, given the responsible design context that frames this project, it is necessary to anticipate usage scenarios of our sensor. In what contexts can such a sensor be useful? How should the implementation be anticipated? We analyse two main utilisation scenarios, one in the Philippinean context and one in the Belgian context and create appropriate framings for data processing.

Chapter 3

Materials and methods

This chapter exhibits the main models used for the characterisation of our sensor and summarizes the experimental steps that were undertaken to verify this preliminary characterisation.

1. First, the general equivalent circuit of the sensor components is presented. The model for the electrical characteristics ϵ and σ of composite structures (such as the membranous nitrocellulose substrate) is exposed. The equivalent electrical circuit for bacteria is also given.

2. Then, we establish an analytical model that determines the value of the equivalent circuit components.

3. Finally, the conducted experiences are explained. The tools used to determine the empirical values of the equivalent circuit components are elaborated.

1 Equivalent circuit and intrinsic properties

1.1 Global equivalent circuit

Figure 3.1 represents a cross section of two fingers of Interdigitated Electrodes (IDE) and the equivalent circuit associated with it. In this section, we describe qualitatively what they consist of and whether or not they're of interest in the sensing mechanism.

R_{EL} is the **parasitic resistance** of the electrodes. Our electrodes are made of aluminium, a conducting material. Since no material is perfectly conductive, a little resistance resides in it. However, we consider that this resistance is small enough to be neglected in any situation.

L_{EL} is the **parasitic inductance** of the electrodes. It translates the tendency of an electrical conductor to oppose a change in the electric current. The flow of electric current creates a magnetic field around the conductor. From Faraday's law of induction we know that any change current induces a change in this magnetic field, which in turn induces an electromotive force in the conductors. According to Lenz's law, this induced voltage created by the changing current has the effect of opposing the change in current.
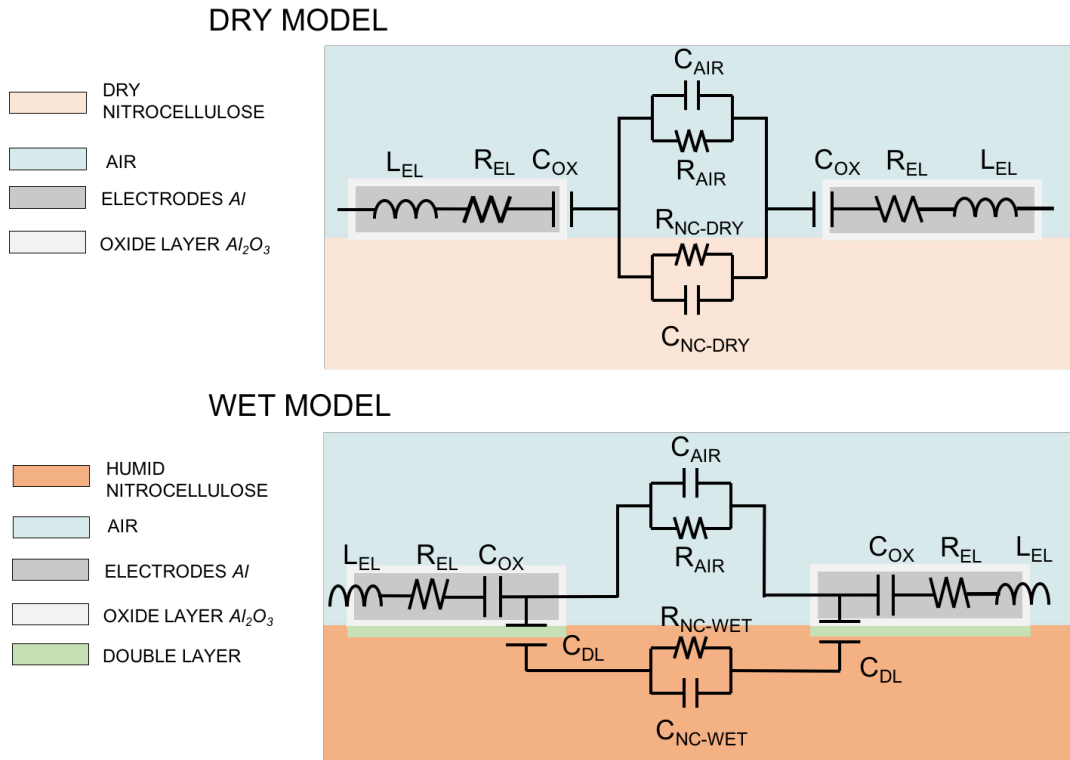
Figure 3.1: Equivalent circuit of the electromagnetic interactions between two IDE fingers

[176] The faster the current changes, the more the back EMF opposes the current and the less the effects of L_{EL} are negligible. According to the analytical model in section 2.1, L_{EL} has an order of magnitude of 10^{-8} H. Since $Z = \omega L$, we neglect the effect of L_{EL} when $\omega < 10^7$ Hz, but we take it into account when $\omega > 10^7$ Hz. In section 3.4.3, we will elaborate how to eliminate the parasitic inductive effects.

C_{OX} is the **capacitance of the insulating oxide layer** Al_2O_3 that has formed on the aluminium electrodes. This layer forms naturally when aluminium is exposed to oxigen in the ambient air. Its thickness can vary between 1 and 10 nm. [92, 177] This layer acts like a passivation layer, but it is not perfect. When the aluminium electrodes are brought into contact with water, the layer thickness may increase due to reaction between aluminum and water. This is even more true when a tension is applied to the electrodes, since this alters the redox potential. [178] In our model, we make the hypothesis that this capacitance is constant. It will be discussed whether or not this is coherent. Since this layer is very thin compared to other electrode dimensions, its capacitance is relatively big, making its impedance relatively small. However, since we do not entirely know the behaviour of the natural oxidation layer, this circuit element can be a source of divergence between the model and the actual experimental data. It is thus better not to neglect this element in the total equivalent circuit.

C_{DL} is the **double layer capacitance**, that was detailed section 3.2.1 of chapter 1. This layer forms only at the interface between electrodes and electrolytes, and is thus

absent when the nitrocellulose is dry. We consider that this double layer only exists at the lower half of the fingers when the nitrocellulose has absorbed a liquid. Thus, we neglect the interactions between a possible water film on the nitrocellulose surface and the side flanks of the electrodes. The value of C_{DL} increases when the ion concentration in the volume increases. In our experiments, we use solutions of which the ionic concentrations varies a lot. In order to stay coherent, we never neglect C_{DL}.

The presence and/or growth of bacteria can alter the presence of ions in their solution, and thus alter the value of the double layer capacitance. This makes C_{DL} a **relevant variable in terms of bacterial detection**. Note that, due to the non-Faradaic nature of the interface, the Warburg impedance and charge transfer resistance, which are elaborated in section 3.2.1 of Chapter 1, can be neglected.

C_{AIR} and R_{AIR} constitute the impedance seen by the IDE of the **upper air layer** above the electrode plane.

C_{NC} and R_{NC} constitute the impedance seen by the IDE of the **lower substrate layer** under the electrode plane. Since the target bacteria are present in the nitrocellulose which is the most significant part of the lower layer, these are also **important for bacterial detection**. Indeed, the presence of bacteria affects the global conductivity and permittivity of the nitrocellulose substrate. We thus require the total impedance to be **sensitive** towards changes in C_{NC} and R_{NC}.

This means that the effects of the latter have to be predominant on the effects of the upper layer impedance, in parallel to them. Even though not "perfectly optimised", we observe that air does a fairly good job. Indeed, its resistivity is very high and its capacitance is quite low: this makes it negligible when in parallel with a "low enough" resistance and a "high enough" capacitance. In practice, the air layer will be "visible" for the sensor when the nitrocellulose is dry (which means its properties are close to those of air) and negligible when the nitrocellulose is humid. For the sake of coherence and completeness, we never neglect C_{AIR} and R_{AIR}, even when their influence is small.

As exposed, R_{EL} and L_{EL} can be neglected when $f < 10^7\ Hz$. Thus, the equivalent circuit mainly boils down to a capacitive behavior at the electrode interface C_{int}, followed by a capacitive and resistive behavior in the volume around the electrodes C_{vol} and R_{vol}. The circuit in figure 3.1 can be simplified to the one represented in figure 3.2 where :

$$C_{int} = C_{OX} \qquad\qquad (dry\ model) \qquad\qquad (3.1)$$

$$= C_{OX} + C_{DL} \qquad\qquad (wet\ model) \qquad\qquad (3.2)$$

$$R_{vol} = (\frac{1}{R_{AIR}} + \frac{1}{R_{NC}})^{-1} \qquad\qquad\qquad (3.3)$$

$$C_{vol} = C_{AIR} + C_{NC} \qquad\qquad\qquad (3.4)$$
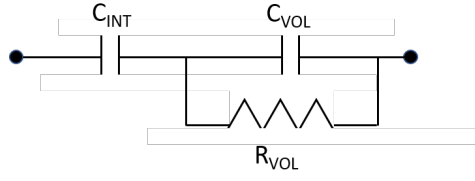
Figure 3.2: Simplified equivalent circuit of the model in Figure 3.1

From this simplified circuit, we can calculate the equivalent impedance Z and its cut-off frequencies.

$$Z = \frac{1}{j\omega C_{int}} + (j\omega C_{vol} + \frac{1}{R_{vol}})^{-1} \tag{3.5}$$

$$= \frac{j\omega C_{vol} R_{vol} + 1 + j\omega R_{vol} C_{int}}{j\omega C_{int}(j\omega C_{vol} R_{vol} + 1)} \tag{3.6}$$

$$= \frac{1 + j\omega R_{vol}(C_{int} + C_{vol})}{j\omega C_{int}(1 + j\omega C_{vol} R_{vol})} \tag{3.7}$$

It appears that the three cut-off frequencies are :

$$\omega_{c1} = \frac{1}{R_{vol}(C_{int} + C_{vol})} \qquad \omega_{c2} = \frac{1}{C_{int}} \qquad \omega_{c3} = \frac{1}{C_{vol} R_{vol}} \tag{3.8}$$
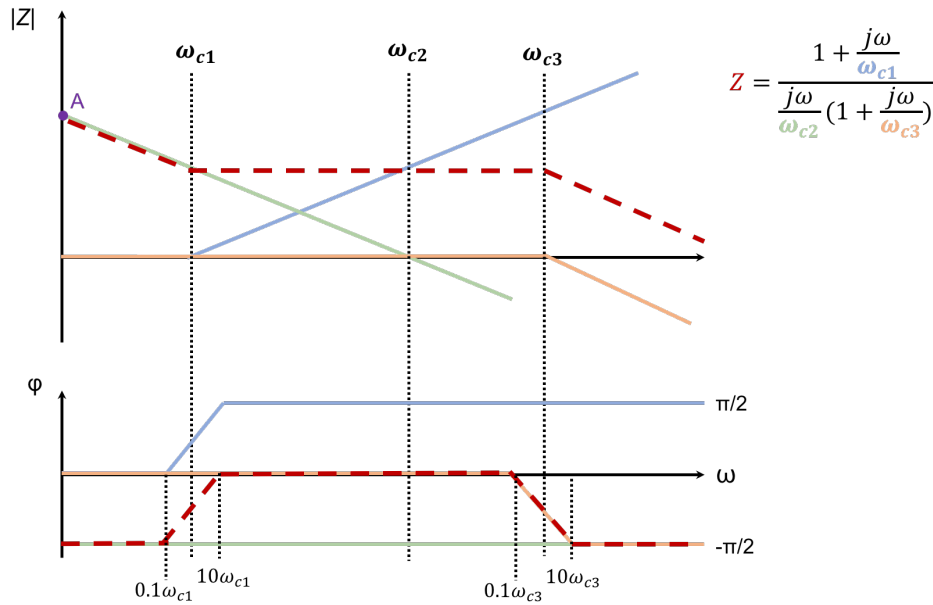
Figure 3.3: Qualitative representation of the Bode plot of simplified equivalent circuit, for the case when $\omega_1 < \omega_2 < \omega_3$

In figure 3.3 we represent in a qualitative way what the Bode plot of the total impedance looks like. Let's consider the case where $\omega_1 < \omega_2 < \omega_3$. This implies that $C_{int} > C_{vol}$, thus that $\omega_1 \approx \frac{1}{R_{vol} C_{vol}}$. We observe that ω_1 marks the transition between the frequency range in which C_{int} is predominant and the frequency range in which R_{vol} is predominant.

The transition between R_{vol} and C_{vol} dominance is given by ω_3. Note that ω_2 does not correspond to a significant transition in impedance behavior. Thus, the exact location has no influence on the phase of Z. However, since the slope always stays the same, the value of ω_2 has a direct influence on the position of the point A on the y-axis, and thus on the offset of the impedance module.

1.2   Electrical properties of composite media

In our model, two main types of composite media are of interest. Both are illustrated in figure 3.4. On the one hand, we have Nitro-Cellulose (NC), a membranous material consisting of interconnected fibers and interconnected pores. On the other hand, we have a composition of separate singularities (bacteria, bioreceptors,...) contrasting with their medium.

Membranous structure : nitrocellulose

Let's first analyse the case of the membranous structure, nitrocellulose. In the samples we use[1], the porosity is estimated to be 75%, which means that 25% of the volume consists of actual nitrocellulose fibers while 75% of the volume are pores. An important characteristic is that the pores are connected: the nitrocellulose sample is a composition of an interlinked fiber-network and an interlinked network of whatever fills the pores. Obviously, the porous structure that combines both substances has different properties than those substances in uniform, separate materials.

We consider two main situations: when the pores are filled with air and when the pores are filled with water.
When the **pores are filled with air**, both the fibers and the pore-content are insulating materials. Thus, we make the assumption that the bulk composition has a conductivity which is near zero. The permittivity of the bulk material is not easily modeled. One reason for this is that data from permittivity NC measurements always involve a membranous structure: it is hard to extract the permittivity of the fibers as such. Furthermore, the fibers are not homogeneously ordered. Thus, we carried out a measurement of the permittivity of dry nitrocellulose, as summarized in section 3.4.4 of this Chapter.
Since both materials form an interconnected network, since their volumic fraction are significant and of the same order of magnitude and since the relative permittivities of both materials are of the same order of magnitude, we approximate the bulk permittivity by the **linear volumic mean** of both values. Given that v is the volumic fraction of the pores, we consider that for dry NC, the permittivity is given by:

$$\epsilon_{dryNC} = v\epsilon_{air} + (1-v)\epsilon_{NC} \tag{3.9}$$

where ϵ_{dryNC} is the bulk permittivity of dry NC and ϵ_{NC} is the "artificial" permittivity of the pure NC fibers. Since we measured ϵ_{dryNC} and since v and ϵ_{air} are known, we can determine a conceptual value for ϵ_{NC} using equation 3.9.
When **pores are filled with liquid**, the same volumic mean principle is used for the permittivity:

$$\epsilon_{bulk} = v\epsilon_{sol} + (1-v)\epsilon_{NC} \tag{3.10}$$

---

[1]Reference: "CN140 unbacked Sartorius"

This time, the total bulk permittivity ϵ_{bulk} is calculated based on the real value of ϵ_{sol} and the articial value of ϵ_{NC} which was determined with the dry NC measurement. Note that this composite permittivity model is very simple and that much more accurate models can be found, for example in [179] and [180].

For the conductivity, the approach is different. Indeed, the different conductivities of the nitrocellulose fibers and the pore content do not have the same order of magnitude at all. NC is an almost perfect insulator ($\sigma \approx 10^{-12}$ S/m), DI water is a less perfect insulator ($\sigma \approx 10^{-6}$ S/m) and ionised water is conducting($\sigma \approx 10^{1}$ S/m). Since the liquid in the pores takes up to 75% of the volume of the bulk material, and since all the pores are interconnected, we assume that the "current path" created by the liquid is not too cluttered. Thus, we assume that the conductivity of bulk volume equals the conductivity of the liquid. Note that this simplification is only valid because of the big difference in order of magnitude of both components. A more complete model can be found in [181].
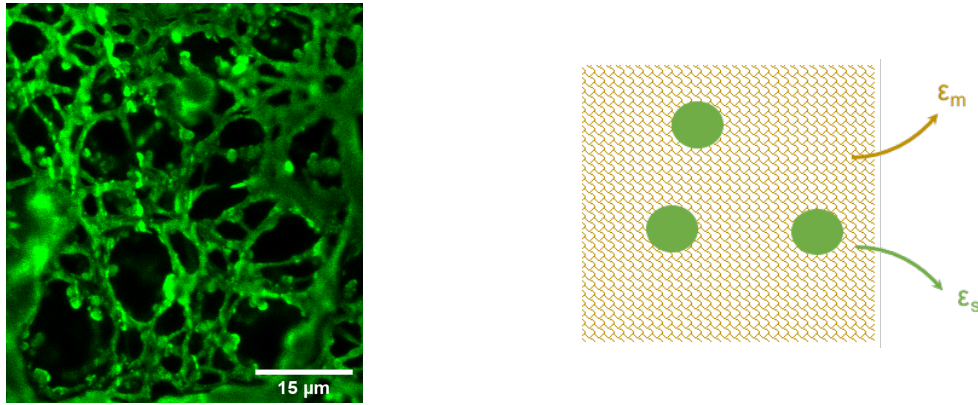
Figure 3.4: Representation of the two types of composite media that are considered. On the left: llustration of the porous structure of nitrocellulose. Confocal image of a CN140 nitrocellulose sample, bio-functionalised with fluorescent phage receptor binding proteins (RBP) [7]. On the right: simplified schema representing the composition of singularities (e.g. bacteria) in a medium of interconnected pores and fibers.

Individual periodical singularities

For **individual periodical singularities**, such as on the right side of figure 3.4, we cannot make the same assumptions. Indeed, since they are not interconnected, there is no "direct path" the current can flow through, as it was the case in the interconnected composite material. An increased conductivity of the singularities is only influential for current flows when they are interconnected. A simple analogy can be found in electrical circuits: when a high and low resistance are in series, the high resistance is predominant. On the other hand, if the singularities have a lower conductivity than their medium, current easily finds it way around them as long as their fractional volume is small enough. In our case, the singularities created by the bacteria are very small in size. Thus, we consider that they have no influence on the bulk conductivity.

For the permittivity, the lack of interconnection is no reason to neglect the singularities, even though they are small. Indeed, the dielectric properties are dominated by the interfacial polarization between the pores and matrices and between the bacteria and their medium. [180] However, since the volume fraction of bacteria is much smaller than the volume fraction of the medium, we cannot use the linear volumic mean approximation that was used for the porous structure. Instead, we apply a periodic singularity composite model, found in [182].

$$\epsilon_{bulk} = \epsilon_2 \frac{\epsilon_1 + 2\epsilon_2 + 2f(\epsilon_1 - \epsilon_2)}{\epsilon_1 + 2\epsilon_2 - f(\epsilon_1 - \epsilon_2)} \tag{3.11}$$

With f the volume fraction of the scattered material and ϵ_1 and ϵ_2 the respective permittivities.

Table 3.1 summarizes the four situations that were discussed.

Pores filled with:		
	Air	**Solution**
No bacteria	$\epsilon_{bulk} = 1.3$ $\sigma_{bulk} \approx 0$	ϵ_{bulk} : see Eq. 3.10 $\sigma_{bulk} = \sigma_{sol}$
Bacteria	ϵ_{bulk} : see Eq. 3.11 $\sigma_{bulk} \approx 0$	ϵ_{bulk} : see Eq. 3.11 $\sigma_{bulk} = \sigma_{sol}$

Table 3.1: Summary of the behavior of the bulk nitrocellulose, with or without presence of bacteria. The value of ϵ_{bulk} when nitrocellulose is filled with air and no bacteria are present, was obtained through measurement. Equation 3.10 corresponds to a volumic mean model while equation 3.11 corresponds to a periodic singularity model.

1.3   Electrical model of bacteria
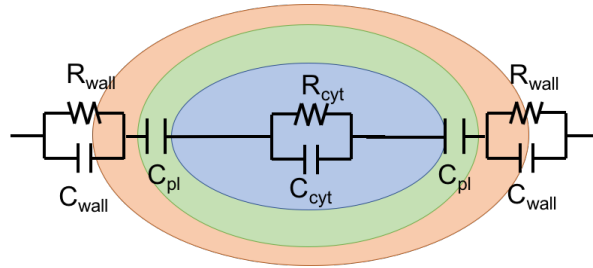
Figure 3.5: Equivalent circuit of a Gram-positive bacterial cell

Bacteria are typically composed of several outer shells, two for Gram-positive bacteria (Bacillus, Staphylococcus,...) and three for Gram-negative bacteria (Escherichia). In this work, we focus on Gram-positive bacteria since we work with Bacillus. A multishell representation, which accounts for the cytoplasm, plasma membrane and cell wall is given in figure 3.5. The electrical properties are summarised in table 3.2. Note that the bacterial cell-wall is ion-penetrable and has therefore a conductivity which is proportional

to the conductivity of the eletrolyte, i.e $\sigma_{wall} \approx 0.4 \cdot \sigma_{sol}$. [183]

The impedance of the bacterial cell is generally characterized by four cut-off frequencies, which are represented in figure 3.6. The first results from the series connection between C_{pl} and R_{wall}, while the second results from the parallel association between R_{wall} and C_{wall}. However, we observe that these cut-off frequencies have little impact on the impedance modulus, since the impact of the wall resistance is actually very small. In fact, in some models, this resistance is not considered at all. [75] We will thus simplify the equivalent circuit in figure 3.5 by grouping the effect of the cell wall and plasma membrane under one "outer capacitance term" C_{out} formed by the series association of C_{wall} and C_{pl}, thus $C_{out}^{-1}=(C_{pl}^{-1} + C_{wall}^{-1})$. To simplify matters, we introduce an equivalent "relative outer permittivity $\epsilon_{r,out}$:

$$\epsilon_{r,out} = (t_{pl} + t_{wall})(\frac{t_{wall}}{\epsilon_{r,wall}} + \frac{t_{pl}}{\epsilon_{r,pl}}) \tag{3.12}$$

Analogically to the development for the circuit in Figure 3.2, we then obtain a simplified expression for the two last cut-off frequencies:

$$f_{cb1} = \frac{1}{2\pi R_{cyt}(C_{out}/2 + C_{cyt})} \approx \frac{1}{2\pi R_{cyt}(C_{out}/2)} \approx \frac{(t_{pl} + t_{wall})\sigma_{cyt}}{\pi d_{cyt}\epsilon_0\epsilon_{r,out}} \tag{3.13}$$

$$f_{cb2} = \frac{1}{2\pi R_{cyt}C_{cyt}} \approx \frac{\sigma_{cyt}}{2\pi\epsilon_0\epsilon_{r,cyt}} \tag{3.14}$$

with d_{cyt} the cytoplasm diameter and the different t, ϵ, σ defined in table 3.2. Note that the thickness of the cell wall and plasma membrane is very small (nm) compared to the diameter of the cytoplasm (μm), which is why C_{cyt} is negligible next to C_{out} in the expression of the f_{cb1}.

At relatively low frequencies, ($f < f_{cb1}$), the bacterial cell behaves as a large capacitance formed by the cell wall and plasma membrane. At larger frequencies, ($f > f_{cb1}$), the cytoplasm dominates: first in a resistive way, then in a capacitive way.

To understand the behavior of bacterial cells in a solution, the cut-off frequencies of the bacterial cells must be compared to the cut-off frequencies of the electrolyte-IDE system, expressed in equation 3.8.
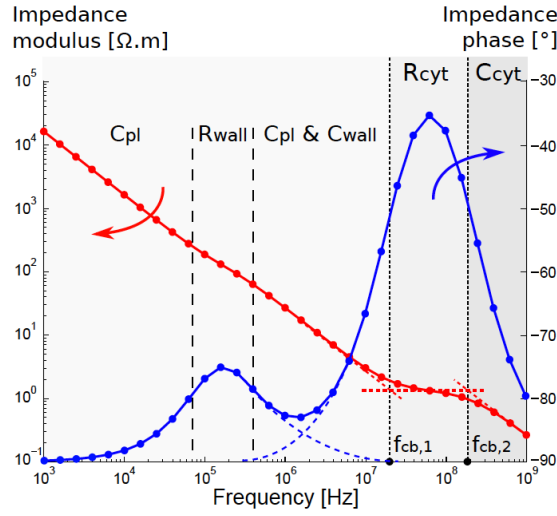
Figure 3.6: Analytical expression of the Staphylococcus bacterial cell impedance modulus and phase versus the applied frequency. [11]

When bacteria are emerged in an electrolyte, a double layer forms around them. For one whole bacterial cell, the double layer capacitance is estimated to be $\approx 70pF$. [184] However, junctions between double layers, atop the electrodes and around the bacterial cell when the bacterial cell is close to the electrodes, cannot easily be modelled analytically. [183]

2 Analytical model of the equivalent circuit

In this section, the formula which are used in the analytical model to calculate the different components of the equivalent circuit, are presented. First, we analyse the electrical behavior of the electrodes and their interface, which is fairly straightforward. Then, we introduce the expressions for the impedance sensed by the IDE in the bulk volume above and underneath the electrode plane. To achieve this, a conformal mapping method is used, which maps the coplanar IDE onto parallel plate electrodes.
The values for the different parameters used in the formula, are summarized in table 3.2.

2.1 Electrode and interfacial properties: L_{EL}, R_{EL}, C_{ox} and C_{DL}

As already explained in section 1.1, we neglect the intrinsic resistance of the electrodes since they are made of aluminium, which is a good conductor. Thus, $R_{EL} = 0$

For L_{EL} we use the general expression for the inductance in a straight wire [197], which is given by:

$$L_{EL} = 2l[2.303ln(\frac{4l}{d}) - 1 + \mu/4 + \frac{d}{2l}]$$

with μ the relative permeability of the wire material, l the cable length and d the wire diameter. In the case of our sensors, L_{el} has the order of magnitude of 10 nH.

Table 3.2: Physical parameters used for the equivalent electrical model

	Symbol	Description	Value	Units	Ref.
Surroundings					
Air	ϵ_{air}	Air rel. perm.	1	-	
	σ_{air}	Air conductivity	e-14	S/m	[185]
FR-4	ϵ_{FR4}	FR-4 rel. perm.	4.4	-	[186]
	σ_{FR4}	FR-4 conductivity	e-12	S/m	[186]
Dry nitrocellulose	ϵ_{NC}	NC rel. perm.	1.3	-	
	σ_{NC}	NC conductivity	e-11	S/m	[187]
	t_{NC}	NC thickness	140	μm	
Solutions					
DI water	ϵ_{DI}	DI rel. perm.	85	-	[188]
	σ_{DI}	DI conductivity	6.6 e-6	S/m	[189]
	λ_D	Debye Length	99	nm	
NaCl 0.5M	ϵ_{05M}	0.5M NaCl rel. perm.	75	-	[188]
	σ_{05M}	0.5M NaCl conductivity	3	S/m	[190]
	λ_D	Debye Length	0.41	nm	
NaCl 1M	ϵ_{1M}	1M NaCl rel. perm.	68	-	[188]
	σ_{1M}	1M NaCl conductivity	3.5	S/m	[190]
	λ_D	Debye Length	0.28	nm	
PBS	ϵ_{PBS}	PBS rel. perm.	80	-	[191]
	σ_{PBS}	PBS conductivity	1.6	S/m	[191]
	λ_D	Debye Length	0.7	nm	[192]
Electrodes					
	t_{el}	electrode thickness	1	μm	
	t_{ox}	oxidation layer Al_2O_3	5	nm	[193]
	ϵ_{ox}	rel. permittivity Al_2O_3	9.1	-	[194]
Type 1	W_1, G_1	finger & gap width	500	μm	
	L_1	finger length	1.2	cm	
	N_1	number of fingers	10	-	
Type 2	W_2, G_2	finger & gap width	200	μm	
	L_2	finger length	1	cm	
	N_2	number of fingers	20	-	
Bacteria					
	V_{bact}	bacterial volume	0.7	μm^3	[195]
	ϵ_{cyt}	cytoplasm rel. perm.	70	-	[11]
	σ_{cyt}	cytoplasm conductivity	0.8	S/m	[11]
	ϵ_{pl}	plasma rel. perm.	16	-	[11]
	t_{pl}	plasma thickness	8	nm	[183]
	ϵ_{wall}	cell wall rel. perm.	60	-	[11]
	t_{wall}	cell wall thickness	20	nm	[183]
	ρ_{max}	maximum concentration	10^8	CFU/ml	[175]

rel. perm. = relative permittivity

ϵ_{NC} was measured in March 2020 in Welcome, UCLouvain (cfr section 3.4.4)

We consider that the permittivity and conductivity of materials is constant between 1Hz and 30MHz [196].

The capacitance of the insulating layer and double layer, C_{OX} and C_{INS} are given by [11]

$$C_{OX} \approx \frac{\epsilon_0 \epsilon_{r,ox}}{t_{ox}} \cdot (N-1)A_e \tag{3.15}$$

$$C_{DL} \approx \frac{\epsilon_0 \epsilon_{r,sol}}{\lambda_D} \cdot (N-1)A_e \tag{3.16}$$

with $\lambda = \kappa^{-1}$ the Debye lenght defined in formula 1.16, A_e the surface of an electrode finger, N the number of electrodes.

For NaCl solutions, we determine the Debye length by using a simplification of equation 1.16 which is only valid for monovalent electrolytes:

$$\lambda = \sqrt{\frac{\epsilon k T}{e^2 N_a 2C}} \tag{3.17}$$

with e the electron charge, C the ionic concentration $[mol/m^3]$, N_a the Avogadro constant and $\epsilon = \epsilon_r \epsilon_0$ the permittivity. For the Debeye length of a PBS solution, we take an empirical value obtained in [198]. The resultant values for λ are summarized in table 3.2.

2.2 Volumic impedance of the IDE: C_{AIR}, R_{AIR}, C_{NC} and R_{NC}

2.2.1 Basic concepts and definitions

For electrical applications, a material has 2 fundamental properties: its conductivity σ and its permittivity ϵ.

Electrical conductivity σ $\left[\frac{S}{m}\right]$ quantifies a material's capacity to conduct electrical current. Its inverse, resistivity ρ $[\Omega.m]$, expresses a material's ability to resist electric current.

The **absolute permittivity** ϵ $\left[\frac{F}{m}\right]$ expresses the ability of a material to polarize in response to an applied electric field. The higher the permittivity, the more the material polarizes, the more energy is stored. The permittivity of a material is often expressed in terms of its **relative permittivity** ϵ_r $[-]$, which is the ratio between its absolute permittivity ϵ and the vacuum permittivity $\epsilon_0 \approx 8.85419 \cdot 10^{-12}[\frac{F}{m}]$.

$$\epsilon_r = \frac{\epsilon}{\epsilon_0}$$

A **dielectric material** polarizes when an electric field is applied but has a high resistivity. Inversely, a **conducting material** has a low resistivity but barely polarizes in response to an applied electric field.

The conductivity and permittivity of a medium depend, among other things, on its temperature and on the applied voltage (i.e its frequency, direction and magnitude).

Let's consider a homogeneous[2] and isotropic[3] material, placed between two planar electrodes (see figure 3.7). The electric properties of this medium can be expressed in

---

[2] A homogeneous material has the same properties at every point.

[3] An isotropic material has the same properties in every direction.

terms of a resistor R and a capacitor C in parallel, forming the equivalent circuit. [176] The values of R and C are calculated as follows:
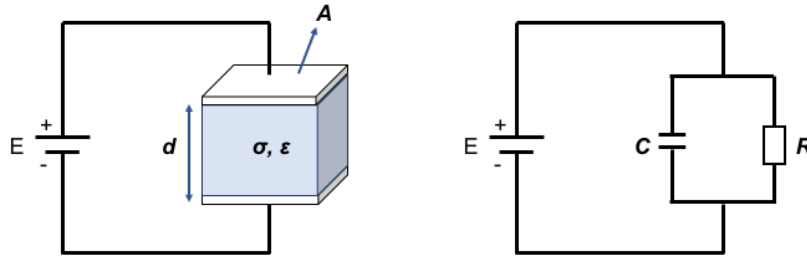
Figure 3.7: Dielectric medium between two parallel plates and its equivalent circuit.

$$R = \frac{d}{A\sigma} \quad [\Omega] \tag{3.18}$$

$$C = A\frac{\epsilon_0\epsilon_r}{d} \quad [F] \tag{3.19}$$

with:

- A $[m^2]$ the surface of the parallel electrodes

- d $[m]$ the distance between the two plates

- ϵ_0 $[\frac{F}{m}]$ the vacuum permittivity and ϵ_r $[-]$ the relative permittivity of the medium

- σ $[\frac{S}{m}]$ the conductivity of the medium

Interdigitated Electrodes (IDE) are two interlocking comb-shaped arrays of metallic electrodes, as presented in figure 3.9. As can be seen in figure 3.8, coplanar electrodes have different interaction field lines than parallel plate electrodes. Due to this, the parallel-plate formula for capacitance and resistance between the electrodes (eq. 3.18 and 3.19) are no longer valid.

Figure 3.8: Parallel plate electrodes and coplanar electrodes

In the next sections, different **geometrical parameters** will be of use:

- G, the gap width
- W, the finger width
- L, the finger length[4]
- N, the number of fingers

- $\lambda = 2(W+G)$, the spatial wavelength
- τ, the thickness of the electrodes
- $\eta = \frac{W}{W+G}$, the metalisation ratio

Unless explicitly stated otherwise, the following **hypotheses** are always applicable in this paper:

1. $L >> \lambda$: so the length of the sensor can be considered infinite from the point of view of the cutting plane on figure 3.10.

2. $W >> \tau$: the thickness of the electrodes can be neglected. Thus, the electric potential of the electrodes is specified at the interface between the upper and lower half planes.

3. By symmetry, the perpendicular planes halfway between the electrodes are **equipotential planes** with a voltage value equal to the average of the values of the opposing electrodes. This is exact for an infinite periodic structure which fingers have infinite length. In a finite structure, the equipotential walls tend to bend closer to the outer electrodes. However, we assume that most of the polarization occurs in the region where the bending of the ground plane is not significant.
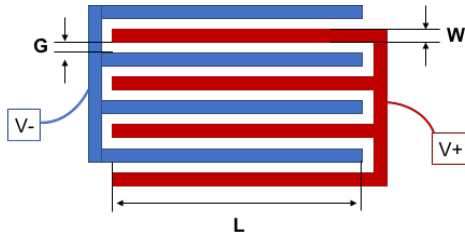
Figure 3.9: Electrode plane
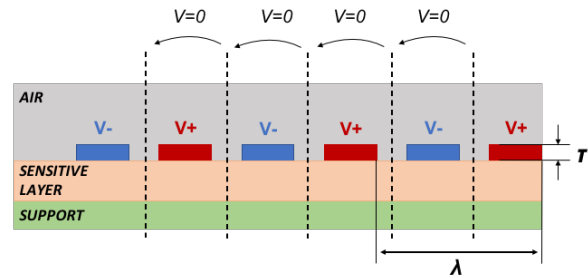
Figure 3.10: Cross-section of an IDE structure with equipotential planes

In the rest of this section, we will invoke the **upper- and lower semi-infinite half plane** several times. This refers to figure 3.8, since we think in terms of cross-section to ease visualisation. Of course, since we suppose that the electrode length is much larger than the electrode width, what is valid for the upper and lower half-plane is also considered to be valid for the upper and lower volume.

2.2.2 Analytical expression of the capacitance of IDE

Linear approximation of an IDE capacitance

The order of magnitude of the IDE capacitance can be roughly estimated by considering the coplanar electrode interactions as parallel plate interactions. This comes down to

---

[4]As can be seen on figure 3.9, the part of the finger that's not flanked by neighbouring fingers, is neglected.

adapting equation 3.19 to take the number of fingers into account. [199] Since the capacitance of the upper and lower half-plane (respectively seen by the green and orange field lines in figure 3.8) are in parallel, both capacitance values are added.

$$C = \epsilon_0(\epsilon_{r,uh} + \epsilon_{r,lh})\frac{W \cdot L}{G}(\frac{N}{2} - 1) \tag{3.20}$$

with $\epsilon_{r,uh}$ and $\epsilon_{r,lh}$ the permittivity of the upper and lower half plane respectively. W, L, G, N are the finger width, finger length, gap width and number of fingers as defined in section 2.2.1. Obviously, this model over-estimates the interception of field lines. It was used in [199] for approximative values but did not prove accurate enough in our case. A more precise model, using conformal mapping between parallel plate electrodes and interdigital electrodes, is elaborated in the following section.

Capacitance model of IDE using conformal mapping

In order to better represent interactions between electrode fingers, two different types of "sub-capacitances" should be distinguished when we analyse the equivalent circuit of the interdigitated capacitances (as represented in figure 3.11).

- C_I, half the capacitance of one interior electrode relative to the potential of the equipotential planes

- C_E, the capacitance of one outer electrode relative to the potential of the equipotential planes
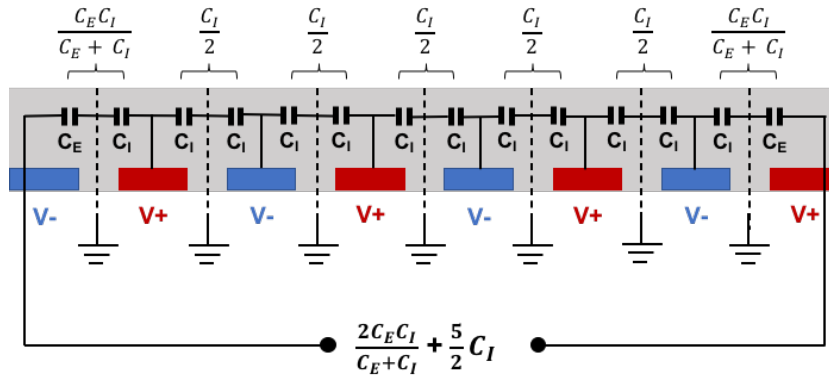
Figure 3.11: Equivalent circuit for evaluation of the semi-infinite top layer
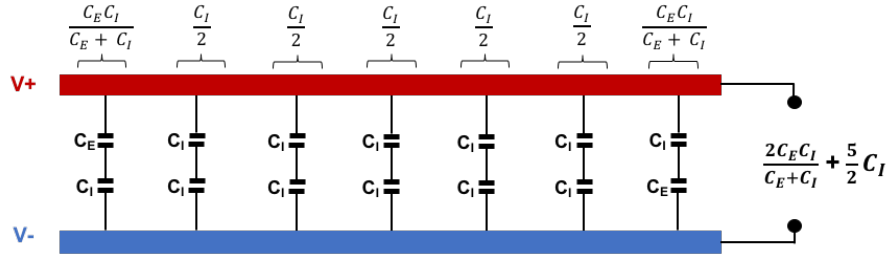
Figure 3.12: Reorganisation of the capacitances on figure 3.11 between the two electrodes

The capacitances network on figure 3.11 can be rearranged as in figure 3.12. The upper-layer capacitance C_u between negative and positive electrodes can thus be expressed as:

$$C_u = L[(N-3)\frac{C_I}{2} + 2\frac{C_I C_E}{C_I + C_E}] \quad N > 3 \tag{3.21}$$

Note that eq. 3.21 is only valid when there are four or more electrodes: indeed, we need at least two outer electrodes and two inner electrodes for this model to make sense.

The capacitance of the lower semi-infinite C_l layer has the same configuration as the upper semi-infinite layer C_u. From an electrode's point of view, these capacitance are connected in parallel. Thus, to obtain the total capacitance seen by the IDE in the half-plane model, C_{tot}, both C_u and C_l should be determined thanks to equation 3.21 and then be summed up:

$$C_{tot} = C_u + C_l \tag{3.22}$$

To determine C_I and C_E in eq. 3.21, a comformal mapping technique is applied. This **mapping varies for the inner and outer electrodes**. Both cases are qualitatively illustrated in figure 3.13.

- For C_I, the mapped region is the region whose horizontal boundary coincides with that of the dielectric layer. The vertical boundaries are the perpendicular line at half the electrode and the neighbouring equipotential line.

- For C_E, the mapped region has the same horizontal boundary. However, it has only one vertical boundary: the equipotential line. In the other direction, the domain extends to infinity.

Quantitatively, the complete elliptical integral of first kind $F(k)$ is the main cantilever for this transformation.

$$F(k) = \int_0^1 \frac{1}{\sqrt{(1-t^2)(1-k^2t^2)}} \, dt \tag{3.23}$$
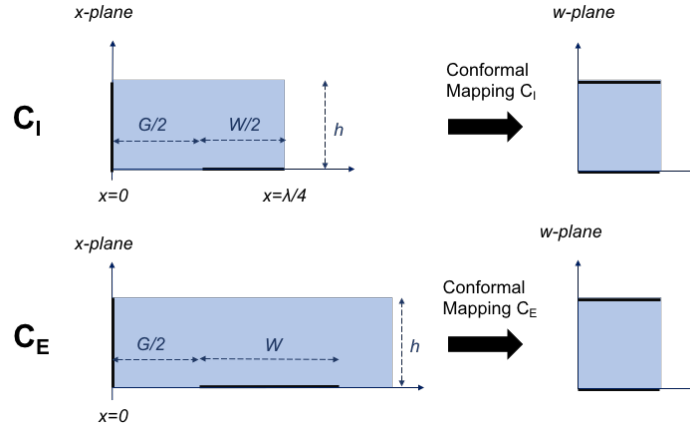
Figure 3.13: Simplified schema of the conformal mapping from a coplanar electrode configuration to a parallel plate configuration. This mapping is different for C_I, the capacitance of inner finger of the IDE and C_E, the capacitance of the outer fingers. Adapted from [118].

Table 3.3 summarizes the analytical expressions for C_I and C_E which emanate from the aforementioned transformation. We consider two types of substrates: either single layer and multilayer. The former corresponds to a situation where the upper and lower halfplanes adjacent to the electrode fingers are each made of a single, homogeneous material. The latter corresponds to a configuration where the upper and/or lower half-plane adjacent to the electrode fingers consist of a stack of different material layers. In the next section we detail the superposition method that leads to this multilayer model.

2.2.3 Multi-layer model for IDE capacitance

For the **half-plane model** in table 3.3, we consider that the IDE has a uniform substrate that fills all the space in its upper-halfplane and another uniform substrate that fills all the space underneath it. This model is useful in situations where the substrates above and underneath the fingers, are homogeneous until "far enough away" from the electrode fingers. A rule of thumb is that this **sensible depth has the same order of magnitude as half the electrode fingerwidth.** [11, 199, 12, 76].

In situations where the substrate varies within the sensible depth, close to the electrode fingers, a more refined model is needed to correctly reflect the impact of the layered permittivity variation. Several authors obtained accurate results by using the partial capacitance technique [118, 119, 201, 202], which is visually explained in figure 3.14. In the two-layered case on figure 3.14, the capacitance seen by the electrodes can be expressed as follows:

$$C_u = \epsilon_{AIR}C_{h=\infty} + (\epsilon_2 - \epsilon_{AIR})C_{h=h_1} + (\epsilon_1 - \epsilon_2)C_{h=h_2} \tag{3.24}$$

with

- C_u the total capacitance of the upper half plane

Table 3.3: Detailed equations needed for the calculations of C_I and C_E for a finite layer as well as for an infinte layer

	Interior electrode	**Exterior electrode**
Multilayer	$C_I = \epsilon_r\epsilon_0\frac{F(k_I)}{F(k'_I)}$ $k'_I = \sqrt{1-k_I^2}$ $k_I = t_2\sqrt{\frac{t_4^2-1}{t_4^2-t_2^2}}$ $t_2 = sn(K(k)\eta,k)$ $t_4 = \frac{1}{k}$ $k = (\frac{v_2(0,q)}{v_3(0,q)})^2$ $q = exp(-4\pi r)$	$C_E = \epsilon_r\epsilon_0\frac{F(k_E)}{F(k'_E)}$ $k'_E = \sqrt{1-k_E^2}$ $k_E = \frac{1}{t_3}\sqrt{\frac{t_4^2-t_3^2}{t_4^2-1}}$ $t_3 = cosh(\frac{\pi(1-\eta)}{8r})$ $t_4 = cosh(\frac{\pi(1+\eta)}{8r})$
Infinite Half-plane	$C_{I\infty} = \epsilon_r\epsilon_0\frac{F(k_{I\infty})}{F(k'_{I\infty})}$ $k_{I\infty} = sin(\frac{\pi}{2}\eta)$ $k'_{I\infty} = \sqrt{1-k_{I\infty}^2}$	$C_{E\infty} = \epsilon_r\epsilon_0\frac{F(k_{E\infty})}{F(k'_{E\infty})}$ $k_{E\infty} = \frac{2\sqrt{\eta}}{1+\eta}$ $k'_{E\infty} = \sqrt{1-k_{E\infty}^2}$

$r = \frac{h}{\lambda}$
λ the spatial wavelength (cfr fig. 3.9)
h the height of a finite substrate, (cfr fig. 3.14)
η the metalisation ratio (cfr fig. 3.9)
$F(k_x)$ the complete elliptic integral of first kind (eq. 3.23)
$sn(z,k)$ the Jacobi elliptic function of modulus k
v_2 and v_3 the Jacobi theta functions [200]

- C_{h1} and C_{h2} the capacitances of the first two -finite- layers, which depend on their height h (through the parameter $r = \frac{h}{\lambda}$ and on the electrode geometry. These values are found by substituting the values for C_E and C_I, which are obtained by using the multilayer model in table 3.3), in equation 3.24.

- $C_{h\infty}$, the capacitances of the third semi-infinite layer, which depends on the electrode geometry. This value is found by substituting the values for C_E and C_I, which are obtained by using the semi-infinite model in table 3.3), in equation 3.24.

- ϵ_n the relative dielectric constants of layers 1 and 2
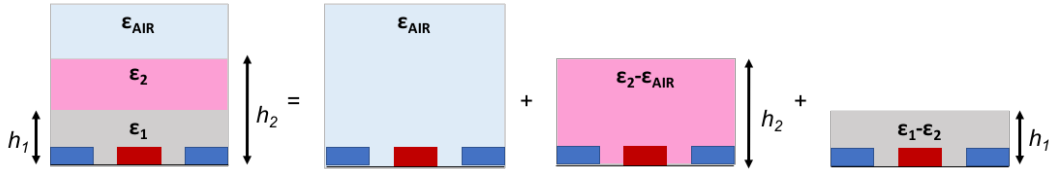
Figure 3.14: The partial capacitance technique: splitting up a two-layered half plane into two individual layers and the infinite air-layer

Note that the calculations for the multilayer model imply Jacobi theta functions and Jacobi elliptic functions, which makes the calculations more complicated and reduces the domain of the different input parameters. [200]

2.2.4 The cell constant K_{cell} and the resistance seen by IDE

The conformal mapping technique (figure 3.13 which results in the formula in table 3.3 for the capacitance seen by IDE, leads to a more general parameter, which is very useful in the analysis of any kind of **coplanar electrodes**: the cell factor K_{cell}. In electrochemistry, this is a geometry dependent parameter that relates the resistance and capacitance measured by the cell to the substrate's conductivity and permittivity.

$$R_{cell} = \frac{K_{cell}}{\sigma_{cell}} \ [\Omega] \tag{3.25}$$

$$C_{cell} = \frac{\epsilon_0 \epsilon_{cell}}{K_{cell}} \ [F] \tag{3.26}$$

with R_{cell} and C_{cell} the electrical resistance and capacitance seen by the IDE, K_{cell} $[m^{-1}]$ the cell factor and σ_{cell}, ϵ_{cell} the conductivity and relative permittivity of the bulk substrate of the upper or lower half-plane.

For parallel plate electrodes, the cell factor is given by the ratio of electrode separation A $[m]$ to electrode area S $[m^2]$:

$$K_{parallel} = \frac{A}{S} \ [m^{-1}] \tag{3.27}$$

This equation holds well for large electrode areas with small separations. In that case, most of the electrode current flows directly between the electrodes, and the small current

in the fringing field can be neglected. Indeed, by combining equations 3.25- 3.26 and 3.27, we obtain equations 3.18- 3.19.

For a coplanar electrode, finding the cell constant is more complicated because in this case all the electrode current flows through the **fringing field**.
Let us consider a situation in which the upper half plane (cfr. figure 3.8) is made of a conductive substrate and the lower half plane is made of an insulating material. Since both resistances are in parallel from the point of view of the IDE, we neglect the lower half-plane.
Olthuis et al. found an analytical solution for the potential distribution by using the method of conformal mapping which was already described in figure 3.13. [203] By doing so, a new coordinate system is created in which the field geometry is more easily solved. The resultant **cell factor for Interdigitated Electrodes (IDE)** and resistance of the upper semi-infinite conducting layer R_u are expressed as follows:

$$K_{planar} = \frac{2}{L(N-1)} \cdot \frac{F(k')}{F(k)} \quad [m^{-1}] \tag{3.28}$$

$$R_u = \frac{K_{planar}}{\sigma_u} \tag{3.29}$$

with L the length of an electrode, N the number of electrodes and σ_u the bulk conductivity of the upper half-plane. $k = sin(\frac{\pi}{2}\eta)$ and $k' = \sqrt{1-k^2}$ and the complete elliptical integral of first kind $F(k)$ is defined in equation 3.23.
Given the complexity of Olthuis' expression for the cell factor, a power law approximation can be used:

$$K_{planar} \approx \frac{2(S/W)^{1/3}}{L(N-1)} \tag{3.30}$$

In [204] it was proven that both models coincide quite well over the whole metalisation ratio range, when $N > 6$.

Since they are based on the same conformal transformation, it is no surprise that Olthius' expression for the cell constant looks similar to the formula in table 3.3. In fact, Igreja et al. [118] refined Olthuis' work by adding two concepts.
Firstly, they took into account the fact that the interactions with the **outer electrode fingers** differ from those with the inner electrode fingers. To illustrate this, let's consider equation 3.21 and consider the two outer electrodes by two extra inner electrodes ($C_E = C_I$). We then substitute C_I by the expression given by table 3.3 for the semi-infinite layer case.

$$C_u = L[(N-1)\frac{C_I}{2}] \tag{3.31}$$

$$C_u = L(N-1)\frac{\epsilon_0\epsilon_u}{2}\frac{F(k_{I\infty})}{k'_\infty} \tag{3.32}$$

Comparing with eq. 3.28 and noting that $k = k_{I\infty}$, we obtain

$$Cu = \frac{\epsilon_0\epsilon_u}{K_{cell}} \tag{3.33}$$

which fits exactly to the initial definition given by equation 3.26. Thus, in for the semi-infinite layer case, Igreja et. al refined the more commonly used Olthius formula. In this work, we initially use the Olthius formula for determining the resistance seen by the IDE and the Igreja formula for the capacitance seen by the IDE. We then compare both.

Secondly, Igreja et al. took into account the possibility of a **multilayer configuration** for determining the total capacitance. However, for the resistance, we only use the semi-infinite model. Indeed, the multilayer model is less useful. For example, given that adjacency is needed for the current to flow, a conducting layer which follows an adjacent insulating layer, has little to no influence on the total resistance.

In the case of our sensor, the lower half-plane contains relevant electrical information. However, the upper half-plane, consisting of air, can not be neglected when the nitrocellulose is dry (and thus, when the conductivity and permittivity of the bulk nitrocellulose are close to the conductivity and permittivity of the ambient air).

Consider that the subscript *tot* corresponds to the total capacitance or resistance seen by the IDE, that the subscript u corresponds to the bulk semi-infinite upper half-plane and the subscript l to the semi-infinite lower half-plane. Both half planes are in parallel from the IDE point of view. We then obtain the expression for the **cell constant considering both the upper and the lower half plane**

$$R_{tot} = (R_u^{-1} + R_l^{-1})^{-1} = (\frac{\sigma_u}{K_{cell}} + \frac{\sigma_l}{K_{cell}})^{-1}$$

$$C_{tot} = (C_u + C_l) = \epsilon_0(\frac{\epsilon_u}{K_{cell}} + \frac{\epsilon_l}{K_{cell}})$$

$$K_{cell} = \frac{(\sigma_u + \sigma_l)}{(R_u^{-1} + R_l^{-1})} = \frac{C_u + C_l}{\epsilon_0(\epsilon_u + \epsilon_l)}$$

with R_{tot}, C_{tot} the total resistance and capacitance of the upper and lower half plane seen by the capacitance (and by extend, the upper and lower volume).

3 Experimental determination of the equivalent circuit

3.1 Fabrication of IDE on nitrocellulose

3.1.1 Nitrocellulose substate

The nitrocellulose membranes which we use, are provided by Sartorius Stedim Biotech [205]. We use two types of membranes: CN95 and CN140. The former has larger pores than the latter. They both have a void factor of approximately 75%, which means that 25% of the membrane volume consists of nitrocellulose fibers and 75% is air (when the nitrocellulose is dry). The thickness of the sheets varies between 110 and 140 μm.

The CN95 membrane is always backed with a $100\mu m$ polyester layer while the CN140 is either backed or unbacked.

The choice between backed and unbacked was always deliberate (the backing offers extra strenght to the membrane which was essential for certain experimental set-ups, as will be explained later). The choice between pore-sizes on the other hand was not deliberate but rather dependent on the stock of available nitrocellulose samples. However, in the range of our applications, this pore size difference did not have a significant impact.

3.1.2 Electrode deposition method

Before the start of this master thesis project, different tests were already done to deposit electrodes on nitrocellulose through inkjet printing. However, the paper feed mechanism (capilarity effect) and improper ink-substrate interaction scaused precision issues. As seen in figure 1.25, a pretreatment of the nitrocellulose is needed in order to avoid this. The scope of this work is to globally characterise the electrical properties of the sensor components as a whole and elaborate a proof of concept. Thus we did not focus on the problems linked to inkjet printing. Instead, we chose an alternative electrode deposition method with devices available in the UCLouvain WINFAB laboratoria: Physical Vapor Deposition (PVD) using electron beam evaporation. Since this fabrication method is time, energy and labor intensive; this can not be used for the final production of a point-of-care device. However, it forms a useful sidestep to understand the fundamental sensing principles and to confirm the analytical model.

The electrodes deposited on nitrocellulose made of **aluminium** and have a **thickness of 1** μm. This thickness is large compared to state of the art electrodes in table 1.3. Indeed, because of the rugosity of the nitrocellulose surface (around 0.5 μm of "mean surface roughness"), a too thin layer presents the risk of connection failure.

The deposition was performed by single and dual E-gun evaporation at the Winfab laboratorium of UCLouvain (see figure 3.15).

Two types of masks were at our disposal: we had two masks for IDE with 500 μm finger width and seven masks for IDE with 200 μm finger with. The resulting electrodes are represented in table 3.4.

Figure 3.15: The VACOTEC Dual E-gun evaporation system (left) and the VST - TFDS 462 (right) in Winfab at UCLouvain, both used for the deposition of aluminium electrodes (thickness $1\mu m$) on nitrocellulose [206]
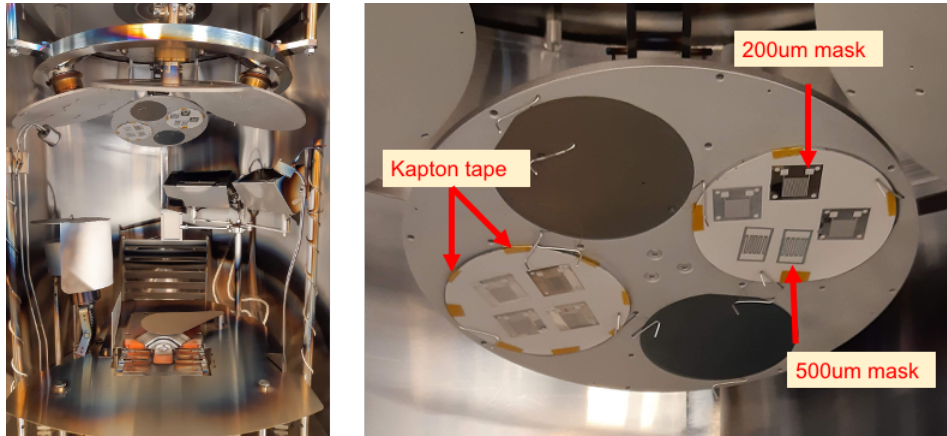
Figure 3.16: Interior of VST - TFDS 462 (cfr. fig 3.15). 4 wafers can be fixed per plate, which have a planetary rotation around the e-gun. We use 2 magnetic wafers on which we attach a nitrocellulose sample with kapton tape. The masks are fixed with the magnetic force of the wafer.
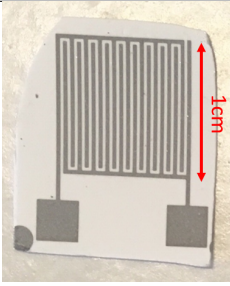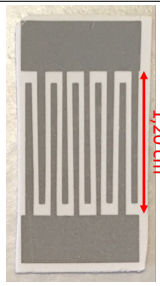
	Electrode 1	**Electrode 2**
Substrate material	Nitrocellulose	
Substrate thickness	140 um	
Electrode material	Aluminium	
Electrode thickness	1 um	
Finger width	200 um	500 um
Finger length	1 cm	1.2 cm
Gap width	200 um	500 um
Number of fingers	20	10

Table 3.4: Characteristics of the electrodes printed by PVD as explained in section 4.1.1, using the VACOTEC.

3.1.3 Storage of the fabricated electrodes

Once the electrodes are fabricated, they have to be stored at constant temperature and relative humidity in order to avoid bias due to residual humidity in the nitrocellulose membrane. This was done in the "temperature and humidity champber" in the Welcome laboratorium at UCLouvain. In an ideal scenario, the duration storage should be the same for all used electrodes in order to avoid differences in the thickness of the oxidation layer. However, due to the sanitary crisis and the subsequent closure of the laboratorium

during the lockdown, some of our electrodes were exposed to ambient air during several weeks. Even though we estimate that the bias induced by this is limited, this should be kept in mind.

3.2 Bio-functionalisation and preparation of bacteria

Nitrocellulose is used for its very good properties of immobilizing biomolecules. Due to the charge interactions, the weak hydrogen bonds and Van der Waals interactions, it allows easy electrostatic binding of proteins through the interaction of the strong dipole of nitrate esters with the strong dipoles of the peptide bonds within the protein. [7]

In order to capture and stabilise bacteria, the nitrocellulose is **functionalised with phage proteins** such as Receptor Binding Protein (RBP) and Cell Binding Domain (CBD) of endolysins. In order to allow optical control of good protein binding, these are made fluorescent using Green Fluorescent Protein (GFP), a versatile biological marker for visualizing protein localisation. Once the proteins are tagged with GFP, they are deposited on the nitrocellulose membrane according to the protocol in Appendix B.
The drying steps is of high importance as the proteins retain its structural integrity while completely dried. Thanks to that and while waiting to be used, the sensor may be stored at ambient temperature (in dry conditions). By rehydrating the proteins by the sample they should be instantly reactive.

The protocol to prepare the solution of bacteria is also detailed in Appendix B. We use GBJ002-bacteria (Bacillus thuringiensis) and suspend them either in PBS or DI water. Figure3.17 depicts bacteria which come from the same strain as the GBJ002 we use, and are marked with GFP.
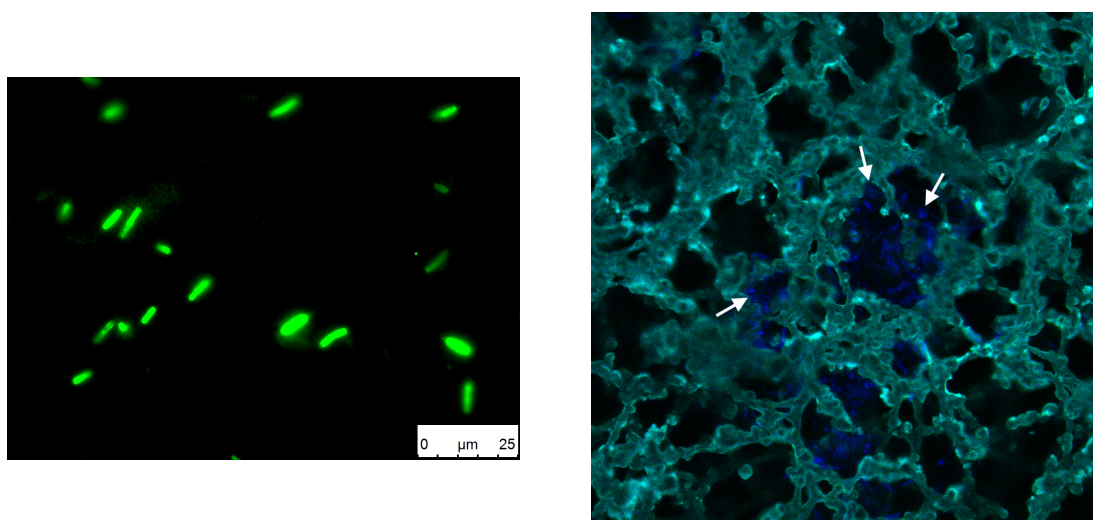

Figure 3.17: On the left: Strains GBJ001 from Bacillus cereus group recognized by fluorescent gp221-CBD. Picture made by Audrey Leprince [175]. On the right: GBJ002 bacteria captured in the nitrocellulose and tagged with CFP (cyan fluorescent protein)

3.3 Electrical connection interface

The electrical connections with the electrodes are made with **BNC connectors**. These are chosen because they allow linkage with a coaxial cable, which is a type of electrical cable consisting of an inner conductor surrounded by a concentric conducting shield, with the two separated by a dielectric (insulating material). Electric and magnetic fields outside the cable are largely kept from interfering with signals inside the cable. This property makes coaxial cable a good choice both for carrying weak signals, that cannot tolerate interference from the environment, and for stronger electrical signals, that must not be allowed to radiate or couple into adjacent structures or circuits.

The BNC connectors are soldered to an FR-4 plate using Sn-Pb solder. FR4 (or FR-4) is a composite material composed of woven fiberglass cloth with an epoxy resin binder that is flame resistant (self-extinguishing). The initial connection between the BNC-connectors and the paper electrodes is pictured on the left size of figure 3.18. A connecting wire was soldered to a copper track which is linked to the BNC connector. This connecting wire (reference AKT 3001) is made of electrolytic silver plated annealed copper, has a diameter 0.254mm and a nominal resistance 34Ohm/100m[207].
The connecting wire was glued to the electrode pad with **conductive epoxy** (reference CW 2400). This setup has the advantage that the used nitrocellulose can be both backed and unbacked: indeed, since the membrane is directly deposed on FR-4, no rigidity issues occur.
However, it has three main advantages:

1. It is not time-efficient. Indeed, the epoxy glue has to dry for at least 8 hours.

2. One can test only one electrode pair per test run, since the membrane cannot be removed without breaking it.

3. At high frequencies ($f > 10^6 Hz$), we observe a huge parasitic impact of the connecting wire.

After a while, a second electrical connection set-up was used. **Toothless crocodile clips** were directly soldered to the copper track. This allows for the electrodes to be connected and disconnected from the BNC-connectors without damage. Thus, it is possible to test multiple electrodes in one run. The high frequency parasitic effects were tempered. Since no more epoxy glue is used, no time was lost during the drying process. However, this set-up has the drawback to be less adapted for the (brittle) unbacked nitrocellulose, since the membrane is not directly supported by FR-4 any more.

3.4 Impedance and permittivity measurement devices

3.4.1 Impedance measurement

There are many measurement methods to choose from when measuring impedance: the bridge method, the resonant method, the I-V method, the RF-IV method, the network analysis method, the auto balancing bridge method,... Elaborated explanations for each method are found in [209].
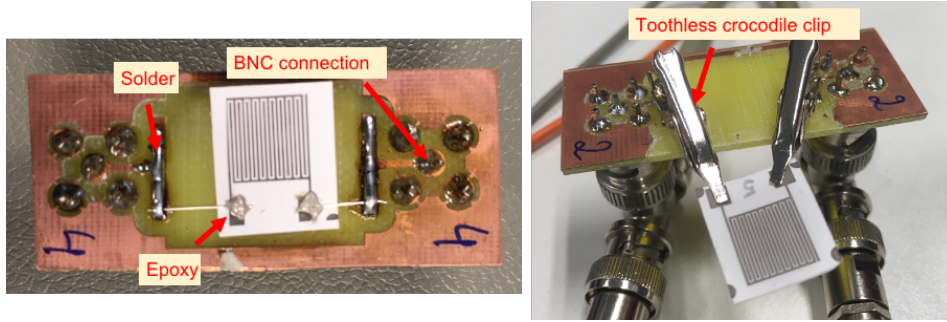
Figure 3.18: Evolution of the connection interface: first with conductive epoxy glue, then with toothless crocodile clips.
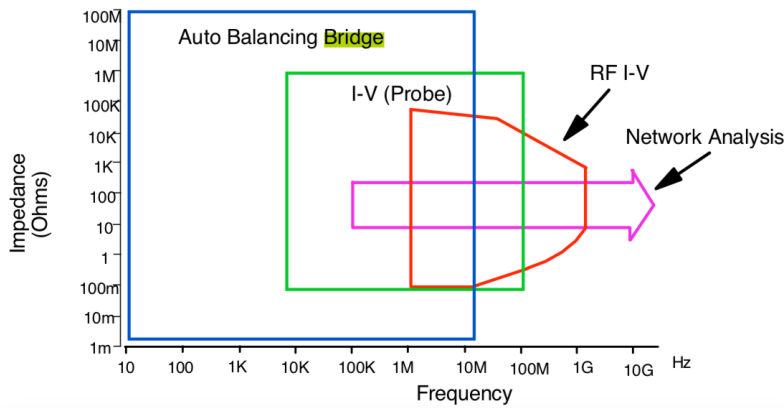
Figure 3.19: Coverage of each impedance measurement technique considering frequency and DUT impedance criteria. [208]

As can be seen in figure 3.19, the auto-balancing bridge provides the widest measurement range with high accuracy. [210]. The I-V technique provides good mid-frequency measurmeent range. RF-I-V method is an excellent choice for high frequency impedance measurement. Network analysis covers the highest frequency range, but it is designed to work around 50Ω, which makes the impedance range rather narrow. [208, 209, 211]

Our choice is to use an LCR-meter with auto-balancing bridge between 10^3 and 10^6 Hz, and a Vector Network Analyser (VNA) up until $10^9 Hz$.

In table 3.5, we summarize the two main devices which are used for impedance measurement of our device. In the following sections, we go into more detail concerning these devices.

Equipment type	Equipment name	Total freq range	Used freq range	Output parameters	Connection type
LCR meter	Agilent 4284A	$20 - 10^6$	$10^3 - 10^6$	ZTD	2p BNC
VNA	ENA E5061B	$5 - 3 \cdot 10^9$	$10^3 - 10^9$	S-parameters	2p N-connector

Table 3.5: Two main techniques for impedance measurement.
$2p = "2port", \ freq \ [Hz]$
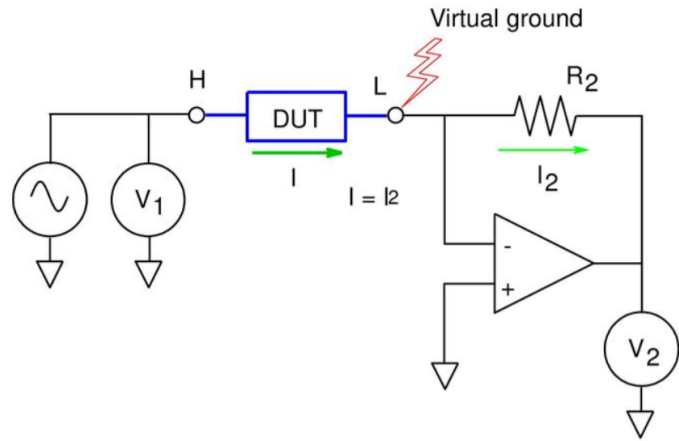
Figure 3.20: Auto balancing bridge main components. [208]

3.4.2 LCR impedance measurement and polar representation

LCR meter is an electronic testing instrument used to measure the inductance (L), capacitance (C) and resistance (R) of a DUT. As explained in section 3.1, these quantities are not measured directly, but determined from a measurement of impedance. [212]
The used LCR-meter, *Agilent 4284A* as indicated in table 3.5, uses the auto balancing bridge method.

Figure 3.20 shows a simplified circuit diagram of the Auto-Balancing-Bridge method. To perform precise impedance measurements, the voltage applied to the device under test (DUT) and the current which flows through the DUT need to be accurately measured. The test signal current that flows through the DUT also flows through the range resistor R_2. The voltage at the low terminal L is constantly monitored and balanced to zero by a feedback loop controlled through an IV converter amplifier. This is called the virtual ground.
The voltage at the high terminal V_1 is imposed and the voltage at the range resistor V_2 can be constantly monitored. Thus, the impedance of the DUT Z_{DUT} can be determined as follows:

$$V_2 = I_2 R_2 \tag{3.34}$$

$$Z_{DUT} = \frac{V_1}{I_2} = \frac{V_1 R_2}{V_2} \tag{3.35}$$

Impedance is represented as a complex, vector quantity. A polar coordinate system is used to map the vector as shown in figure 3.21, where quadrants one and two correspond to passive inductance and passive capacitance respectively, quadrants three and four correspond to negative resistance. The output of the used *Agilent 4284 A* is represents the impedance in its "$Z - \theta$" format, which incorporates the modulus Z and the phase θ of the impedance as represented in figure 3.21. With equation 1.11, this polar representation can easily be transformed into the carthesian impedance respresentation.
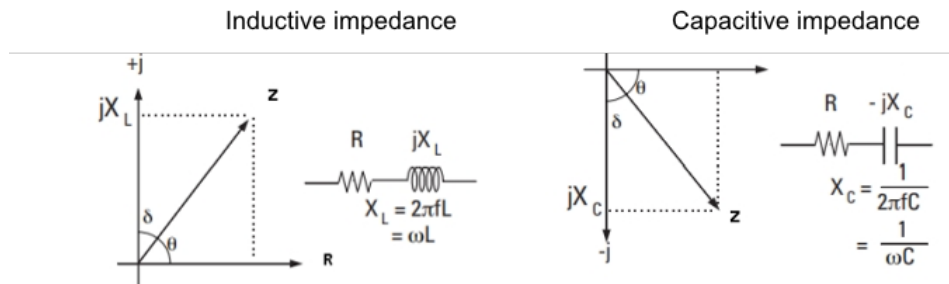
Figure 3.21: Impedance representation in the polar coordinate system [213]

Correction of the LCR-meter measurement

Generally, impedance measurement instruments have a reference plane to define the measurement accuracy at the terminals of its front panel. A test fixture is connected to the reference plane. Test fixtures degrade the total measurement accuracy by their residual impedance. To improve this degradation, error correction should be applied. The OPEN/SHORT correction is the very popular correction technique used in recent impedance measurement instruments. [214]

The Agilent 4284A that we use, has an internal setting that allows for the elimination of the electrical effects due to the cable length. We always perform an OPEN measurement to correct the LCR result. For the epoxy set-up, on the right of figure 3.18 this is done by gluing the connective wire with epoxy on a piece of nitrocellulose on which no electrode is printed. For the crocodile clip set-up, this is done by clipping a blank piece of membrane between both clips.

A special attention is required for the set voltage. When the nitrocellulose is dry, the impedance is very high and thus $1V$ is applied. When the nitrocellulose is humid, the impedance is lowered. The applied voltage is $20mV$ in order to stay maintain a linear response of the device. [81]

3.4.3 VNA impedance measurement and S-parameters

The Vector Network Analyser (VNA) characterizes high-frequency passive and active devices in their linear mode of operation by measuring their network parameters, called S-parameters, as a function of frequency.
S-parameters describe the complete linear behavior of a high frequency device or circuit in linear mode of operation. The main function of a vector network analyzer is to provide S-parameters as a function of the frequency.

Consider a load connected to a sine wave generator through a piece of cable. The sine wave generator has a certain source impedance and the electrical power travels across the wire from the source to the load as the combination of an electric and magnetic field. The propagation speed v_p depends on the dielectric properties of the medium and is a fraction of the speed of light. The wavelength, λ, is defined as a function of the

propagation speed and the sine wave generator frequency f_0:

$$\lambda = \frac{v_p}{f_0}$$

When f_0 is low, the wavelength is large and the length of the cable is negligible compared to the size of the wavelength. As a result, the measured voltage and current are independent of the location on the cable. However, when f_0 increases, the wavelength reduces and eventually becomes smaller than the length of the cable. In that case, the measured voltage and current will depend on the position. Measuring the voltage with a voltage probe is impossible because it depends on the probe's position. In this scenario, the analysis is more complex since it involves **transmission line theory**.

Using transmission line theory, one can think of the electrical power traveling along the line starting from the source. While traveling on the line, a certain voltage and current relation is imposed by the electrical properties of the line. In fact, the cable itself will behave such that it is characterized by an inherent impedance that does not change as long as the properties of the line or cable do not change. This impedance is called the characteristic impedance (Z_0).
As the electrical power hits the load, the voltage to current relationship is now imposed by the impedance of the load. Under the condition where the load impedance is equal to the characteristic impedance, the power is fully absorbed. If the load impedance is different from the characteristic impedance, the ratio of voltage and current will change at the point where the medium changes. As a result, the load will not absorb all the power, resulting in a portion of the power traveling back towards the source. Given this characteristic, the system has both an **incident and reflected wave**.[215]
The incident wave propagates from the analyzer to the Device Under Test (DUT) while the reflected wave travels in the opposite direction from the DUT back to the analyzer.

In general, as illustrated in figure 3.22.A, both incident waves a_1 and a_2 can be non-zero. In that case, we have:

$$\begin{bmatrix} b_1 \\ b_2 \end{bmatrix} = \begin{bmatrix} s_{11} & s_{12} \\ s_{21} & s_{22} \end{bmatrix} \cdot \begin{bmatrix} a_1 \\ a_2 \end{bmatrix} \tag{3.36}$$

s_{11}, s_{12}, s_{21}, s_{22} are called the **scattering parameters**.

A Vector Network Analyzer contains both a source, used to generate a known stimulus signal, and a set of receivers that characterize the response of the device - with the help of a separation hardware- by measuring the phase and amplitude of the signals that are both incident to and reflected from the DUT [215, 216]
Linear networks, or nonlinear networks operating with signals sufficiently small to cause the networks to respond in a linear manner, can be completely characterized by S-parameters measured at the network terminals without regard of the contents of the networks. [217]

To characterize the performance of such a network, other parameters than S-parameters (equation 3.36) can be used, for instance admittance Y-parameters (equation 3.37) and impedance Z-parameters (equation 3.38). As can be seen in figure 3.22, there are four
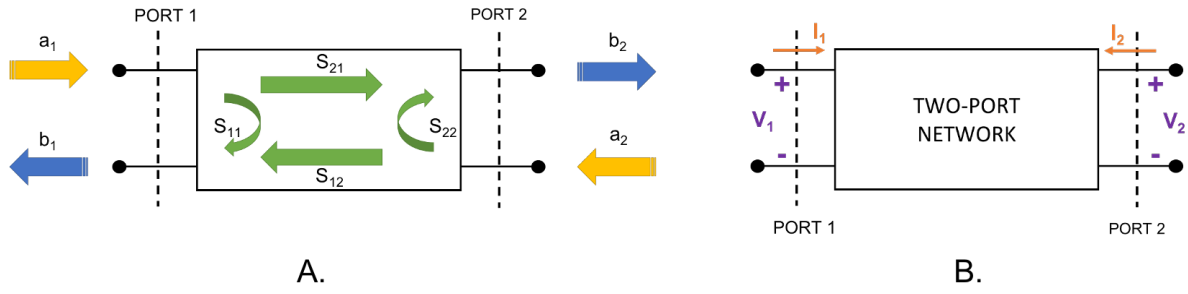
Figure 3.22: Schematisation of S-parameters (A.) and general representation of a two-port network (B.)

variables related to a two-port network: the incoming current and the potential difference at each port. Each parameter set is related differently to these four variables. In general, two of these variables represent the excitation of the network (independent variables), and the remaining two represent the response of the network to the excitation (dependent variables). The Y-parameters express the dependent current variables I_n as a function of the excitation parameters V_n, while the opposite is true for Z-parameters.

$$\begin{bmatrix} I_1 \\ I_2 \end{bmatrix} = \begin{bmatrix} y_{11} & y_{12} \\ y_{21} & y_{22} \end{bmatrix} \cdot \begin{bmatrix} V_1 \\ V_2 \end{bmatrix} \tag{3.37}$$

$$\begin{bmatrix} V_1 \\ V_2 \end{bmatrix} = \begin{bmatrix} z_{11} & z_{12} \\ z_{21} & z_{22} \end{bmatrix} \cdot \begin{bmatrix} I_1 \\ I_2 \end{bmatrix} \tag{3.38}$$

Other sets of parameters correspond to other combinations of dependent and independent variables. However, all parameter sets contain the same information about a network, and it is always possible to calculate any set in terms of any other set.[218, 219, 217] Note that all parameter are have imaginary values.

In our measurements, the S-parameters that are the output from the *ENA E5061B* are directly transformed in the Y-parameters and Z-parameters, which is the most useful for us. However, the four impedance Z-parameters are not directly comparable to the single impedance $Z - \theta$ output from the LCR-meter. A simplification is needed.
For reciprocal networks, **simplified equivalent circuits** exist. A network is called **reciprocal** when the response at port 2 due to a stimulus at port 1, is the same as the response at port 1 when that same stimulus is applied at port two. In terms of Y- and Z-parameters, this means that $z_{12} = z_{21}$ and $y_{12} = y_{21}$.
In that case, an equivalent T- and Π-circuit exist for the Z- and Y-parameters respectively, as shown in figure 3.23. Since the LCR-measurement gave an impedance value for the "through" impedance and not the "shunt" impedance. Thus, the value obtained with the LCR-meter corresponds to $Z_{11} + Z_{22} - 2Z_{12}$ in impedance parameters obtained with the VNA.

Calibration of the VNA

We use a two-port measurement and make the connection to 2 coaxial cables with N-connectors.
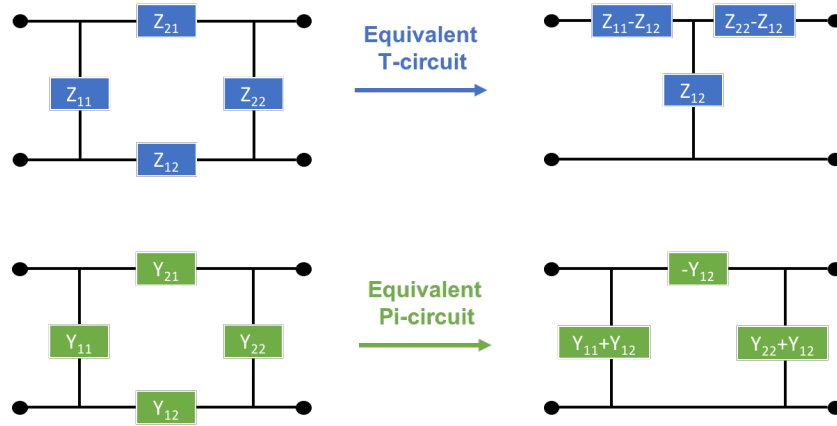
Figure 3.23: Equivalent T- and PI circuit for impedance and admittance parameters, given that the network is reciprocal.

The calibration of the VNA is done by an OPEN, SHORT and LOAD element which are connected to each coaxial cable separately. These circuit elements correspond to a characteristic impedance of 50Ω and respect the theory of transmission lines. The OPEN and SHORT elements both reflect the wave but at a different phase. The LOAD element is exactly 50Ω and thus absorbs the whole wave.

A THOUGH measurement is also made by interconnecting both coaxial cables. The calibration is considered "successful" when a the S11 parameter stays between $-10mdB$ and $10mdB$ over the whole target frequency range when a reflexive circuit element (either open or short) is connected to it.

Correction of the VNA measurement

Our device does not respect the theory of transmission lines since our interconnections do not have a characteristic impedance of 50Ω. This means extra de-embedding is needed by using both the closed an open circuit measurement of the device. For the open circuit measurement, the same set-up is used as for the LCR measurement. For the closed circuit measurement, we use a membrane sample which is completely covered by $1\mu m$ of aluminium (recovered from residual nitrocellulose surface after Physical Vapor Deposition (PVD) with the VACOTEC, cfr section 3.1).

Let the subscript D correspond to the target device measurement, the subscript O correspond to the open circuit device and the subscript C to the closed circuit device.

We first perform an open de-embedding of the target device measurement admittance $\overline{\overline{Y_D}}$ by substracting the open measurement admittance from the obtained device admittance.

$$\overline{\overline{Y_{DO}}} = \overline{\overline{Y_D}} - \overline{\overline{Y_O}}$$
$$\overline{\overline{Z_{DO}}} = (\overline{\overline{Y_{DO}}})^{-1}$$

We then perform a closed de-embedding of the target device measurement by substracting the closed measurement impedance from the open deembedded impedance $\overline{\overline{Z_{DO}}}$.

However, if we substract the closed measurement impedance from the open deembedded impedance, they have to be in the same reference plane. Thus, we cannot use $\overline{\overline{Z_C}}$ as such, we must first perform an open de-embedding of the closed circuit device measurement in order to obtain $\overline{\overline{Z_{CO}}}$.

$$\overline{\overline{Y_{CO}}} = \overline{\overline{Y_C}} - \overline{\overline{Y_O}}$$
$$\overline{\overline{Z_{CO}}} = (\overline{\overline{Y_{CO}}})^{-1}$$

$$\overline{\overline{Z_{DOC}}} = \overline{\overline{Z_{DO}}} - \overline{\overline{Z_{CO}}}$$

In the epoxy set-up, the closed measurement correction should enable to undo the parasitic inductive effect of the connective wire. However, in practice, this is not so easy, since both the closed an open device measurements result in very noisy signals.

3.4.4 Permittivity measurement device
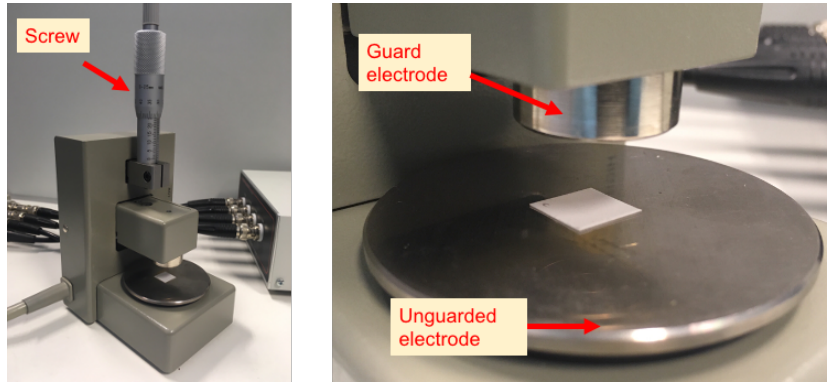
Figure 3.24: Permittivity measurement (Parallel plate) with Test-Fixture 16451B connected to Novocontrol LCR meter. The screw allows to precisely lower the guard and guarded electrode in order to determine the spacing between the parallel plate electrodes exactly. In the ideal case, the spacing between the electrodes is exactly the same as the sample thickness t_a.

By using the Test-Fixture 16451B shown in figure 3.24, the permittivity of sheet materials can be measured. This test fixture is connected to the NovoControl, which is an LCR-meter with roughly the same functionalities as the Agilent 4284 that was already mentioned.

This device allows us to experimentally measure the values for ϵ_r and σ, in order to compare them to the model in section 1.2 of this Chapter.

The role of the guard electrode represented in figure 3.25 is to remove the additional edge measurement error due to the edge capacitance. It permits to measure the permittivity of the sample only which is between the two parallel plates. Indeed, only the characteristics of the sample are desired and thus the guard electrode helps to remove the ambient air characteristics and to obtain purer results.
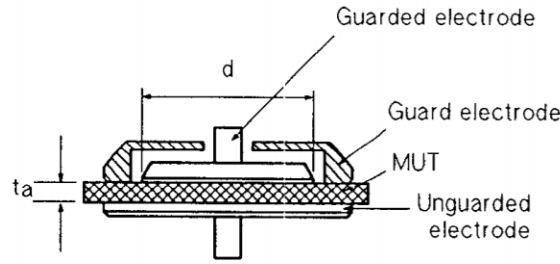
Figure 3.25: Illustration of the guarded and guard electrode in a parallel electrode setup [220]

The relative permittivity is a complex-valued number, represented by a real part ϵ_r' and an imaginary part ϵ_r'' [221]:

$$\epsilon_r = \epsilon_r' - i\epsilon_r''$$

and is given by the machine thanks to impedence measurements.

The **real part** of the relative permittivity ϵ_r is found thanks to the capacitance measurement:

$$\epsilon_r' = \frac{t_a \cdot C_p}{A \cdot \epsilon_0}$$

with t_a the average thickness of DUT [m], C_p the equivalent parallel capacitance of DUT measured by the Test-Fixture [F], A the area of the guarded electrode [m^2], and ϵ_0 the vacuum permittivity [F/m].

The **imaginary part** is found in a similar way thanks to the other impedance measurements. From the imaginary part ϵ_r'', we can deduce the conductivity of the material by the following equation [222]:

$$\sigma = \omega\epsilon_0\epsilon_r'' \tag{3.39}$$

The dielectric loss factor is defined by the ratio of the imaginary part and the real part of ϵ_r. This characterises where the material is situated between dielectric and conductive behaviour :

$$\tan(\delta) = \frac{\epsilon''}{\epsilon'}$$

Calibration of the Test Fixture

No calibration or correction is needed. However, in order to control if all the settings are correct, a control measurement with a reference sheet of Teflon should be carried out.

3.5 Control and data treatment

3.5.1 Control

When doing measurements with bacteria, different types of control are effectuated in order to verify that the observed difference in electrical signal is indeed the consequence of an increased presence of bacteria.

1. **Control using a functionalization-free sensor**: measurement with bacteria but without functionalisation on the nitrocellulose.

2. **Control by optical means**: Not suitable for point-of-care and compact sensors, optical monitoring of the sensor surface can nevertheless be performed in laboratory during electrical sensing to assess the binding of bacteria, proteins,... For example, this is done in figure 3.17

3. **Control using the solution without bacteria**: measurement without bacteria, in order to differentiate possible interactions of ions in the solution.

3.5.2 Analysis of the experimental data

In order to validate the analytical electrical model, we should extract the values of the equivalent circuit elements in figure 3.1 from the obtained measured data. To do so, we use the software "ZView for Windows" [223], which is a useful tool for analysis of EIS data. The data input are *.txt* files with the real and imaginary parts of the measured impedance, for different frequencies. Zview allows to easily plot Bode and Nyquist plots and to filter out singular data points. The user can chose the form of an equivalent circuit, after which ZView determines the values of the equivalent circuit element in order to fit the obtained impedance as closely as possible.

Chapter 4

Results

This chapter discusses several aspects of the obtained results and offers perspectives for future research.

1. First, discuss the fitting of the analytical model. 3.1

2. Then, we elaborate different factors that can be improved in the measurement set-up.

3. Finally, we introduce a reflection towards more selective and sensitive bacterial detection and towards a fully operational device.

1   Analytical model

1.1   Simplification of the equivalent capacitance

In the previous chapter, in figure 3.1 we established the equivalent circuit on which we base our analytical model. In this section we attempt to validate the layers that are considered in the dry and wet model. Indeed, this model only considers a semi-infinite air top-layer and a semi-infinite nitrocellulose bottom layer, but this is not the case in the real set-up: the nitrocellulose is either deposed on FR-4 (in the epoxy set-up) or surrounded by air (in the clip set-up), as can be seen in figure 3.18.
To validate this single-layer configuration, we consider different multilayer-configurations in figure 4.1 and try to establish under what conditions these models converge.
A, B and C are reference configurations with a lower semi-infinite halfplane consisting of respectively air, dry nitrocellulose or FR-4.

Then, we study the behavior of two cases which correspond to the real set-ups:

- Case D: the lower half-plane consists of nitrocellulose followed by a semi-infinite layer of air, which approximates the clip-configuration (cfr section 3.3 of Chapter 3).

- Case E: the lower half-plane consists of nitrocellulose followed by a layer of 2.3 mm of FR-4 and then by a semi-infinite layer of air. This approximates the epoxy-configuration (cfr section 3.3 of Chapter 3).
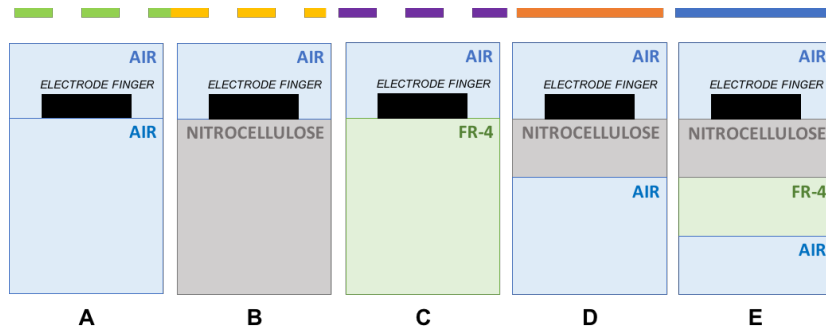
Figure 4.1: Schematic representation of the five geometrical configurations of the lower semi-infinite half-plane. The corresponding linestyle of the plots in figure 4.2 are added above. The used material properties are summarised in table 3.2

.

In figure 4.2 we plot the total capacitance seen by the $500\mu m$ IDE, according to the analytical model, as a function of the thickness of the nitrocellulose layer, for each configuration. We consider that the nitrocellulose is dry.

Of course, configurations A, B and C do not involve nitrocellulose and are thus constant with varying NC thickness. Since air has the lowest relativity and FR-4 the highest (see table 3.2), it makes sense that the semi-infinite layer of air causes the lowest capacitance while the semi-infinite layer of FR-4 causes the highest one.
Note that we consider that the three cases have a semi-infinite upper layer of air. In agreement with equation 2.2.2, this layer of air forms a parallel capacitance, thus "offsetting" the three total capacitance values by the capacitance of the upper air layer. Thus, the ratios between the relative permittivities in table 3.2 are not transposable to the total capacitance values obtained in figure 4.2.
Since in both cases D and E the nitrocellulose is directly adjacent to the electrodes (see figure 4.1), the total capacitance converges towards the semi-infinite nitrocellulose layer capacitance when the NC layer gets thicker.
When the nitrocellulose layer becomes very thin, case D converges towards semi-infinite air. Case E converges towards semi-infinite FR-4 but seems to flatten before reaching it. This can be explained by the fact that we consider only 2.3mm of FR-4 which is followed by a (less influent) semi-infinite air. For a given NC layer thickness, since $\Delta\epsilon_r$ is smaller between air and nitrocellulose than between FR-4 and nitrocellulose, it makes sense that $|C_{tot,\ E} - C_{tot,\ B}| > |C_{tot,\ D} - C_{tot,\ B}|$.
We thus conclude that the analytical model is **coherent in terms of relative behavior between different sorts of materials**.

In figure 4.2, we can see that at the actual thickness of the nitrocellulose sheet of our device (120 μm, cfr table 3.4), the presence of FR-4 can almost be neglected. A vertical line is plotted at 120 μm. We observe that the difference between scenarios D and E on the one hand, and scenario B towards which they converge on the other hand, is very small.

Figure 4.2: Analytical model the total capacitance seen by the 500um finger device (cfr table 3.4) as a function of varying thickness of the nitrocellulose layer. Figure 4.1 summarizes the five different cases. The upper half-plane is always air while the lower half plane varies. The dry nitrocellulose has a relative permittivity of $\epsilon_r = 1.3$.

Can the presence of FR-4 also be neglected in the **wet model?** For this, we consider a "generic" version of soaked nitrocellulose, with a relative permittivity $\epsilon_r = 50$. The total capacitance in the case of a semi-halfplane with only NC is thus much higher than that with only air or FR-4. Again, case D and E converge towards the infinite NC case with a growing NC thickness. Since the relative permittivity of wet NC is much bigger than that of air and FR-4, and since NC is the layer closest to the electrodes, the NC-layer is predominant in terms of behavior. This explains why this time the difference between case D and E is very small when the NC thickness decreases, which was not the case when NC is dry. It also makes the fact that we neglect the FR-4 layer in the analytical model even more acceptable: indeed, the difference between E and B at $NC_{thickness} = 120 \ \mu m$ is even smaller than in the dry scenario.

We can thus conclude that, when the thickness of the nitrocellulose layer is $> 100 \ \mu m$, it is **acceptable to neglect the presence of any material adjacent to the nitrocellulose sheet**, as long as nitrocellulose stays adjacent to the electrodes and as long as the next substrate has a relative permittivity which is "the same order of magnitude or smaller" than the NC permittivity.
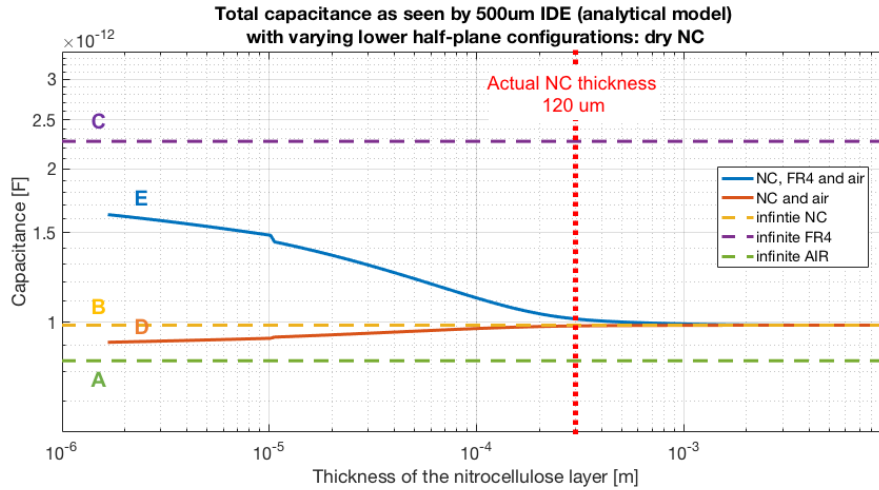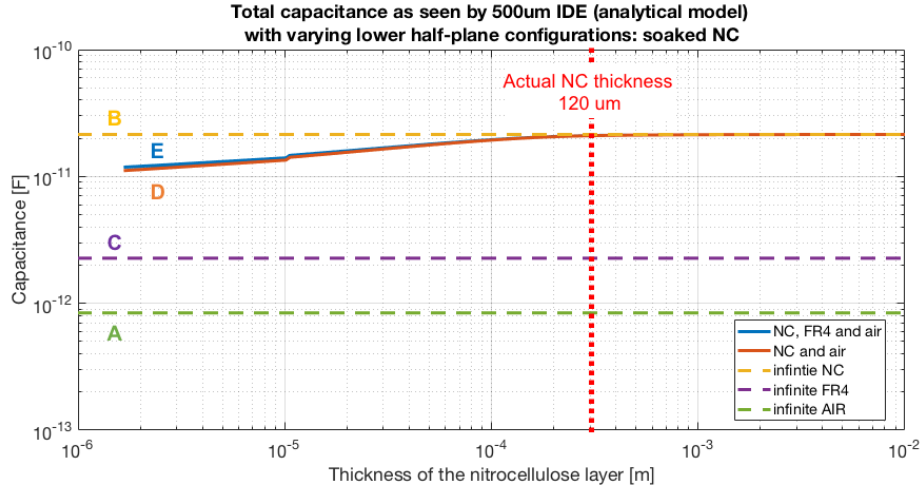
Figure 4.3: Analytical model the total capacitance seen by the 500um finger device (cfr table 3.4) as a function of varying thickness of the nitrocellulose layer. Figure 4.1 summarizes the five different cases. The upper half-plane is always air while the lower half plane varies. The soaked nitrocellulose has a relative permittivity of $\epsilon_r = 50$.

1.2 Analytical values of the equivalent circuit components

Tables 4.1 and 4.2 summarise the different values of the circuit elements in figure 3.1 obtained by the analytical model. As explained by equation 3.1, C_{DL} and C_{OX} for the interfacial capacitance C_{int}, C_{AIR} and C_{NC} for the volume capacitance C_{vol} and R_{AIR} and R_{NC} for the volume resistance R_{vol}. We see that, expect for the dry measurement, the effect of the air layer is small.

To get a qualitative better understanding of the influence of C_{int}, C_{vol} and R_{vol}, figures C.2, C.3 and C.4 in appendix C show the variation of the total simplified impedance function as a result of variation of every component.

Electrode 1 (200 um) with $C_{AIR} = 0.863[pF]$ and $R_{AIR} = 1.05[P\Omega]$				
	C_{DL} [F]	C_{OX} [F]	C_{NC} [F]	$R_{NC}[\Omega]$
DI	$2.89 * 10^{-7}$	$6.12 * 10^{-7}$	$5.61 * 10^{-11}$	$1.59 * 10^{6}$
0.5 mol	$6.15 * 10^{-5}$	$6.12 * 10^{-7}$	$4.90 * 10^{-11}$	3.5
1 mol	$8.17 * 10^{-5}$	$6.12 * 10^{-7}$	$4.45 * 10^{-11}$	3
PBS	$5.28 * 10^{-5}$	$6.12 * 10^{-7}$	$5.22 * 10^{-11}$	6.58
DRY	/	$6.12 * 10^{-7}$	$1.12 * 10^{-12}$	$1.05 * 10^{12}$

Table 4.1: Results of the analytical model of the equivalent circuit elements represented in Figure 3.1 with electrode 1 (200um).

Electrode 2 (500 um) with $C_{AIR} = 0.504[pF]$ and $R_{AIR} = 1.85[P\Omega]$				
	C_{DL} [F]	C_{OX} [F]	C_{NC} [F]	$R_{NC}[\Omega]$
DI	$4.11 * 10^{-7}$	$8.7 * 10^{-7}$	$3.24 * 10^{-11}$	$2.81 * 10^6$
0.5 mol	$8.75 * 10^{-5}$	$8.7 * 10^{-7}$	$2.86 * 10^{-11}$	6.17
1 mol	$1.16 * 10^{-4}$	$8.7 * 10^{-7}$	$2.60 * 10^{-11}$	5.29
PBS	$7.5 * 10^{-5}$	$8.7 * 10^{-7}$	$3.05 * 10^{-11}$	11.57
DRY	/	$8.7 * 10^{-7}$	$6.55 * 10^{-13}$	$1.85 * 10^{12}$

Table 4.2: Results of the analytical model of the equivalent circuit elements represented in Figure 3.1 with electrode 2 (500um).

2 Experimental validation of the model

2.1 Dry equivalent capacitance

As described in Chapter 3 (section 3.1.1), we use both backed and unbacked nitrocellulose paper. To validate the aforementioned single layer hypothesis experimentally, we measured the impedance of the same $500\mu m$ electrodes printed on three different types of supports:

- unbacked nitrocellulose CN140, fixed on FR-4

- backed nitrocellulose CN140: one fixed on FR-4 and one fixed with clips

- unbacked nitrocellulose CN140, deposited on a stack of 5 layers of unbacked nitrocellulose and then fixed on FR4

Figure 4.4 plot the capacitances obtained in these three situations. Note that, since the phase angle is always $> 87°$, we simply divide the whole impedance modulus by the frequency. We observe that the three cases are indeed quite close to each-other.

The multilayer measurements have a capacitance $C \approx 0.963\ pF$, which is really close to the infinite nitrocellulose model ($C \approx 0.985$) in figure 4.2.

The unbacked measurement fits almost perfectly to to multilayer analytical model (case E in figure 4.1).

The backed measurements exhibit a slightly higher capacitance, which is due to the backing (polymer) that is adjacent to the nitrocellulose and has a relative permittivity $\epsilon_r \approx 4.4$. Note that the thickness of NC in a backed sheet is slightly smaller ($\approx 110\ \mu m$) than in an unbacked sheet ($\approx 140\ \mu m$). The relative difference between the capacitance of the backed and unbacked devices is around 15%. This is non-negligible but we will often neglect the impact of backing anyway for two reasons:

1. Adding backing to the model implies a significant complexification of the mathematical model, cfr table 3.3

2. This is a maximum deviation. Indeed, once the nitrocellulose gets humidified, this deviation significantly decreases as it was seen in figure 4.3.
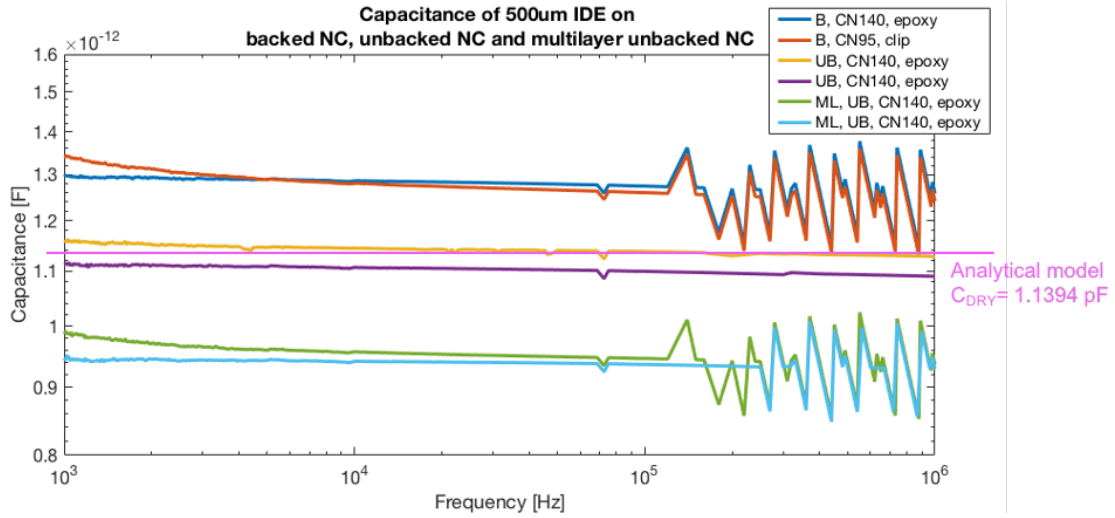
Figure 4.4: $|Z/\omega|$ seen by the 500um fingers in different configurations: *Acronyms: B Backed, UB UnBacked, ML Multilayer.* The pink line corresponds to the expected value computed with the analytical model.

2.1.1 Experimental permittivity of dry nitrocellulose

Dry CN140 unbacked	Dry CN95 backed
n=7	$n = 13$
$\epsilon'_r = 1.37 \pm 0.0026$	$\epsilon'_r = 1.558 \pm 0.0011$
$\epsilon''_r = 0.009 \pm 0.00097$	$\epsilon''_r = 0.0169 \pm 0.00028$

Table 4.3: Complex permittivity of dry undbacked CN140 and backed CN95 nitrocellulose. n is the number of analysed samples per case. Data type: $M \pm \sigma$ with M the mean (over frequency) of the mean frequency behavior (over the n samples) and σ the standard deviation (over frequency) of the standard deviation per frequency value of the n measurements.

The parallel plate test-fixture was used to determine the bulk relative permittivity of both backed and unbacked dry nitrocellulose. Since the polymer backing has a relative permittivity around $\epsilon'_r = 4.4$, it makes sense that the backed nitrocellulose has a slightly higher real relative permittivity.

2.2 Humid model validation

2.2.1 Results

We focus on the $500\mu m$ electrodes which absorbed $30\mu L$ of a 0.5M NaCl solution. A visual control of the samples confirms that the nitrocellulose is saturated with the liquid and that there is no liquid film on the electrode surface.

Based on table 4.2 and equations 3.1 to 3.8, we obtain the three cut-off frequencies of the impedance seen by the IDE:

$$f_1 = 2.99 \cdot 10^4 \ Hz$$
$$f_2 = 1.85 \cdot 10^5 \ Hz$$
$$f_3 = 6.73 \cdot 10^8 \ Hz$$

It was qualitatively explained in figure 3.3 that ω_1 and ω_3 form the transition between interface capacitive, resistive and volume capacitive behavior. This is confirmed by the blue plot that corresponds to the analytical model.
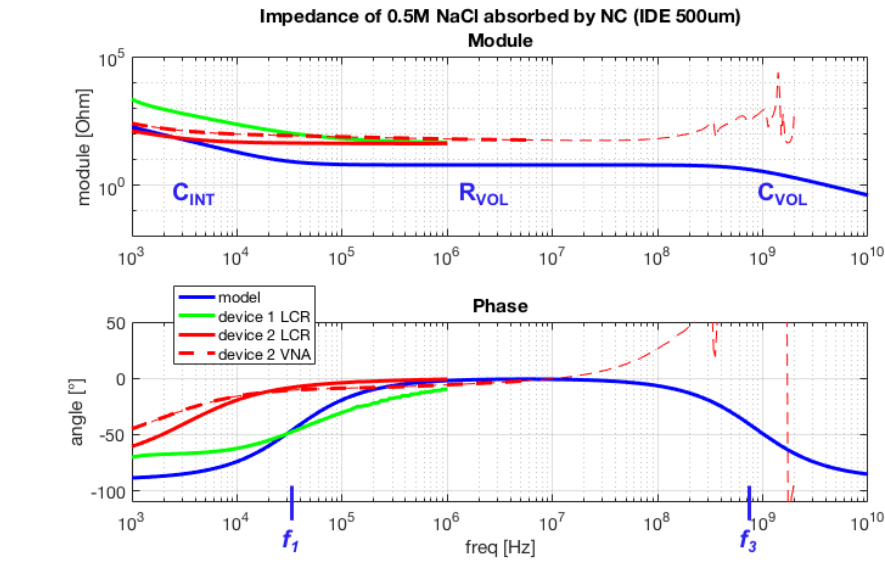
Figure 4.5: Impedance seen by the 500 μm electrodes when the nitrocellulose is saturated with a 0.5M NaCl soluation. The blue line corresponds to the analytical model. Device 1 (green curve) consists of electrodes printed on CN140 unbacked nitrocellulose in the epoxy-setup. Device 2 (red curves) has a CN95 backed nitrocellulose substrate in the clip-setup. (cfr figure 3.18 for visualisation of the set-ups)

The green line represents an LCR measurement made on a CN140 unbacked device. The VNA-data have been de-embedded with an open and closed circuit as was explained in section 3.4.3 in Chapter 3. However, due to noise in the open and close circuit, this deembedding is only reliable up to $10^7 Hz$. We observe that it follows the same trends as the model in terms of frequency. However, an offset is present in the modulus. In particular, the impedance stalls at a higher value on the "flat zone" after the first cut-off frequency.

The red lines represent a LCR and VNA measurement made on a CN95 backed device. Both measurements follow the same tendencies between 10^3 and $10^6 \ Hz$, which confirms the coherence of the measurements. They also converge towards the same resistive plateau as in device 1.
However, between 10^4 and 10^6, we observe that the resistive phase is reached a frequency
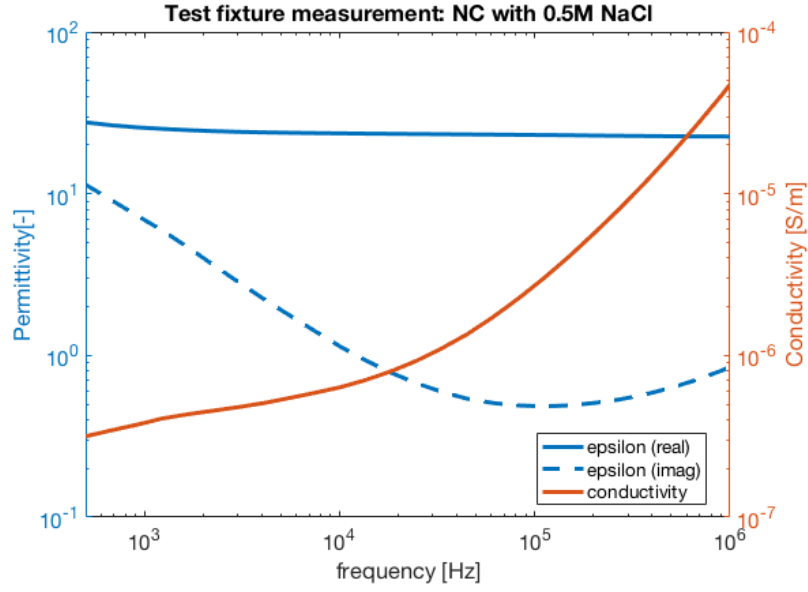
Figure 4.6: Measurement of the real and imaginary relative permittivity of a nitrocellulose sample saturated with a 0.5M NaCl solution

decade earlier.

Based on the data in table 3.2 and the composite membranous structure model described in Chapter 3, we expect the bulk permittivity of the nitrocellulose to be $\epsilon_r = 56.8$ and the conductivity to be $\sigma = 3[S/m]$. Using the test-fixture, we verify whether the experimental permittivity and conductivity correspond to the permittivity and conductivity of our model. The results are plotted in figure 4.6.
The real relative permittivity ϵ'_r is constant over the whole frequency range: $\epsilon'_r = 23.76$ with a relative standard deviation of 4.8%. The imaginary relative permittivity ϵ''_r however, varies significantly over the frequency range. So does the conductivity, which we calculate using from ϵ''_r using equation 3.39.
The mean average loss factor, $tan(\delta) = 0.09$, is higher than for the dry nitrocellulose. This makes sense since a 0.5M NaCl solution is way more conductive than air.

2.2.2 Analysis

Qualitatively, when analysing the difference between the red and blue lines with the help of figure C.3, it looks like the R_{vol} seen by the IDE is larger than in the model. This would explain both the fact that it rises earlier and the fact that the resistive behavior range stalls at a higher impedance. Furthermore, this also corresponds to the fact that modulus of both cases seem to converge towards the same asymptotic value when the frequency goes under $f = 10^3\ Hz$.

Let's analyse the difference between these curves **quantitatively**, in terms of equivalent circuit elements. In table 4.4 we present the results of datafitting with Zview, for the first and second device. Since the experimental data do not reach the frequency range in which C_{vol} is predominant, it was not possible to find any relevant value for this capacitance with

ZView. We compare these values to the theoretical model values and to the "Test fixture" values which combine the measured permittivity and the theoretically obtained cell factor.

	C_{int}	R_{sol}	C_{sol}	χ^2
Model	$8{,}75{\cdot}10^{-5}$	6,17	$2.86{\cdot}10^{-11}$	-
Test Fixture	-	$1.85 \cdot 10^5 \pm 187\%$	$1.23{\cdot}10^{-11} \pm 5.4\%$	-
Device 1	$8{,}91{\cdot}10^{-8} \pm 6{,}5\%$	$76{,}2 \pm 5{,}4\%$	-	0,964
Device 2	$1{,}256{\cdot}10^{-6} \pm 2{,}1\%$	$52{,}6 \pm 1{,}5\%$	-	0,092

Table 4.4: The values of C_{int}, R_{sol} and C_{sol} given by the analytical model and compared to the calculated value with ϵ_r, σ obtained with the test fixture and to the results obtained by data-fitting for Device 1 and Device 2 (done with ZView for Windows). Device 1 and 2 are generical names for correspondance with figure 4.5

We can see that indeed, the model largely under-estimates the resistance seen by the IDE.

Concerning the interface capacitance, a large variation is present in the experimental results: device 1 has an interface capacitance which is one order of magnitude below the model capacitance while device 2 has an interface capacitance which is 37% higher than in the model.

This might be because of varying thickness of the oxidation layers. It can be observed in table 4.2 that C_{DL} is negligible next to C_{OX} when in series. According to equation 3.15, the capacitance is reduced when the thickness of the oxidation layer increases. The electrodes that constitute device 1 have been exposed to ambient air for several months during the lockdown (at controlled relative humidity) while device 2 was used two days after production.
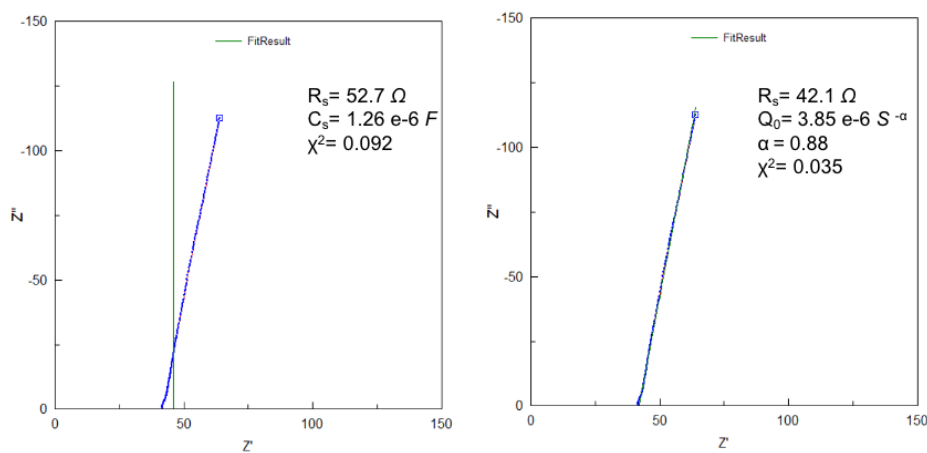
Figure 4.7: Nyquist plot of the impedance measurement made on device 2 (cfr figure 4.5 by the LCR. Datafitting done with ZView for Windows.

It was mentioned in section 3.2.2 of the State of the Art that interfacial capacitances do not perfectly behave like a capacitance. We illustrate this in figure 4.7 with the example

of the measurement made on device 2 with the LCR-meter. As already mentioned, the experimental data does not reach the zone where C_{sol} is predominant, which corresponds to the fact that no half-circle (typical behavior for a parallel RC circuit) is observed in the Nyquist plot. This forces us to neglect C_{vol} during the data fitting. Thus, figure 3.2 boils down to a simple series R-C circuit, which is used for the fitting on the left. For the fitting on the right, we have replaced C by a Constant Phase Element (CPE) (cfr figure 1.17). As a reminder, for a CPE,

$$Z = \frac{1}{Qj\omega^{\alpha}}$$

Conclusion concerning the model

- The values for the permittivity of the dry nitrocellulose obtained by the test-fixture measurement, fits the analytical model and the measurements made with the LCR meter. We observe a difference due to backing. This is also present in the dry LCR measurement but negligible once the nitrocellulose is wetted.

- The experimental results confirm the trend of the analytical model but highlight that this model over-estimates the bulk conductivity.

- A large variation in C_{int} is observed between 2 different electrodes. This is not visible in the dry model when C_{int} is negligible next to $C_o x$ but it makes a difference in the wet measurement. We dedicate this to varying oxidation layer thickness.

3 Bacterial detection

Two media were used for bacterial suspension: both PBS and DI. The bacterial concentration is always $10^8 \ CFU/ml$. [175] We begin by analysing the measurements made by the parallel plate test fixture, after which we introduce measurements made with the $200\mu m$ electrodes.

3.1 Electrical characteristics of the NC with bacteria

In order to avoid perturbation of the result due to electrode cell constant variability and external perturbations that might induce inter-electrode variations, we chose to first focus on the electrical properties of the membranous structure directly, through a parallel-plate measurement with the Test Fixture.

The results for bacteria dilluted in PBS are given in figure 4.8.
We first note that the tendencies of both ϵ' and σ are roughly the same as in figure 4.6.[1] This makes sense since both are ionic solutions.

Due to excessive noise and because of the limited number of sample measurements, we have no reliable signal for the measurement with PBS and bacteria between $500Hz$ and

---

[1]In figure 4.8 the permittivity has a linear y-axis for readability reasons, due to the error bars.

$5000Hz$. We see that above that frequency range, no significant difference exists between the two situations.

Figure 4.8: The real and imaginary relative permittivity of a backed CN95 nitrocellulose membrane, humidified with PBS. The error bars represent the standard deviation over the n different measurements per given frequency. 6 measurements were made without bacteria and two were made with bacteria.

Since the permittivity and conductivity of cytoplasm are very close to that of PBS, it is hard to detect the presence of bacteria in cytoplasm. This is why we chose a solution which has properties that are more distinct from that of living cells: desionised water (DI). As mentioned in table 3.2, DI is barely conductive while cytoplasm is fairly conductive.

Figure 4.9 presents the results of the test fixture measurement for bacteria suspended in DI. Both ϵ' and ϵ'' show a different trend between both scenarios. The trend in ϵ' is rather small and subject to large standard deviation (in the case where bacteria are present). Thus, further tests should be made before any conclusion can be drawn. On the other hand, the trend for ϵ'' is more explicit and less varying. Furthermore, when applying equation 3.39, we observe a global increase of the conductivity in the case where bacteria are present, which lays in the line of the expectations.
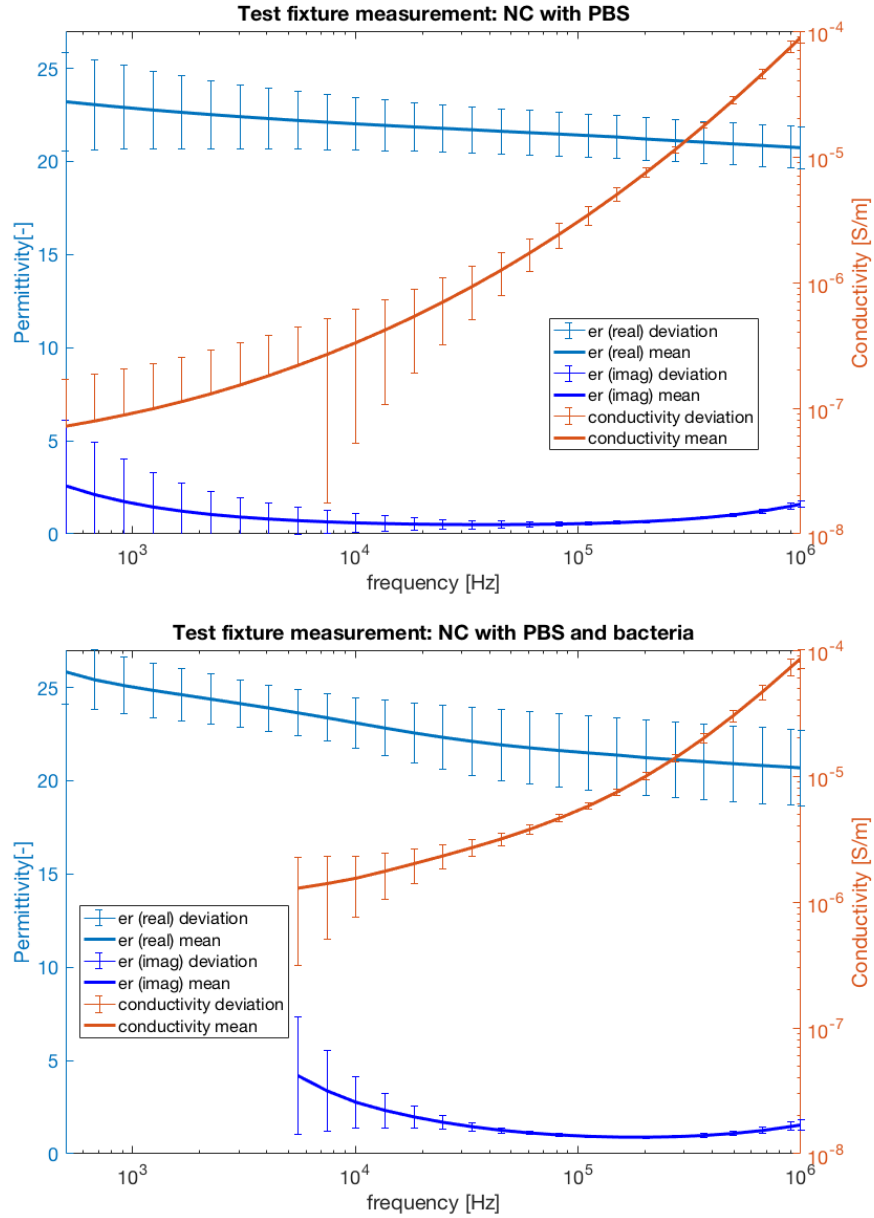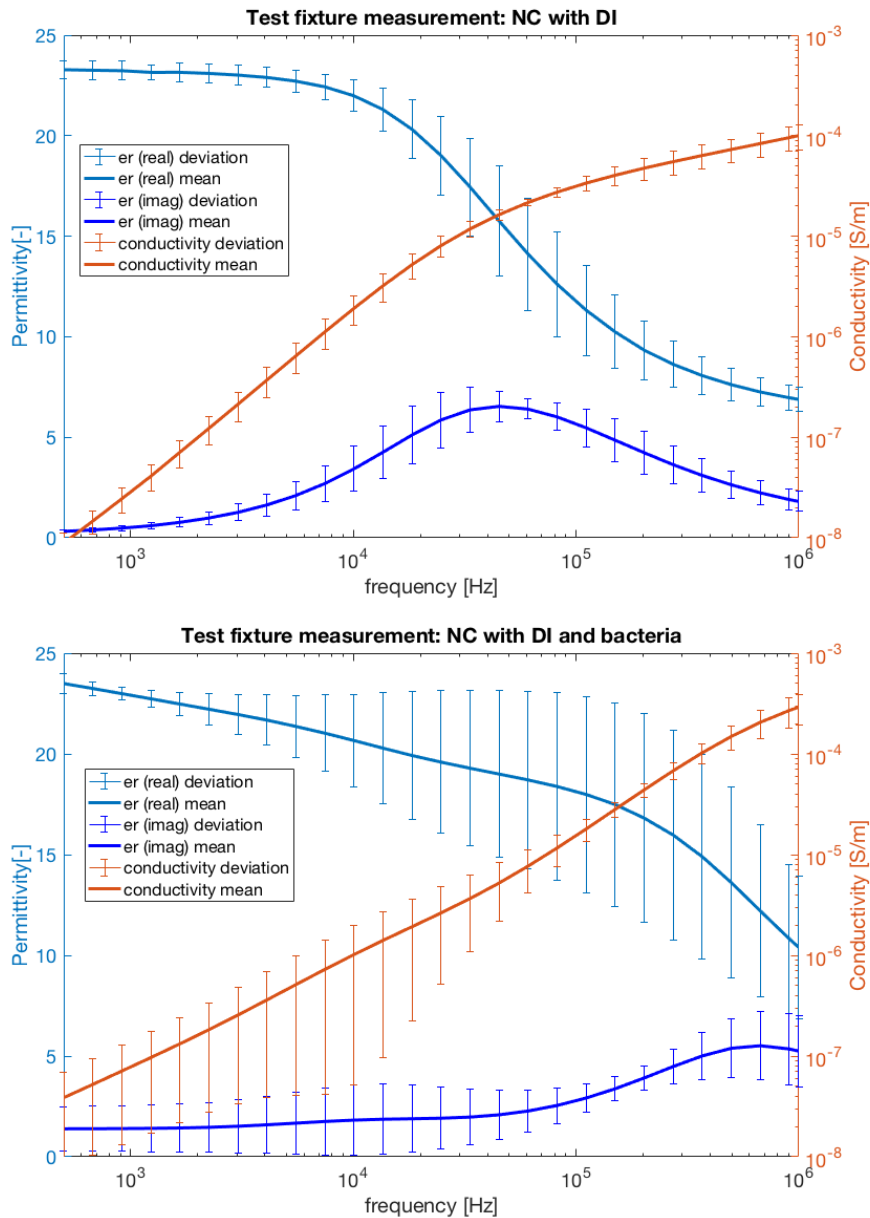

Figure 4.9: The real and imaginary relative permittivity of a backed CN95 nitrocellulose membrane, humidified with DI water. The error bars represent the standard deviation over the n different measurements per given frequency. 4 measurements were made without bacteria and 6 were made with bacteria.

	Humid w/ bact	Humid with bact	Dried w/ bact	Dried with bact
PBS	$n = 6$	$n = 2$	$n = 4$	$n = 2$
	$\epsilon'_r = 21.8 \pm 0.44$	$\epsilon'_r = 22.69 \pm 0.31$	$\epsilon'_r = 1.7 \pm 0.069$	$\epsilon'_r = 1.6 \pm 0.013$
	$\epsilon''_r = 0.97 \pm 0.92$	$\epsilon''_r = /$	$\epsilon''_r = 0.04 \pm 0.008$	$\epsilon''_r = 0.04 \pm 0.022$
DI water	$n = 4$	$n = 6$	$n = 3$	$n = 2$
	$\epsilon'_r = 16.6 \pm 0.8$	$\epsilon'_r = 18.9 \pm 1.8$	$\epsilon'_r = 1.65 \pm 0.0008$	$\epsilon'_r = 1.71 \pm 0.024$
	$\epsilon''_r = 3.15 \pm 0.4$	$\epsilon''_r = 2.68 \pm 0.35$	$\epsilon''_r = 0.016 \pm 0.00047$	$\epsilon''_r = 0.043 \pm 0.0258$

Table 4.5: Complex permittivity of the nitrocellulose membrane in different situations. n is the number of analysed samples per case. Data type: $M \pm \sigma$ with M the mean (over frequency) of the mean frequency behavior (over the n samples) and σ the standard deviation (over frequency) of the standard deviation per frequency value of the n measurements. Drying process: 3 hours outside on a hot summer day, no direct sunlight.

Table 4.5 shows a comparison between measurements made on CN-95 backed nitrocellulose in different conditions. We distinguish the medium in which the bacteria are suspended: either PBS or DI water. The, we consider two situations:

1. The nitrocellulose is saturated with the applied liquid: either with or without $10^8 \ CFU/ml$ of bacteria suspended in them.

2. The nitrocellulose after 3 hours of drying outside, in the shadow, on a warm sunny day.

The manipulations with DI were done as follows: dry measurement, wetting with DI, drying, wetting the same samples with DI + bacteria, drying. Thus, the solution with bacteria is applied to the membranes that already contained a DI-solution without bacteria. For the manipulations with PBS however, we had to take different samples with or without bacteria: indeed, once pure PBS evaporates, it may leave behind residual ions (which are theoretically absent in DI) and thus compromise the correctness of the next measurment on the same membrane.

The **humid cases** are plotted in figures 4.8 and 4.9. The values in this table are averages, both over n different samples and over the frequency range. Relatively, the real part of the permittivity varies less than the complex part of the permittivity.
We observe that the **loss factor** $tan(\delta) = \frac{\epsilon''}{\epsilon'}$ **is larger when the nitrocellulose is humid** than when it is dry. This makes sense since the electrolyte filling the pores is more conductive than ambient air.
A sample manipulation error created excessive noise in the measurement of the relative permittivity for PBS with bacteria. Thus, an averaged value is not available for its imaginary part. When $f > 10^4 \ Hz$, the behavior of ϵ''_r is similar to the scenario without bacteria. For $f > 10^4 \ Hz$, we can not tell with certainty.

In the **dried PBS** case, we observe a small difference in ϵ''_r compared to the dry case in table 4.3. When comparing the dried NC with and without bacteria, it is clear that the observed difference is not due to bacteria in particular, but to residual ions which

remain in the PBS in general.

In the **dried DI** case, we observe a difference between the ϵ_r'' of the dried sample without and with bacteria. However, only two measurements are available for the latter situations and the standard deviation σ is relatively big. Thus, we must not jump onto premature conclusions.

3.2   Detection with electrodes

3.2.1   Bacteria in PBS

In table 3.2, we observe that the permittivity and conductivity of PBS are very close to those of cytoplasm: $\sigma_{PBS} = 1.6$, $\sigma_{cyt} = 0.8$, $\epsilon_{PBS} = 80$, $\epsilon_{cyt} = 70$. When considering bacteria as little "lumps" of cytoplasm spread over the volume of the nitrocellulose, and when using the simplified model for composite media described in section 1.2, the analytical calculations do not expect any visible change in the electrical signal.

Even if the analytical results did not promise any significant change, we did several sets of measurements anyway: indeed, the model being very simplified, it does not very accurately take into account the electrical properties at the interface between bacteria and its solution. It was worth trying.

We used $200\mu m$ electrodes, both functionalised and unfunctionalised, to analyse PBS solutions with and without bacteria. We observed a spectral behavior which was similar to the one discussed in section 2.2 of this Chapter. No relevant tendency was found in terms of bacterial detection. However, there were a lot of inter-electrodes variations. This uncovered that the $200\mu m$ have a cell factor that varies a lot, cfr figure C.1 in appendix C.

3.2.2   Bacteria in DI

Even though tests with PBS revealed an large variation in the cell constant of $200\mu m$ electrodes, we continue using these for the tests with bacteria in DI. The reason for this is simple: while we have only two masks of $500\ \mu m$ electrodes, we have 7 masks for the $200\mu m$. Given that a large enough number of measurements is required to confirm trends in the data, and given that one run of electrode production is very time-consuming, we opt for the latter. This implies that measurements can only be analysed by comparing results per electrode pair: while the absolute changes in value are not expected to be the same over different electrodes sets, the relative changes per sensor should follow the same trends.

In figure 4.10, the blue curves compare two different states of the same electrode pair which we generically call "sample 1". Note that in figure 4.5 the lower frequency limit was $f = 1\ kHz$, while in this case we go down to $20Hz$ in order to get a better grisp on the interfacial phenomena. The full blue line corresponds to the impedance seen by $200\mu m$ electrodes deposited on a NC membrane with pure DI water. After drying, these same electrodes are humidified again, this time by a DI solution with $10^8\ CFU/ml$ of bacteria. As expected, we observe a clear **drop in the impedance modulus**: around $1.8 \cdot 10^5\ CFU/ml$. When $f > 10^5 Hz$, we note a phase shift that goes in the same

direction when we compare it to figure C.3: a drop in R_{vol}.

The red lines represent the average relative difference between absence and presence of bacteria over 3 similar tests, in the same conditions but with different electrodes. The trend is confirmed in all the tests, but with different orders of magnitude. However, the minimal relative difference of the impedance modulus for each sensor is at least 30%, which is significant enough.
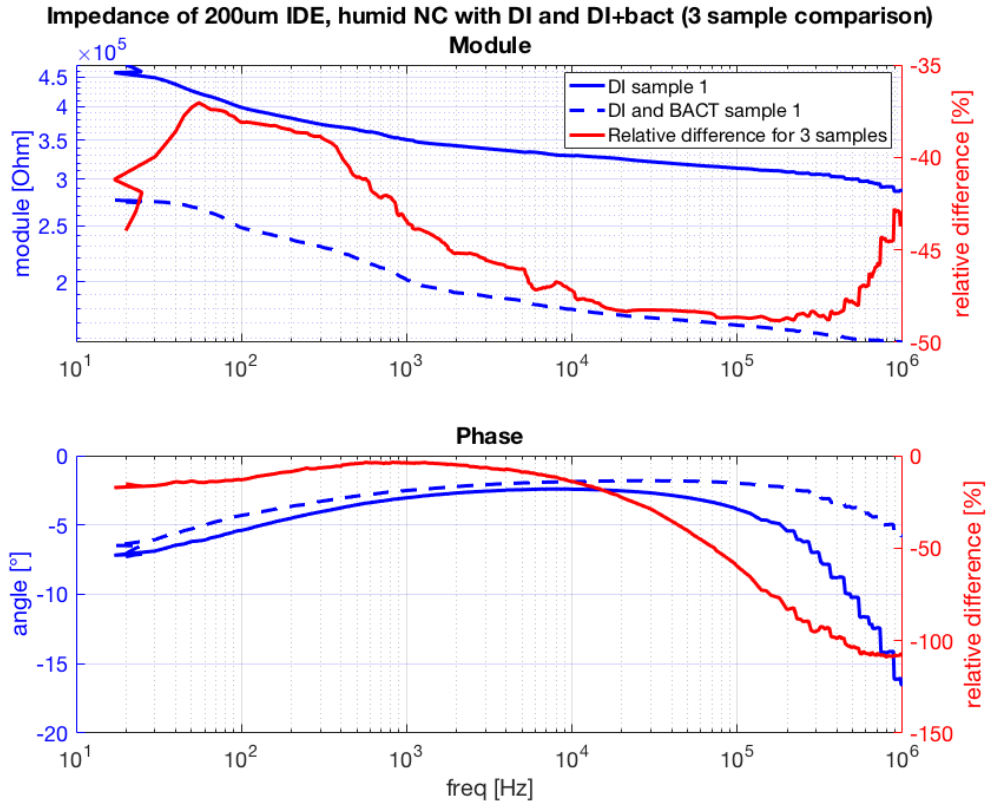
Figure 4.10: In blue: absolute values of the change induced by bacteria in one electrode pair. In red: relative change averaged over 3 samples.

Let's define these observations made for "sample 1" quantitatively, in terms of equivalent circuit. For this, we fit the data to an equivalent circuit using ZView for Windows. To simplify matters, this fitting is done in two steps: one in the frequency range where the interfacial behavior dominates and one in the frequency range where the volume phenomena dominate. As opposed to figure 4.6, the zone where C_{vol} is predominant starts in the measured frequency range. This is because R_{vol} is much larger in DI water than in the solution with 0.5M NaCl, thus all the cut-off frequencies of the impedance are shifted to the left (cfr figure 3.3).

	From DI to DI+bact
Q_0 of CPE_{int}	$+34\%$ ($\sigma = 22\%$)
C_{vol}	-38.09% ($\sigma = 28\%$)
R_{vol}	-25.61% ($\sigma = 18\%$)

Table 4.6: Relative variation of the interfacial and volumic elements of the simplified equivalent circuit. Data formal: M (σ) with M the relative value that is added or substracted to the "pure DI" value in order to obtain the "DI and bacteria" value. M is the average value for four measurements on 4 different electrodes. σ is the standard deviation.
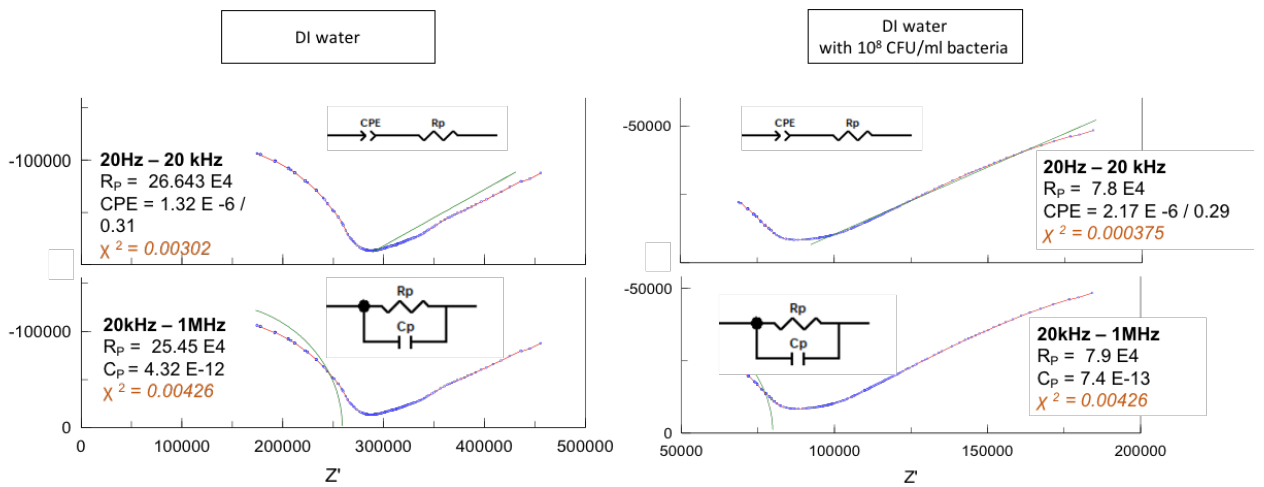
Figure 4.11: Nyquist plot of the impedance seen by $200\mu m$ electrodes. The membrane is humidified either with pure DI water or with DI water in which 10^8 CFU/ml is suspended. Between 20Hz and 20kHz, the interfacial constant phase element dominates. Above 20kHz, the volumic capacitance and resistance dominate.

In table 4.6 we show the relative change in the data fitting results per circuit component, with and without bacteria. Over 4 measurements, the trends were identical (increase vs. decrease) but varied a lot in terms of magnitude (large variation vs small variation).

Conclusion concerning bacterial detection

- The detection of bacteria in PBS is not possible at this point. This is not only due to electrode design: with the parallel plate test fixture, no significant signal was detected either. This was predicted by simulation and is due to the fact that inherently, the electrical properties of bacteria are very similar to those of PBS.

- The presence of bacteria in DI causes a significant shift (order of magnitude 10^5 Ω) in the modulus of the impedance seen by 200 μm IDE.

Chapter 5

Discussion and Perspectives

1 Fitting of the analytical model

The analytical model is merely a simplification of the real physical phenomena. This creates an unavoidable difference between the measured data and the predicted data by the model. In order to minimise these divergences in the future, we present the phenomena which we believe to be the main causes of divergence and enunciate possibilities to avoid them or model them more accurately.

1.1 Interface phenomena

The thickness of the oxidation layer is not constant

Immediately after the deposition of electrodes, when they come into contact with ambient air, a natural oxidation layer forms on the electrode fingers. Since the production is done in the same conditions during the PVD process, and since the ambient air of the WINFAB laboratorium is monitored to be at approximately the same conditions, it is fair to expect that the initial natural oxidation layer is roughly the same for all electrodes. The electrodes are kept in a humidity- and temperature controlled chamber in order to avoid disparities as much as possible. Nevertheless, it is unclear to what extend the "storage time" impacts the electrode oxidation. Indeed, even if we could manage to store the electrodes in the same ambient conditions, we were unable to guarantee that the storage time was approximately the same for all electrodes. Due to the sanitary crisis and the subsequent closure of laboratoria, some electrodes were kept in that chamber for more than eight weeks while others were kept in that chamber for only 12 hours. This could explain the difference in interfacial capacitance between the two electrode pairs studied in section 2.2.

Furthermore, during the measurements with humid nitrocellulose, the electrodes did not have the same exposure time to water. Indeed, some measurements took more time than others, sometimes a setting was faulty and the measurement had to be made again, etc. Here again, it is unclear to what extend this affected the oxidation layer.

Thus, even though we consider that C_{OX} is constant over time and equal for all electrodes of the same geometry, we know that this is not entirely true.

The passivation layer is not perfect

We supposed that no charge transfer occurs between the ionised solution and the electrodes. However, we do not have the guarantee that the natural oxidation layer forms a perfect passivation layer. This may cause corrosion of the electrodes when they are put under tension. Thus, we can not for sure exclude that a little charge transfer occurs.

In order to avoid variability of the interface behavior, it is possible to **coat the electrodes with a passivation layer**, as was done in [11, 199].

1.2 Volumic phenomena

Permittivity and conductivity of the composite material

Measurements of the bulk permittivity of the nitrocellulose membrane with the parallel-plate electrode do not fit the results obtained with the composite media model (section 1.2, Chapter 3) very well. For instance, when the nitrocellulose is humidified with a 0.5M NaCl solution, we expect $\epsilon_r = 56.8$ while the parallel plate measurement indicates it to be around $\epsilon_r = 28$.
Of course, the linear model in equation 3.10 is only a rough approximation, which could explain a deviation. However, since a deviation of 50% is quite large, we suppose that other factors intervene as well.

- **Erroneous void factor:** the void factor of 75% is mentioned in the datasheets of the used nitrocellulose membranes. We did not verify this void vector experimentally. Since the relative permittivity of the liquid is much larger than that of the nitrocellulose, this would have a significant impact on the bulk permittivity.

- **Compression of the membrane:** Since physical contact is needed between the parallel plate electrodes and the membrane, it is possible that the parallel plate electrodes significantly compress the membrane, thus reducing the void factor and increasing the volumic ratio of fibres and pores.

- **Imperfect saturation:** it might be possible that small air cavities remain in the nitrocellulose membrane after humidification. In other words, the pores would not be perfectly filled with the applied solution. The presence of these cavities can reduce the volume fraction occupied by the liquid, which alters the resulting permittivity in the same way as a wrong void factor.

The compression of the membrane can be avoided with an experimental set-up in which an uncompressible dielectric frames the membrane under test partly or completely. The thickness of frame should be as close as possible to the actual thickness of the DUT. The presence of air cavities in the membrane and the void factor can be determined by microfluidic experiments.

Permittivity and conductivity vary with frequency

The data mentionned in table 3.2 are averages over the $10^3 - 10^6$ frequency range. We did not detail their validity outside this frequency range. Typically, once $f > 10^8 Hz$, we

can expect non-negligible variability from these averages. [191]

The results from the measurements with the parallel plate electrodes show a relatively stable permittivity ϵ_r' over the measurement range ($500\ Hz - 1MHz$) but a varying ϵ_r''. This should be investigated further: is it a typical behavior or is it characteristic for the membrane-ion interactions? Tests could be done be a probe which is put directly in the liquid in order to avoid the membranous effect and compare both results.

2   Sample handling and measurement set-up

In this section, we get highlight two aspects that could be improved in future measurement protocols. First, we enunciate several possibilities to increase the quality of the measurement results. Than, we elaborate how the measurements can be controlled better.

2.1   Quality and reproducibility of the measurements

Several factors contribute to the variability of measurements.

Drying process

The **drying rate** of a nitrocellulose membrane is subject to large variability, depending on whether the membrane is functionalised or not, how much water was absorbed, the ambient temperature and humidity,etc. Figure 5.1 shows different behaviors shown by (supposedly) similar nitrocellulose membranes who have undergone (supposedly) the same handlings. However, we observe that the blue and red curves do not show the same trends. The blue dried line shows an amplitude that converges towards the blue initial (dry) blue line, but with a significant shift in phase. The red dried line has a constant off-set from the initial (dry) red line but a smaller phase difference.
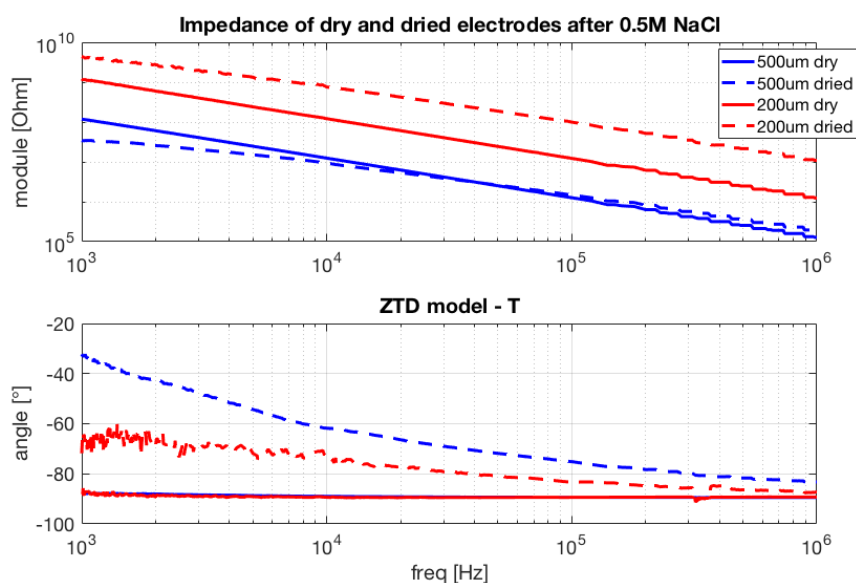
Figure 5.1: Drying results of a 500um and 200um electrode pair, kept overnight in the same conditions

This should be further investigated. First, we should get a better grips on the drying process of the membrane: its expansion, how much residual humidity is left behind, how ions behave if they recombine once their solution evaporates,... Secondly, we should eliminate as much variability as possible from the sample manipulation and the exposure to external perturbations. It is not excluded that, for instance, one of the electrodes in figure 5.1 suffered a mechanical blow that the other did not.

Variance due to external factors

To better understand the causes of this differences, and to eliminate as much variability as possible, it is advised to think of a set-up that allows different electrodes to be printed on the same membrane. For instance, one could imagine a set-up such as in figure 5.2. The idea is to have one collector pad for the fluid of interest, which would spread the liquid over the whole membrane due to capillarity. With the clip setup (cfr figure 3.18), one could subsequently connect the electrodes to the measurement device without damaging the membrane.

- **Homogeneous liquid distribution**: if we assume that the microfluidic flow is uniform, the liquid on the collector pad would spread evenly over the membrane volume. Thus, every printed sensor is exposed to the exact same humidity, and every surface unit of the membrane has the same drying rate.

- **Exposure to the exact same conditions**: the risk of measurement variability due to handling differences of different ambient conditions is reduced since all electrodes are on the same sample.
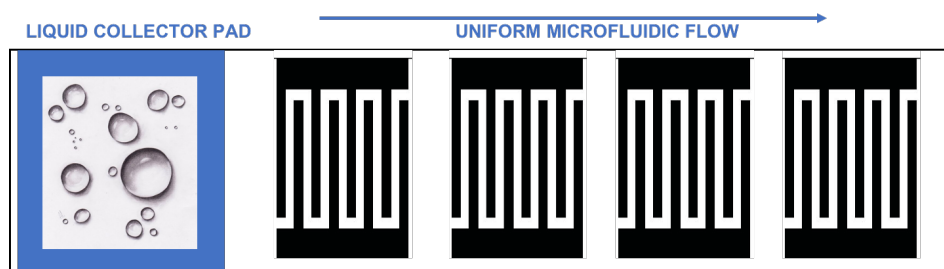
Figure 5.2: Suggestion for a set-up to avoid variability due to different drying rates.

This set-up may be very useful if one wants to analyse the effects of electrode geometry: by printing two electrodes of geometry A and two electrodes of geometry B on the same membrane, we are less at risk to induce bias in the measurement results due to external factors than if they are printed on 4 separate membranes. The same can be done to analyse the effects of bio-functionalisation: we can functionalise the two electrodes on the right and compare them to two unfunctionalised electrodes on the right. Note that the other way around is not advised since the flow goes from left to right: we would not want residues of the functionalisation to contaminate the two electrodes that are supposed to be unmodified.

Variability in water absorption

It was observed that functionalisation alters the absorption properties of the nitrocellulose membrane. Figure 5.3 shows two examples of this. Due to altered absorption capacitance of the paper, the electrodes are exposed during a longer time to humidity before the measurement can be made. This can induce bias due to oxidation. Furthermore, since the absorption is that altered, it is not excluded differences occur within the pores as well, for instance with air cavities. This may affect the bulk permittivity since the volumic fraction of liquid within the membrane would be smaller. The reason for this altered membrane behavior should be studied further in order to analyse if it can be avoided or tempered.

Making the device suitable for RF analysis

It was shown in figure 4.5 that a part of the VNA-measurement range is useless due to noise in the signals for open and closed de-embedding of the electrodes (cfr section 3.4.3 of Chapter 3). For future set-up design, the transmission line theory should be considered in order to facilitate conversion with a signal source that has a characteristic impedance of 50Ω. [218]

Large trend observations

In figure 5.2, we suggested a set-up that allows for several individual measurement on electrodes that are exposed to external conditions which are as equal as possible. Another -complementary- multiple-sensor set-up can be imagined that requires only one actual measurement: we could connect a large number of sensors in parallel and only measure the two extremities of the connection track. This would require to create a new
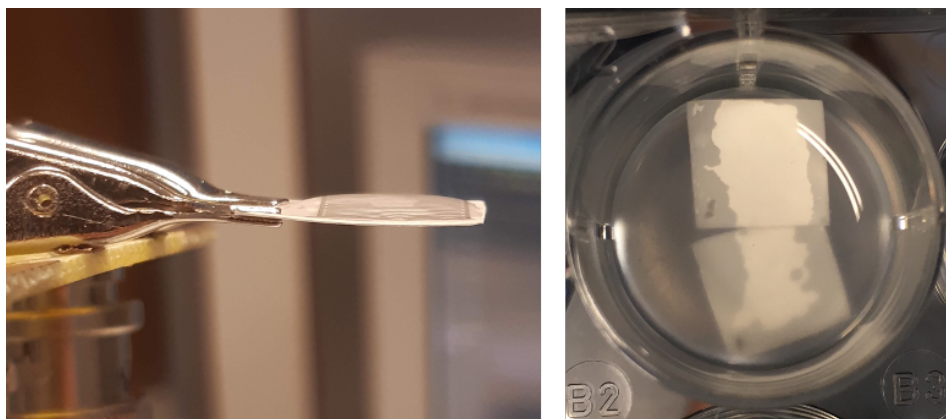
Figure 5.3: On the left: $200\mu m$ electrodes on CN95 backed nitrocellulose which are functionalised and do not easily absorb water. On the right: functionalised backed nitrocellulose membrane immersed in DI water for at least 30 minutes. The white spots clearly indicate a zone in which the water penetration has not yet happened.

mask in which both the IDE as such and the connective tracks are integrated. It offers the major advantage of observing mean trends over several electrode pairs in only one measurement. Since this method does not offer the possibility to trace back individual singularities, so it should be used once the system is mostly understood.

2.2 Measurement control

Control of biological phenomena

Biological phenomena cause different uncertainties. We focus on three of them.

1. It is relatively well known how a colony of bacteria survives in a PBS solution, but it is more difficult to determine **how "well" bacteria survive in DI water**. During our tests with bacteria in DI-water, we visually determined that "some" bacteria were still metabolically active due to the turbity of the solution, but it was not clear if the initial 10^8 CFU/ml were still alive. During the proof of concept, we proved that the bacteria could be detected, but we did not seek to quantify them. However, for further refinement of the sensor, it will be crucial to know how many bacteria are brought in the nitrocellulose. **Real-time visual control** (i.e analysing the solution under a microscope right before applying it to the NC) offers a precise but time-consuming solution. Another- less precise but easier- solution consists of establishing a rough "population curve" of bacteria in DI over time. This can be done colony counting (cfr section 1.2 in Chapter 1) the bacteria in a DI sample every 15minutes.

2. We do not know **how the bacteria spread in the nitrocellulose volume**. Are they blocked by the pore-sizes? If they are applied directly on the electrodes, do they stay at the surface or do they spread over the whole volume? This should be verified visually by taking a cross-section slice of nitrocellulose and analysing the presence of bacteria over the membrane (for instance through fluoroscopy).

3. It is unclear if bacteria survive in the membrane once the humidity is evaporated. As it will elaborated in the next section, the drying period could offer a lot of opportunities for bacterial detection. To enable these possibilities, we should know at what relative humidity of the nitrocellulose bacteria start to implode/explode due to osmotic effect. This could also be determined visually by monitoring the rate of fluorescence of a membrane sample while controlling its relative temperature and humidity.

3   Towards bacterial detection

A proof of concept for bacterial detection was given, which is encouraging to continue prototyping and improving the design.
On the one hand, we should get a better understanding of the bacterial behavior when it is suspended in an ionised solution. On the other hand, we should improve the sensing mechanism in order to work on its selectivity and sensitivity.

Analysis of the bacterial response

We are not yet capable of distinguishing bacteria PBS. Indeed, PBS is very conductive (thus field lines easily find their way around the non-conductive cell wall of bacteria) and the cytoplasm of bacteria has a relative permittivity which is very similar to that of PBS (80 vs 75). Currently, the detected bacteria were suspended in DI water. However, in practice, when bacteria are present in drinking water they are always surrounded by other living cells and ions.
In future steps, these "perturbative" elements should be considered step by step in the measurements, in order to understand the behavior of the bacteria when they are surrounded by ions. For instance: how does the double layer around the bacterial cell membrane affect the global measurement?
The first step after DI, could be to work with **diluted PBS** (e.g 1:1000) as was done in [11]. This allows to observe the interaction of bacteria in ionised solutions, whilst maintaining the visibility of the bacteria.

Sensitivity of the measurement

Compared to table 1.3, we use IDE with very large fingers. This increases the "sensible depth" (which is our objective since we aim at sensing the nitrocellulose volume instead of the electrode surface) but decreases the 'sensitivity per depth unit'. In [224], where bacteria are only bound to the electrode surface, it is said that *"to provide high sensitivity to bacteria, the transducer typically consists of IDEs with finger gap and width of similar size to bacteria. These micrometer dimensions enhance the sensitivity, thanks to a larger active area for bacteria binding and a more confined electric field around the adherent bacteria."*

Several options are worth trying in order to improve the sensitivity of the sensor despite the large finger width.

- The use of **nanoparticles** can help increase the visibility of bacteria. Figure 4.5 shows that there exists a "plateau" where R_{vol} dominates. Such a constant impedance over a relatively long frequency range is an interesting asset for differential comparison. When we oscillate around a given frequency which is far enough from the plateau borders, a difference in impedance can be entirely assigned to a resistance offset without having to consider the slope of the impedance function. Conductive nanoparticles could make a significant contribution to this offset.

- When increasing the used frequency to the **radio-frequencies**, we can specifically target one of the resonance frequencies of bacteria in order to amplify their visibility. A resonator based capacitive sensor was studied in [225].

- **Transient monitoring** has not been encountered a lot in literature but seems to offer possibilities. When the bacteria are in an ionised aqueous solution, they hardly cause any difference in bulk permittivity and conductivity. When the sample is completely dried, the ions recombine while the bacteria supposedly die due to osmotic effect. It is interesting to further explore the transient phase between "completely soaked" and "completely dried" nitrocellulose. Indeed, before dying, the maintain their conductivity while their medium starts becoming less and less conductive (since atoms are recombining) and capacitive (since air takes up more and more volume). We expect that a transient analysis, monitoring the impedance of the system during the drying process, would reveal different trends with and without bacteria.

The latter option is the most feasible with the material at our disposal right now. Indeed, this could be done with the current electrical connection interface. Using multiple electrodes on the same sheet as in figure 5.2 in a humidity controlled chamber could help guarantee that the same humidity is seen by all the electrodes, thus avoiding as much variability as possible.

The use of nanoparticles and RF are possible in the middle and long term. Indeed, the former requires extensive biological preparation and characterisation while the latter requires to adapt our device and its interconnection interface to RF measurement equipments.

4 Towards a fully operational device

Technology readiness level

The area of paper-based biosensors is in its infancy. Thus, a gap remains between the advanced research undergone at academia and clinical applications. This is mainly due to challenges such as substrate fragility, mass production, sample preparation and system integration. Currently, there is a huge amount of research ongoing in order to solve these issues, which is reflected in the peer-reviewed literature with 693 articles on paper biosensors published in 2017. [90]

To be reliable in conditions that differ from "ideal laboratorium conditions", **inherent control** should be added to the sensor.

- **Negative control** should verify that the target bacteria do not go beyond the bio-functionalised zone, thus, that they are indeed captured.

- **Parallel control** should verify the selectivity of the sensor. For instance, if another type of living cell is known to be also responsive to the bio-functionalisation (which may bias the measurement), the potential presence of this cell in the drinking water sample should be verified in a parallel channel.

- **Ambient conditions** should be controlled in order to correct the measurement. For instance, a "dry electrode" (not subjected to the drinking water sample) could be used to measure the air resistance R_{air} and capacitance C_{air}. This should be substracted to the actual measurement according to the equivalent circuit in figure 3.1 in order to suppress the influence of ambient variations of the volume above the electrodes as much as possible.

Performing the measurement

To perform EIS, a precise power-source and impedance measurement device is needed. Currently, existing electrochemical micropads are often equipped with a bulky equipment device, which prohibits proper point-of-care use. [88] More compact measurement devices are often expensive.
However, several initiatives exist to develop cheaper and compacter equipments for PoC electrical measurements. For example, an inexpensive, open-source potentiostat, so called 'CheapStat', was also developed based on a microcontroller-based electronic circuit. [226] This device is capable of carrying out various electrochemical protocols and providing sufficient performance in chemical and biomarker detections.

A study in [227] aims to develop low cost, portable and compact impedance analyzers. that can operate in a frequency range of $10^3 - 10^5$ Hz. Self-calibration functions are implemented. The device can calculate optimal gain values before measurement to avoid errors due humidity and temperature. Gain resistors can be automatically switched accordingly. [82]

Ideally, the sensor requires no further equipment than what citizens "currently" posses. It would be a major advantage if the EIS signal could be directly generated by a smartphone. Several other embedded systems for EIS are reviewed in [78, 93, 212]
Linkage to the smartphone could also help for data treatment and dispolay[228]. The sensing device could be connected to an application that displays the measurement result in a user-friendly manner.

Chapter 6

Responsible design: usage perspectives

1 Towards responsible design

Technologies are not neural. Several critical aspects may condition the manufacturing of the technology in the long term, such as the availability, access and extraction of raw materials, the impacts of typical elements for biosensor developments (materials and energy-consuming processes) and its impacts on the environment (e.g. toxicity). Along with the raw material impact assessments, societal implications of technologies must be collectively managed towards socially robust decisions on their development and implementation.

Our team is conducting innovative researches with the aim to develop appropriate, alternative, sustainable biosensors for affordable water quality assessments. Such disruptive ways of electronics design require multidisciplinary impact assessment studies about how these alternative products could be more appropriate than the current counterparts. Specifically, there is a critical need to integrate holistic impact assessments (performances, environment, socio-economic) at the technology design level to anticipate new technology-related consequences hidden at first sight, and to make deliberate and informed choices with these consequences in mind.

As researchers in the applied science field, we emphasise on considering the limits of our skills and techniques in solving societal problems. We therefore insist on the necessity to be surrounded by experienced mentors in the explored fields when conducting such an evaluation. Technology assessments require **multidisciplinary, systematic methodologies**, applied on the whole technology value chain. **Life Cycle Thinking** is the general approach which recognizes that a balance is necessary across the three pillars of sustainable development: environmental, social and economic. In order to integrate all the possible dimensions in a holistic methodology, we question the technology considered at the system level (i.e. integrated solution: production, device and information system in a societal ecosystem).

When we think about the development of a user product, we tend to think in economic terms: is it profitable? However, for a product to be sustainable, it must not only be
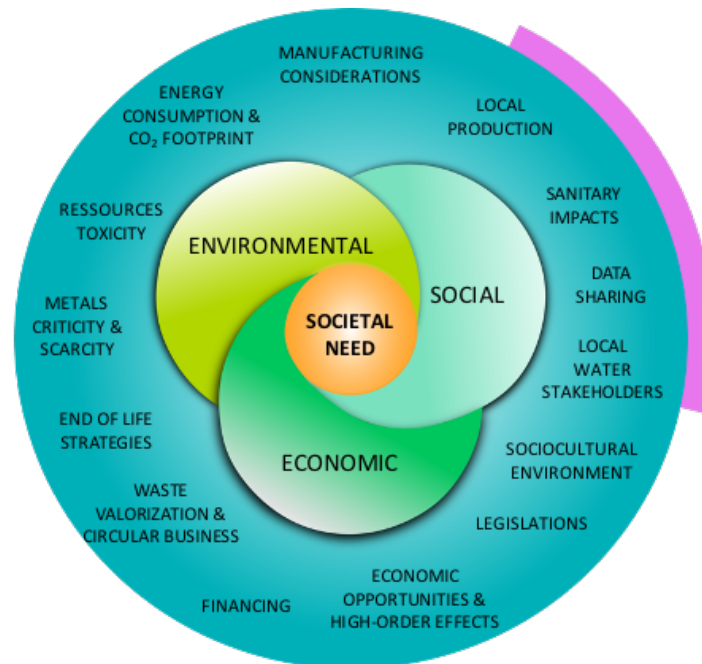
Figure 6.1: Emergence of research questions for the multidimensional analysis of affordable water quality sensors. Life cycle thinking applied to the three sustainability pillars shows the emergence of questions all along the technology value chain, and from Cradle-to-Grave. The scope of this chapter is indicated in pink.

profitable in terms of financial benefits: in the long term, it must also provide social and environmental benefits. A useful tool for systematically analysing these three levels, is the Triple Layer Business Model Canvas (TLBMC) (appendix D).

In the context of the PhD project that led to this master thesis [3], several multidisciplinary impact assessments are involved. 2019-2020, two parallel assessments were concluded:

O. Crahay carried out a simplified LCA [7] comparing nitrocellulosic paper to PDMS as a material supporting the microfluidics of the sensor. Two environmental indicators have been selected to be studied in this assessment: the embodied energy and the CO2 footprint. Both materials and manufacturing processes are contributing to the environmental impacts. Manufacturing processes and, in particular, some of the microfabrication steps included in the sensor development process, are highly energy-consuming and have a significant CO2 impact due to the chemical used. The choice of raw materials can also be critical because of the often significant embodied energy and CO2 footprint associated with their extraction and/or production.

Alongside production process and materials, a usage-oriented assessment was made in this work. Indeed, an accessible and cheap sensor might become widely spread, thus adding a lot of information in community structures. However, this information can be biased in many ways: due to a fault in sensor design, due to wrong sensor handling, due to misreading or even intentional information manipulation. From a usage perspective,

this sensor gives consumers an unprecedented access to information concerning the quality of a vital good: water. What is the fairest and most accurate way to manage this information? How to anticipate usage faults leading to inconvenient and non-desirable consequences right from the sensor design?

2 Drinking water is a matter of trust

The stakes of water are double: water is both a matter of **access and quality**. Access to water on the one hand is fundamental for life, water quality on the other hand is crucial for health. Water-security also has an important role as socio-economic catalyst, as was explained in the introduction.

Water security is determined by the complex interactions between:

1. **Hydrogeological aspects:** both the abundance and the quality of available water vary a lot due to geographic disparities.

2. **Technological aspect:** harnessing, transport and purification techonologies have key roles in water management. They can even counterbalance geological short-comings.

3. **Societal aspect:** water security is largely dependent on governance systems, infrastructure management and user needs and values.

As long as access is not acquired, quality is a secondary variable. Indeed, given the necessity of water for our organism, the choice is easily made between "bad water" and "no water". However, once access is abundant, quality will influence water access accommodations strongly. When we have a choice between different accesses to water, quality becomes one of the decisive factors in that choice. Therefore, quality is called an **economical variable**.

However, the quality of water is never completely certain: one can only be sure for a 100% that the water did not contain pathogens after the water has been consumed. This makes water is an **experience good**: its quality can only be evaluated during and after consumption. Thus, drinking water is a matter of trust: "given the other options that I have, and given that I need to consume water somehow, do I trust this water enough to drink it?". From an economical point of view, quality and trust are very closely related. When selling water, it is not about selling the best quality, it's about having the best reputation concerning the sold quality.

Since the risks of drinking water are not known beforehand, **institutions** are created in order to manage these risks: they have a function of expertise, control and vigilance. **Legislation and certification** are tools used by institutions in order to guarantee a minimum quality. Legislation marks minimum and/or maximum thresholds for components in water. As can be seen in figure 6.5, the "human scale" water cycle contains different stages, on each of which quality alteration may occur.

- What is the water quality at the captation point? Is there any form of contamination?

- Is the water filtered and treated? If so, to what extent does that improve quality?

- Does water transport harm its quality? Are there leaks or local sources of pollution?

Answers to these questions are inherently incomplete. Indeed, not every drop of water is monitored at every moment and at every location. Furthermore, the existing monitoring data is not equally accessible to all actors. This may be for self-interest, for example when a company does not benefit from being known to pollute soil; or for efficiency considerations, for example when a distribution company publishes monthly reports summarizing the data rather than publishing each data point separately.
Thus consumers do not possess the same information than water accommodation and distribution actors. Even between these actors, there can lots of disparities: one may have more or less information than the other. It is said that water quality is often subject to **information asymmetry**.

Laws and standards are used to ensure a minimum required symmetry in the information asymmetry: they can oblige actors to publish reports on quality and give powers to institutions to monitor the follow-up of imposed minimum and maximum concentrations. In general, when these institutions are functional, the trust of consumers in the water quality is maintained. However, when these institutions are non-functional, the trust of consumers is altered. In that case, they rely on other actors than these institutions to make their choice, such as **labels** by independent organisations or the "reputation" of a distribution company.

Apart from asymetry of information, society is also subject to **expertise asymmetry**: not all citizens have the knowledge or scientific background to understand what water quality is, by what parameters it is determined and how these parameters can be monitored. This can even intermingle with the socio-cultural context of citizens and can generate general beliefs such as "water that creates enough foam, is qualitative water". **Training and education** are crucial tools to rectify the existing expertise asymmetry as much as possible.

3   Citizen science as a trust-tool

Water is a matter of trust, but this confidence can be based on a multitude of factors, science being one of them alongside cultural and local beliefs, personal experience, reputation and mimetic thinking.
The implementation of a sensor is only useful when citizens trust its outcome. However, **trusting a sensor and the science behind it, is not self-evident.**
For the most precarious communities, the gap between science and citizens can be critical. The trust in scientific research can be very unstable, leading to for example the non-acceptance of the sensor result.

Furthermore, since members from these communities are underrepresented in the scientific community, research objectives might be irrelevant for them. Scientists and institutions bring their own preconceptions, motivations and biases, often in the form of

implicit assumptions that are based upon their personal, professional and social experiences. These assumptions are expressed when proposing research questions, collecting data and interpreting data, and making recommendations. They may however strongly differ from the assumptions and interests of the affected public. These influences and assumptions mean that "**science itself is an object of representation and misrespresentation, in a wide variety of settings**". [229] Without engaging a broad public that includes underserved communities, scientific projects are at risk to becoming blind to the concerns of those communities, thus reinforcing existing inequities.

Citizen science offers a lot of perspectives in **bridging this gap**. It addresses the importance of engagement and relevance to diverse communities, offering improvements in both ways: on the one hand, citizens feel closer to science by learning to use the sensor. If the project is framed properly, citizens participating to the project have the opportunity to get a grip on the scientific principles behind the sensing mechanism. **Since they are given the possibility to understand the establishment of the measurement, they become more likely to trust its outcome.** On the other hand, the scientific community becomes more aware of the diverse realities of local communities, enabling them to make their research topics more significant.

Success stories on that regard have been reported. For instance, community based participatory research (CBPR) is a research methodology in which power is distributed among community and scientific partners in all aspects of the scientific method in order to improve decision making and/or stimulate action and policy changes. It intentionally spans both research and advocacy to address complex environmental issues affecting underrepresented communities. [230, 231, 232] For example, local groups in Namibia and Nigeria have initiated and developed partnerships with scientists for monitoring uranium mine sites that had provided little accountability to local communities regarding radon hazard and safety precautions. [233] In the US, the standards for the fracking industry were enforced after a citizen science project highlighted large concentrations of benzene, hydrogen sulfide, and formaldehyde near fracking sites. [234]

It will be discussed that the structural organisation of the citizen science projects framing the use of the sensor may vary according to the social context. However, to ensure the quality of the measurements, and thus, **to make the citizen science project trustworthy and relevant, there are some basic observations to consider.**

Firstly, it was already introduced in the State of the Art that not all citizen observations are created equal. [169] Indeed some observation events are more valuable than others due to differences in temporal and spatial resolution. If the project involves a common database, it is important that the spatial and temporal resolution are high enough in order to make the dataset as a whole reliable. This **optimisation** may vary a lot depending on the research question.
For instance, the air-quality mapping project from Over.Meten, which is described in the State of the Art, benefits from the smoothest possible distribution of data points, both in the temporal as in the spatial scale. For a water quality sensing project, the optimisation of data point resolution is different when the objective is to know the

quality of water over the whole length of the river, than when it is to monitor the water quality at one specific point where water is drained. The latter is more "usage-oriented" while the former is "global mapping".

Secondly, a big inequity is added to the dataset due to variables at the moment at which the sample is taken. Indeed, **bias can be introduced by both varying ambient conditions and sample handling.** As mentioned in chapter 5, the former bias can be partly neutralized by differential measurement, which are inherent to the sensor and do not require any human intervention.

The latter bias however, is inherently human. One of the reasons of fluctuating sample handling is **asymetry of expertise**, also referred to as "interobserver skill biases" [169], which covers the fact that some users will be more qualified to do the manipulations than other users. Further sampling biases can be due to the fact that citizens have more or less time, more or less equipment,...

The number of biases to take into account needs to be reduced as much as possible, allowing for both simpler statistical data processing techniques and more reliable results. Thus, a clear and rigorous **protocol** should be established. The manipulations should be as simple as possible, requiring as less time and equipment as possible. In the end, experts trust citizens to make the measurements correctly. It is thus interesting to note that in order to have a fruitful citizen project, mutual trust is key

Thirdly, the confidence of citizens is highly dependent on the forms of **communication** towards them. As explained in [235], "all environmental communication must be relevant, transparent, credible, accurate, verifiable and not misleading." Depending on the usage scenario of the sensor, this can take shape in different ways. In any case, the span of the sensor must be displayed very clearly throughout this communication: the sensor "only" measures a bacterial germ count and is not an absolute guarantee of potability. In order to be relevant and credible for a local community, the content of the output display must consider as much as possible the "local truth" of these communities.

4   Societal impact of the sensor

Our goal is to take a forward leap to the last step of figure 2.1. We think about what roles our sensors can play, whether these make sense and how they can impact society. As we mentioned earlier, technology is not neutral: **choosing between sensor designs is choosing between future impacts**. In order to tend towards responsible engineering, it is crucial to consider what impact the new design can have on society, for better or for worse.

On a master's thesis level, we anticipate not only the potential impacts of the design of the sensor itself but also the impacts of the information system that is supposed to accompany it in collecting, storing and interpreting the sensor data.

This is a complex problem which is multidimensional and constantly evolving. A systematic analysis tool consists of developing a framework for critical thinking that recognizes the complexity and the interdependence of the system. One approach is to split the problem in layers as illustrated in figure 6.2. The fourth stage is the most challenging
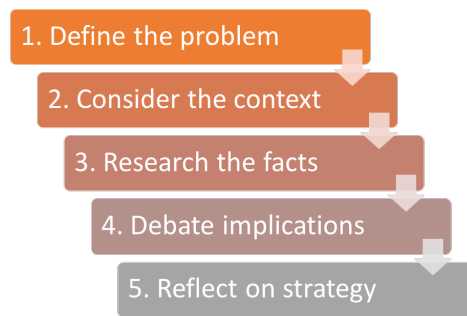
Figure 6.2: Layering as a way of thinking about complex problems. (based on [236])

for a systematic analysis because it weighs up elements that are difficult to quantify and compare, such as personal judgement and cultural values.

In the following subsections, we introduce the problem statement. Then, we consider the context of two reference situations. The first is in Belgium, where the tap water is generally trusted to be qualitative. The second is in the Philippines, where the trust in tap water quality is low. The ARES-PRD BIMWAM project provided us with very valuable information and insights to establish the latter case scenario.
We initiate a (non-exhaustive) fact-finding for both situations and discuss the implications the introduction of the sensor can have in both situations. Finally, we propose a usage strategy of the sensor.
This analysis is not intended to be complete, rather it attempts to set out an initial analysis of usage scenarios, which is to be refined later.

4.1 Definition of the problem

For the final sensor usage scenarios, three **hypotheses** are made:

1. The sensor is made of accessible and cheap materials

2. Its manufacturing is easy and has a production process which is accessible for the targeted communities

3. The sensor output can be sent to and processed by an electronic device such as a smartphone [228]

If we consider a community as a (relatively) balanced system, enabling a wide use of such sensors will put a whole lot of new information into this system, thus creating a **new equilibrium** point around chich the system balances.
In this new equilibrium point, the **(a)symetry of information is altered:**

- Citizens who never had access to any kind of information about their drinking water, now have access to information about its microbial pathogen content

- The sensor may give a different outcome than the information that was already available for (certain) citizens.

- Even though technology lowers the barriers to information, social structure still plays a decisive role in who can effectively access and use this information. This is also true the other way around: creating new accesses to information can alter societal structures.

Based on this, **we formulate the problem as follows:**
Given the easy access to a measurement result of this sensor, the majority of the population can fluently obtain information about the number of bacteria in his/her drinking water. However, the quality of drinking water is a complex matter that has many more facets than just the number of one particular bacterium species.

- What is the best way to translate the measurement result for the user, knowing that this result only reflects a part of the reality and also that not all users have some kind of scientific background that allows them to look at the result critically?

- Moreover, the sensor is intended to be widely distributed. This increases the number of measurements, but also the number of potential errors. Causes of wrong measurements can be linked to wrong manipulation of the sensor, wrong manipulation of the sample or production errors in the sensor itself. What consequences can these errors have? How can these consequences be minimized?

4.2 Contexts, fact-research and implication study

4.2.1 Case 1: drinking water in Belgium

For this study, we analyse the situation in Flanders. We focus only on one part of the country since water management is a regional competence. Of course, the conclusions are transposable to Brussels and Wallonia.

As in most countries, **distribution networks** form a major access point to water. The installation of this structure requires huge fixed entry cost (the investment cost to build up the network), while the marginal cost per trans- ported volume unit of water is relatively constant and very small. High entry cost creates a situation of **natural monopoly**. In such a situation (see [237] for a first formalization), multi-firm production is more costly than production by a monopoly". Thus, autorities have created a **legal monopoly** for the distribution network: it is operated on a regional basis by an appointed organisation.

The Flemish territory is divided into 10 zones which are run by 10 different distribution companies. The Vlaamse Milieu Maatschappij (VMM) is the overarching body who oversees the drinking water control and the applications of the standards which are elaborated by AquaFlanders and BelAqua. Flanders imports 16% of its drinking water from Wallonia and Brussels. The remaining 84% are half groundwater and half surface water. [238] Wastewater is managed and treated by Aquafin before being released back in surface water flows.

In general, it is trusted that the water distribution **accommodations are functional**, that the **legislation is adequate** and that there are enough checks on compliance

with the standards. Drinking water companies publish trimesterial reports[1] and the VMM publishes yearly reports of the global drinkwater quality.[2] The drinking company FARYS reported to have effectuated over 10.000 measurements in 2019. [239] The VMM effectuates **systematic controls** in public buildings and random controls at any point of the distribution grid.

Information asymmetry is present but rather small: both polluting companies and drinking water distributors are submitted to numerous controls and are obliged to publish reports. However, the trust of citizens is not dependent on these reports. [240] Indeed, few citizens spontaneously read these: they only consult it in specific situations (e.g when considering to buy a water softener). Citizen's confidence stems from a general confidence in public institutions on the one hand, and the proximity and availability of drinking water distributors. If citizens have doubts or complains about their drinking water quality, the distributor comes within 12h to take a sample of the water and analyse it. FARYS reported to have had 51 complaints concerning water quality in 2019, of which 31 were well-founded.

Expertise asymmetry exists but concerns mainly the technical and detailed aspects of water composition: indeed, the majority of citizens is capable of understanding the main matters and stakes of water quality. This also implies that a lot of citizens have a basic grip on what the device measures, which **fosters confidence in the sensor outcome**.

Other sources of drinkable water are available, such as **bottled water** in supermarkets. Choosing for that type of water is not a necessity nor a quality issue: it is a mere matter of taste and practical considerations.

Given the existing trust in the distribution system, we expect the same behavior as with the Over.Meten project explained in the State of the Art. Because citizens feel no real need to have extra control of their drinking water quality, the sensor will be purchased mainly out of **curiosity**: we therefore expect a modest interest from people who have time to make the measurements.

On the opposite of the Over.Meten project, a common database would make less sense here. Indeed, in the Over.Meten project, the air quality measurements are done automatically every hour once the sensor is installed. The temporal resolution is thus the relevant enough to map the data points per hour and create a general overview of the air-quality in the city. In the case of our water sensor, interested citizens will test their drinking water regularly but -if the quality of water is as good as it is trusted to be- the interest will eventually fade out. Thus, the **temporal resolution of the measurements becomes less and less relevant**. Moreover, the sensor is likely to be used by the minority of people that has doubts about their drinking water (for instants, the 51 people who complained to FARYS about their tap water). In the end, the database will be extremely biased since these bad samples will be the majority of datapoints, while in reality they form a minority.

If a test were to indicate an unhealthy amount of bacteria present in drinking water, given the existing trust tapwater quality, the first element that would be questioned is the measurement itself: was the sensor faulty? Was the sample well manipulated?

---

[1]e.g. https://www.farys.be/nl/watersamenstelling-en-hardheid-in-jouw-gemeente
[2]https://www.vmm.be/publicaties/kwaliteit-van-het-drinkwater-2013-2018

Figure 6.3: Water quality trust chain in Flanders (Belgium). If an error were to occur, the first insitution in which citizens will lose their trust are the local drinking water distributors such as FARYS or De Watergroep. If this proves insufficient, the overarching and controlling organism, Vlaamse Milieu Maatschappij, will be questioned. Next, the norms imposed by the European Union will be challenged. Finally, if the pathogen is caused by a phenomenon that is not even considered in the standards, the scientific community will be disputed.

Once the result is confirmed, citizens will reconsider their trust in institutions following a 4-step **trust-chain**, which is schematized in figure 6.3:

1. Is the accommodation of the distribution network near my home as reliable as I thought?

2. Are the routine tests and controls, effectuated by the VMM, complete enough?

3. Do the experts of the Flemish government have sufficient knowledge? Are the norms of the European Union sufficiently accurate?

4. Can "science" be trusted? Is there a source of pathogens that "the scientists" have not yet discovered?

From the moment the VMM is started to be widely questioned, a common database becomes relevant: intrigued citizens will start to make more and more measurements, thus making the temporal and spatial resolution of the database relevant.

In conclusion, as long as the water quality stays maintains its current quality, a point of care pathogen sensor will not be used daily on a large-scale. Even though it may attract some curious participants in the beginning, this will eventually fade out as was the case in the Over.Meten project explained in the State of the Art.

However, this does not preclude the sensor from being of interest for **niche applications**:

- Cooling water of industrial processes is a breeding ground for the legionella bacteria. In 2019 there was an outbreak of legionella in Ghent due to a paper factory that had discharged cooling water into the canal. [241] This caused the hospitalisation of more than 30 citizens and the unfortunate death of one patient. This proves

that there is still work to be done: companies have to monitor the quality of the water they discharge very well but at the same time are not eager to spend a lot of money on this. A cheap point-of-care sensor with which a daily test can be done is a possible solution for this. [242]

- When the Belgian army engages in civil or military actions abroad, an environmental check is carried out by the veterinary service of the army. The current field laboratory is equipped with a PCR machine to check the number of bacteria. This already works quite well, but it is relevant to be able to do tests in a more frequent and faster way. [243]

- In the light of recent COVID-19 pandemic, the importance of "strategic stock" has become clear to policy makers. It is not unthinkable that the current water infrastructure will one day reach its limits, for example with an uncontrolled outbreak, a bio-terrorist attack, etc. Thus, even though the relevance of a wide-scale usage of such a sensor might nowadays seem small in Belgium, it might be useful to have them ready "in case of".

- Also due to the COVID-19 pandemic, the resilience of the Belgian and European health-care institutions is pushed to its limits. A sensor which is similar to the drinking water sensor could be imagined in order to detect pathogens in bodily fluids. This is briefly discussed in section 5.1.2 of this Chapter.

4.2.2   Case 2: drinking water in the Philippines (ARES-PRD BIMWAM)

In the Philippines, the water distribution accommodations are inefficient. They are mainly privatised and very scattered. In some regions the accommodations is run by the government, in others by local organisation. Some regions have a mix of both while others have none.

Philippinean institutions lack structure, drive and resources; making it impossible to guarantee sufficient quality of water from the distribution network. Furthermore, insufficient legislation causes the impunity of polluting industrial activities and insufficient organisation causes uncontrolled waste dumping. This implies that other -natural- water resources, if available, are at high risk to be unhealthy. Private companies with government labels sell purified water at **refilling stations**; making potable water accessible but relatively expensive: the selling price depends on the reputation of the company and varies between €0.25 for 20 liters to €1.25 for 20 liters. For a lot of citizens, this is a significant part of their budget.
This causes a **separation of water use** according to its origin: water from the network is used for washing, cooking, outdoor applications,... while drinking water is bought at specific refilling stations where citizens fill their bottles.
The **information asymmetry** is rather significant. Industries are not held accountable in terms of pollution, and given the disparity of the distribution organisation, water quality data are not clearly bundled. Some consumers have no information at all about their tap water, they refer to "its reputation" and "its aspect". This may imply important **expertise assyemtry**: not all citizens have a grasp on what determines their water quality.

In order to empower citizens in their choice of drinking water supply, the need for daily water quality checks is substantial. This could help people to **be more informed and make a conscience choice** between (more expensive) refilling stations water, (cheaper) tap-water and other sources such as groundwater, which is however not always available and has a risk of being contaminated by garbage and/or chemical pollution.

The easy availability of the sensor is essential, but not sufficient for its use to be widely spread and relevant. As it is pointed out in [168], it is not self-evident that citizens who effectuate a measurement **take ownership of its content**, let alone adapt their behaviour according to the measurement results: "If I do not see direct side-effects of the water quality, or in other words, if I do not see my neighbours get sick, would I really pay more money or do more effort to find another water source, just because a certain device told me that that is a good idea?"

Given that everyone needs qualitative water, **social inertia** and societal structures are very important catalysts: "on my own I would not be eager to pay more for access to better water, but if my whole neighbourhood is willing to participate, I am too."

In this case, creating a citizen-science based database can have several advantages

1. Creation of a sense of community, which can be a leverage to adopting change in behavior or change in organisation of access to water

2. Comparison with other measurements in the neighbourhood allows to filter out singularities due to, for example, a faulty sensor.

3. A robust database gives more credibility and arguments to appeal to the authorities for improved water management and distribution.

When creating a common database however, it is crucial to avoid as much bias as possible in order to allow for useful statistical analysis. Figure 6.6 compares the types of bias that can occur due to wrong information transmission or insufficient expertise of the participating citizen. We distinguish two cases: when the participant reads the result and encodes it manually in the database, and when the result reading and transmission to the database is completely autonomous. It is clear that the latter offers a better **bias-mitigation**. However, this automatic completion of a database requires special attention at two levels.

First, in order for citizens to trust the results of the measurement, they should **trust the downstream analysis** which is made after they effectuate the handling.

Second, if the data-process is too automated, it might not consider contextual characteristics which influence the data. The societal and environmental circumstances of each area must be considered in the automated data process. This requires some form of human supervision of the algorithms.

To counter both pitfalls, it is important to have a **qualified and trustworthy relay between the data processing software and the humans effectuating measurements**. This role can be filled by a local NGO, university,... On the one hand, they should establish proximity to the citizens so that these feel involved in the project, trust the data processing and take ownership of their part in the project. On the other hand, they should update the contextual factors considered in the data processing
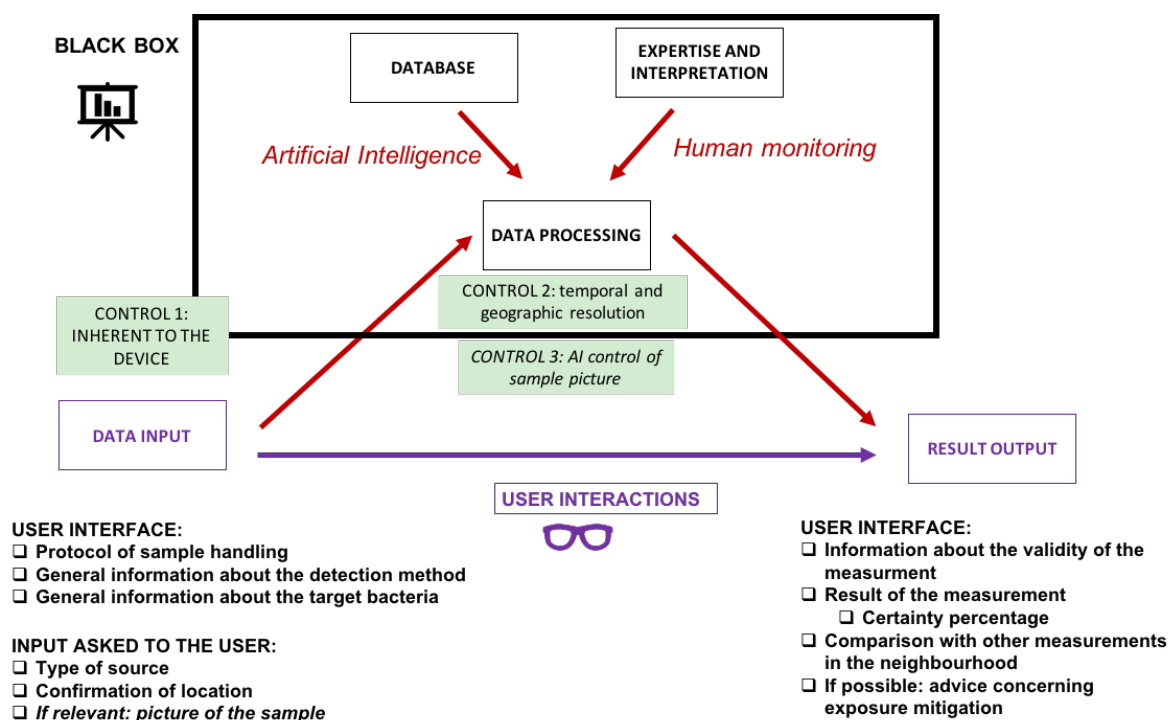
Figure 6.4: Process of an automated measurement linked to a central databank and supervised by local experts.

algorithm and intervene when results do not fit the local reality. They can also play an important role in transforming the results into **factual recommendations** for better water management, which are of course very dependent on local reality.

4.3   Strategy

As a result of the discussions above, we conclude that two main types of utilization exist for the sensor: individual measurements which are not linked to a centralised database - such as niche applications in Belgium- and measurements which are linked to a centralised database - such as wide use in the Philippines.

In both situations, as explicited in figure 6.6, it is relevant to make the measurement as automatised as possible, for instance by coupling it to a smartphone that does the data processing. [228]

In the Belgian scenario, the **individual measurement** would be processed by an algorithm which is pre-implemented and invariable. The main control consists in the differential control which is present on the device itself, as explained in chapter 5. The output information would be the estimated concentration of bacteria and whether a "healthy" threshold is exceeded or not. A disclaimer, explaining that bacterial concentration is not the only indicator of potability, should be added. If possible, one can add a degree of certainty of the measured result.

A schematic representation of the automated measurement process with **database**, such as in the Philippine scenario, is given in figure 6.4. From the point of view of the user,

the manipulation is straightforward: following the instructions on the screen, answering a few questions about the sampling location and waiting for the results to appear. The user makes the measurement according to manipulations described in the User Interface (UI), which can for instance be integrated in a smartphone app. The device and data processing as such are a complete black box for the user: this avoids disparities due to information and expertise asymmetry. However, too much automation has the pitfall of not being adapted to the specific conditions. Thus, a golden mean is a processing algorithm which is supervised by local expertise.

Three types of control are possible in this case.

The first control on validity of the data is the **differential control** which is inherent to the sensing device itself (as explained in chapter 5).

A second form of control is based on **comparison with other nearby datapoints** (both in space and in time) in the database. "If my neighbours have had measurements indicating bad quality of water from the distribution network all day, and I am the only one whose sensor indicates good qualtiy, maybe I should check twice."

A third form of control can be done by asking the user to take a **picture** of his set-up. Through artificial intelligence, the image can then be analysed to verify e.g. if the turbidity threshold of the water is not exceeded. If so, too much dirt is in the water, causing too much perturbation in the measurement and thus making it invalid. This form of control requires the access to a decent camera, which is why this control can be optional.

Comparison with other neighbouring measurements, as referred to for the second type of control, should be well-conceived to avoid panic and backlashes. In order not to rush any premature results up to the user, if the database suspects a **singular behavior compared to nearby measurements** (both in time and space), the user should be asked to make the measurement again without any further information (*"re-take the measurement please, data are not recorder correctly"*). If the second measurement confirms the first measurement, the singularity is most probably due to the actual sample quality and not to sensor failure. In that case, the platforms can propose an action plan to neighbours possessing a sensor in order to find out the origin of the singularity. For instance, based on the database, the platform can determine which access points are connected to the singular one and are thus potentially contaminated as well: this makes it possible to send a warning to all the users who were recently reported to use this water access. In this scenario, an integrated map with all registered water accesses and their origin (distribution network, well,...) can be useful.

These are strategical options that require further elaboration. For example, how are the experts paid? How is data processing checked for neutrality? How do the results get a legal value?

5   Discussion

Concerning drinking water, Belgian institutions are relatively well trusted to maintain tap-water qualitative. As long as this quality is maintained, we established that there would be no large-scale interest in such a sensor, making a common data-base unnecessary

and even harmful since a minority of bad results would constitute the majority of the uploaded data points, distorting reality. However, the sensor may be useful in some **niche-applications** as well as in other domains where the resilience of the institutions is pushed to its limits, for instance for the management of the COVID-19 pandemic. This is briefly discussed in section 5.1.2.

In the Philippinean context, distribution water is often a commodity of uncertain quality or is simply a matter of shared ignorance (the owner of the well or source, or the owner of the distribution system knows no more about the characteristics of the water than the consumers to whom it is sold). The health and economic consequences can be dramatic. The time and cost of analysis can be high while the analysis system may be unreliable. As a result, consumers do not systematically trust the water distribution operator. Public health events have shown how difficult it is to produce safe drinking water and expertise in water analysis . In this context, a collaborative approach to monitoring with recurrent water quality analysis is a particularly welcome solution since it can reduce the problems of expertise (knowledge) asymmetry and information assymetry on the characteristics of the distribution water.

A point-of-care watersensor can offer a lot of perspectives: it can help individuals to make a **balanced choice** between the different available water sources, according to the planned usage. If performed well, these measurements enable to **avoid accidents** linked to consumption of contaminated water.

The two contrasted situations between Belgium and the Philippines prove that different management of the information is required in different situations. Contrary to popular belief, adding additional information to a system does not systematically lead to a state that is, from a collective point of view, preferable. From the point of view of society as a whole, **additional information does not systematically have a positive value**. It may have a negative value: all actors are worse off when they have more information. Thinking about the design of a sensor and its information system means anticipating precise questions concerning information gathering and transfer. We give an example of some of these questions in the context of the database-scenario in the Philippines.

- **What information should be disseminated and to whom?** A message such as *"The measured bacterial concentration is* 10^3 *CFU/ml. The standard deviation is* 8%*. An uncertainty of* 12% *is added due to the water turbidity which is* 20% *"* is too technical for the end-user, especially in a context of high expertise asymmetry. The end-user benefits from a more concise message, such as *"The bacterial concentration is below the maximum threshold and therefore does not present a significant danger to your health"*. A color-code (green, orange, red) may be useful. While not beneficial for all citizens, the aforementioned technical data can be relevant for the database and experts who manage the database, in order to make the data processing more accurate.

- **When should the information be disseminated?** If the measurement shows a singular behavior compared to neighbouring measurements in the database, it is better to ask the end-user to re-take the measurement in order to exclude sensor-failure, before displaying the obtained data.

- **In what format should the information be displayed?** Should the user interface only display *"The bacterial concentration is higher than the maximum threshold"*? Or should it add recommendations such as *"A chlorine tablet improves the water potability. If this is not available, boiling the water before consumption may prevent contamination"*? This is highly dependent on the local context, which underlines -once again- the significant role of a local expertise group managing the database.

This work is only at the beginning answering these crucial questions. We elaborated that information quality can be improved by a clear measurement protocol and automation of (a part of) the measurement (cfr figure 6.6). The information transfer can be optimised and improved through shared data-processing. However, intentional human can still be induced, both at the measurements themselves as at the "black box" level. (cfr figure 6.4). Furthermore, the data-processing is by nature limited to the finite amount of factors that are mapped and can therefore never guarantee a correct analysis with 100% certainty.

Proximity between the sensor developing team and the end-users is crucial in order to map the factors that can cause contamination as accurately as possible. **Inter-universitary research** offers great opportunities in that regard. This can also help the elaboration of trustworthy collaborations in order to mitigate the risk of intentional human information bias as much as possible.

Apart from only offering a first response to the crucial questions concerning inforamtion quality and information transfer, this work is also limited in the scope of the water cycle it focuses on. Analysing figure 6.5, we note that we mainly target the water cycle between a catchment point and consumers connected by a distribution network. We assume that consumers have little to no access to different infrastructures. We proposes a configuration of an information system focusing on tap water: a crucial point of analysis to help maintain confidence in the quality of water and its distribution operator. However, this does not stand alone: the whole cycle should be considered. We introduce this briefly in section 5.1.1.

5.1 Future research

5.1.1 The circular economy of water

Correctly performed and managed measurements can offer two major advantages when bundled, for instance in a database: analysis of the data can help understand the causes of pollution or contamination and large-scale objective data collection can cantilever pressure on local and national authorities to improve water access conditions.
However, the effects of this pressure are rarely direct: structural improvement organised by the government is a slow and cumbersome process. Citizen science has a substitute role to play, while waiting for authorities to act. It can be a tool for **optimising and organising available information and expertise in both society and scientific circles** in order to help communities with the appropriation of the potable water distribution.
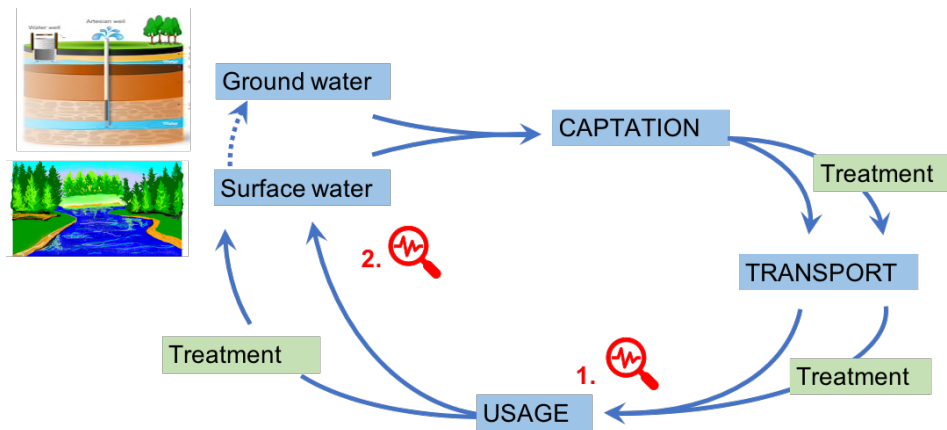
Figure 6.5: The small human water cycle. The magnifying glass corresponds to points in the water cycle where water quality analysis is most crucial: both before usage and before releasing used water back into nature. We mainly focus on the first analysis case.

Taking ownership of the water cycle in figure 6.5 as much as possible, is key to empower communities. This means that **both water treatment processes and quality control should be disposable and manageable on "community scale"**.
It involves the possibility of **taking action according to the result of the sensor**, which goes beyond the scope on this work that mainly focuses on the analysis as such. In concrete terms, if the result of a bacterial concentration measurement is unfavourable, other water sources should be available or citizens should have the possibility to purify water themselves. Although very interesting, the re-use of water, as well as its social acceptance and incorporation of the technologies linked to it, require an extensive analysis that we do not carry out here.

For human needs, the most crucial point at which the water quality has to be guaranteed, is right before consumption. However, somehow, consumed water is rejected back in nature. If the quality of wastewater is insufficient, this has long-term effects on the environment and may also affect long-term human health.
Communities can take over control of water quality, both before consumption and before disposal, with a point-of-care biosensor such as the one we describe in this master thesis. But what if the results of the testing reveals inadequate quality? As already mentioned, tests provide objective arguments for citizens to demand infrastructure improvements from their governments. Could citizens have the possibility to act on their own according to the result, without having to wait for the steps taken by the authorities? Could citizens **take ownership of the water purification process**?

This faces a lot of constraints. Since water is an experience good, it is crucial that citizens trust the purification device and understand the need of the purifying process. In [244], a review was made of factors influencing public acceptance of drinking water alternatives. These factors are very diverse in nature and strongly dependent on the societal context. A study in [245] analyses the public acceptance of the use of nano-materials in point-of-use "in-home" water purification devices was mapped out. This study indicates that the vast

majority of 1642 people analyzed (mainly in Atlanta, Phoenix and Philadelphia) were quite reticent about the idea, but at the same time more than 90% of them had never heard of it before.

Both papers endorse the importance of citizen science, which can play a crucial role in bringing applied science closer to citizens, and thus **build the necessary trust in purification systems and the idea of drinking consumed water**. Water quality sensors as the one discussed in this master thesis can play a key role in building up confidence in this kind of systems.

5.1.2 Focus: COVID-19 in Belgium

In the light of the corona pandemic that hit our country and the whole world in recent months, it is interesting to reflect on what paper-based electrical biosensors can offer in terms of pathogen detection.

Although on average in Belgium we can rely on the good and robust organisation of medical accommodations, we have now been confronted with the limitations of this system. A crucial element in managing the crisis situation is the **rapid detection of infection**. This has not been self-evident in recent months: at certain times, tests were only available for the most serious cases and for medical staff. Even at the time of writing, at the beginning of August 2020, tests are not available to everyone: only for those who have been in contact with a diagnosed person.

During this whole chapter, we oriented ourselves towards pathogen detection in water. An interesting insight is that contamination hotbeds can be detected through wastewater analysis, given that the viral DNA is present in the faeces of infected persons. [5] By analysing the **waste water** of a neighbourhood, it is possible to determine how at what degree contamination is present in that neighbourhood. [246] This technique has already been used for the detection of Hepatitis-A outbreaks [247] as well as for the follow up of the effectiveness of poliovaccin campains. [248]

However, our sensor could also offer possibilities for detection of pathogens in **human body fluids**. Let's consider a paper-based biosensor which is capable to detect whether someone is a carrier of the SARS-CoV-2 virus, based on a drop of saliva or blood. This sensor is cheap, easy to produce (printable on paper) and gives solid results.

Such a sensor could therefore be a key element in the management of a similar sanitary crisis. Where the widespread use of a drinking water sensors in Belgium is less relevant because of the already functional and reliable accommodations, such a viral sensor can serve as a complement for the current health facilities to detect infections.

Although in this case, as in the Philippines, it is useful on a large scale, the data should be treated differently. In the case of drinking water coming from the tap, it is useful to be able to share data with neighbours: it is indeed unlikely that the water from your tap is perfectly potable if that from all your neighbours' tap is not potable. This is because the water from all the faucets in the street has travelled the same way. The origin of an infection therefore has to be found mainly in one place. So, the aggregation of data per geographical region provides added value for the quality of the data: error measurements are easily detected.

Concerning the spread of a virus through droplets in the air, the possible causes are

varied and have multiple facets. There is no guarantee that you will have it when all your neighbours have it: it depends on who (and your neighbours) have had contact with. Comparing your measurement with that of your neighbours gives little guarantee on the correctness of your measurement itself. Of course, this changes when the measurements are linked to a tracing, which keeps track of where you were when (and how much contact you actually had with your neighbours). Here, however, we are entering the domain of privacy and we navigate on ethically slippery ice.

MANUAL MEASUREMENT READING

| SAMPLE PREPARATION AND HANDLING | MEASURMENT | SENSOR OUTPUT | DATA PROCESSING | RESULTS | INTERPRETATION |

INFORMATION			Wrong lectutre of output data	Intentional or accidental data distortion	Wrong , incomplete or distorted results publication	
EXPERTISE	Sensor manipulation (eg. Drying time, sample preparation,...)	A direct link exists between expertise of the manufacturer and quality of the results		Inadequate data processing technique	Wrong conlusion of the processed data points	Erroneous interpretation can be given to the outcome results.

AUTOMATED MEASUREMENT

BLACKBOX FOR THE USER

| SAMPLE PREPARATION AND HANDLING | MEASURMENT | SENSOR OUTPUT | DATA PROCESSING | RESULTS | INTERPRETATION |

INFORMATION				Intentional or accidental data distortion		
EXPERTISE	Sensor manipulation (eg. Drying time, sample preparation,...)	A direct link exists between expertise of the manufacturer and quality of the results				Erroneous interpretation can be given to the outcome results.

Figure 6.6: Completely manual measurement vs. centralised database and automated data processing: differences in bias due to information assymetry and expertise assymetry.

Note that the centralised database can also give an interpretation of the results. However, this has an important condition: the database must somehow take into account the local context of a user in a specific area in order to give a meaningful recommendation linked to the results.

Chapter 7

Conclusion

Improving water security is a global challenge. Point of Care devices are a key tool to monitor quality and prevent illness. This thesis focuses on impedimetric detection of bacteria in drinking water with a paper-based biosensor, which offers the advantage of having a low environmental impact. The goal is to directly deposit electrodes on the paper membrane and detect the bacteria through Electrical Impedance Spectroscopy (EIS).

In this work, we prototyped a rudimental sensing device in order to establish a proof of concept.

A production process was elaborated to deposit electrodes on nitrocellulose membrane samples by Physical Vapor Deposition (PVD). Two kinds of Interdigitated Electrodes (IDE), one with $200\mu m$ and $500\mu m$ finger width, are used. These electrodes are then bio-functionalised with phage endolisine, specific to the target Bacillus bacteria.

An equivalent electrical circuit of the nitrocellulose-electrode system was established and an analytical model to quantify the different circuit elements was elaborated, in order to determine the whole impedance seen by the IDE. Different frequency ranges of EIS where compared. With the fabricated devices, the model was tested and discussed in three cases: when the nitrocellulose is dry, when it is humidified with an electrolyte NaCl solution and when bacteria are applied.

The deposition of electrodes was successful for both electrode sizes. Because of imperfections of the paper surface, the electrical signal from the $500\mu m$ fingers is more repeatable than the signal from the $200\mu m$ fingers. The current bio-functionalisation process impacts both the volume properties of the nitrocellulose membrane and surface properties of the electrodes. While the former were correctly quantified by the analytical model, further research is needed to better understand the latter variations.

The analytical model was validated: the main electrical detection phenomena are correctly quantified. However, the electrical impact of the oxidation of aluminium electrodes under 100kHz needs further research.

The optimal frequency range for operation of the prototype was between 10^3 and 10^6 Hz.

We succeeded in detecting 10^8 CFU/ml of Bacillus Thuringiensis suspended in DI water with the $200\mu m$ electrodes. The presence of bacteria decreased the blank signal over almost 50%, which is a variation far above the noise threshold.

This result is promising and encourages further refinement of the sensor design.

The main obstacle towards a fully operational device is selectivity of the measurement: the device should be able to distinguish bacteria from ions and other particles in water. The next development steps thus require to focus on the particular electrical responses of bacteria in an aqueous medium and determining under which conditions these can be optimised. We highlighted that interesting possibilities are offered by direct parallel plate measurement to determine these responses as accurately as possible, without variability induced by electrode deposition. Furthermore, we elaborated that a transient comparative measurement may offer interesting possibilities in sensing bacteria during drying of the nitrocellulose membrane.

Since this project frames in a responsible design approach, it is essential to anticipate the usage scenarios in order to obtain a final product which is socially relevant. The approach of "responding to a need rather than creating a need" offers some interesting design insights. We are convinced that multidisciplinary studies carried out in parallel with the development of a product offer many advantages, both for the quality and the usefulness of the final product. In the context of this master thesis, a socio-economical impact assessment was made, elaborating different ways to manage the output information from the sensor according to the societal context. The importance of trust, both in the science behind the sensor as in the data treating process, are discussed.

Two contrasting scenarios in terms of drinking water management and accessibility are compared: the case of Belgium and the case of the Philippines. For each scenario, the situation of access to current drinking water is analysed using relevant aspects from water economics as developed in academic research. A water network is a complex infrastructure on which problems may arise that affect water, its flow, treatment and drinkability. Problems can occur at the source as well as elsewhere in the network and affect a variable number of consumers, depending on their density and position in the network. In both scenarios, the specific needs that can be met by a paper-based point-of-care sensor are identified. In Belgium, this has proved to be relevant in several niche applications, while in the Philippines a regular and large scale use is of interest: the latter case is studied, among others, with the scientific literature on citizen science.

As the sensor is connected to a smartphone, the data processing (shared or not) and the user interface must be adapted to the intended use. For each use case, the architecture of an information system is established in a global way, based on three criteria.
Firstly, the information system must be robust to human error (unintentional misuse, intentional distortion of data,...) and to regional variations of external conditions. Second, the information must be accessible and relevant to all users, regardless of their level of education and material resources. Thirdly, the result must be accepted by the user. The scenarios corresponding to these criteria are validated by different actors and researchers in water management, active in the respective regions. These studies make it possible to orient the design of the sensor towards a final design that is relevant not only at the technical level, but also at the environmental and social level. This is still too much ignored in most design processes nowadays.

Appendices

Appendix A

MATLAB code

Appendix B

Protocol for biological manipulations

1 Functionalisation of the nitrocellulose membrane

The protocol of deposition of RBP phage proteins on a nitrocellulose membrane (either CN140 unbacked, CN40 backed or CN95 unbacked) is as follows: [7]

1. Put the nitrocellulose membrane at equilibrium at a certain relative humidity (RH).

   - Prepare the salt sursatured solution by putting $5-10\%$wg more than the needed salt mass for water saturation in heated water.
   - Make the solution get colder. The extra salt forms a layer at the bottom of the recipient.
   - Put the solution and the membrane in a closed enclosure for night at a certain temperature in function of the wanted RH.

2. Cut a square of 1cm x 1cm in the membrane.

3. Prepare the 0.1 mg/mL solution of proteins by dilution with ultra pure water and put in in the centrifuge at 1 rpm for 10 seconds. Keep the solution in the dark by covering it with aluminium foil.

4. Apply 40-50 µL of solution on the membrane by covering all the piece of membrane. Keep the membrane with proteins in the dark by covering it with aluminium foil. It is advised to apply the solution to the side which was in contact with belt during the manufacture of the membrane (shinier one) as it rarely presents physical irregularities.

5. Wait at least 10 min.

6. Wipe the excess solution.

7. Make holes in the aluminium foil and dry the membrane at 37°C during 1h to take out the water excess in the membrane.

8. Keep the membrane in the desiccator (< 30°C) for at least 30 min to fix proteins.

9. Rinse the membrane with distilled water (2 baths of 2 minutes).

10. Wipe the excess solution.

11. Dry the membrane 30 min at 30°C in the desiccator.

12. Stock in the fridge and in the dark to keep the fluorescence of proteins.

2 Solution of bacteria

For our tests, we suspend the GBJ002 (Bacillus thuringiensis) bacteria either in DI water or in PBS. This is prepared by Audrey Leprince [175] as follows:

1. Incubate the bacteria overnight in LB medium at 30 °C with an agitation of 120 rpm.

2. Centrifuge the overnight culture (6000g - 5min)

3. Wash the overnight culture with PBS once

4. Wash the overnight culture with DI water once

5. Resuspend the bacterial pellet in 5ml of distilled water or 5ml of PBS

Appendix C

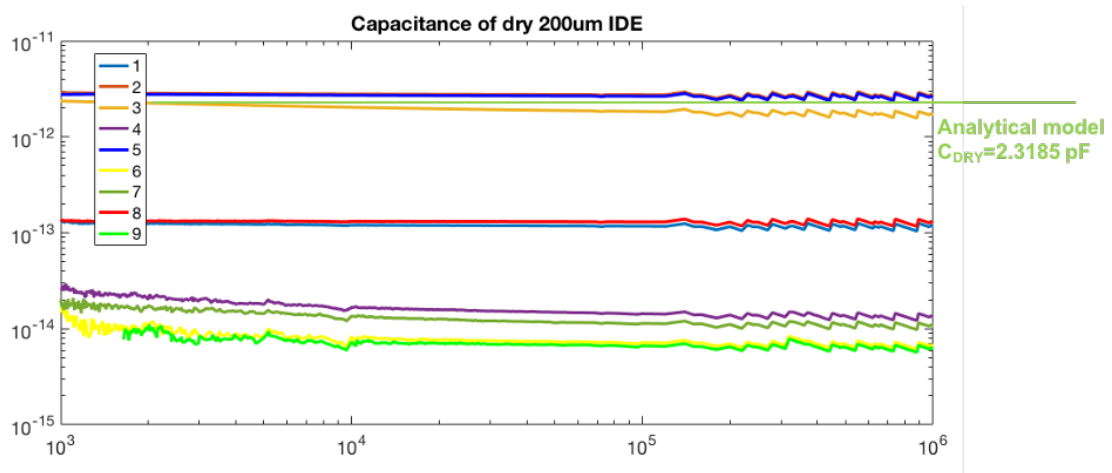# Extra results

1 Variability among the 200um electrodes.

Figure C.1: $|Z/\omega|$ seen by the 200um dry electrodes. 1 to 7 are deposited on a CN95 backed membrane and measured with the clip-setup (fig 3.18). 8 and 9 are deposited on a CN140 unbacked membrane and measured with the epoxy set-up. The green line corresponds to the expected value of the model.

In figure C.1, we observe that the capacitance for dry 200μ is subject to large variations. The explanation for this large variety in cell constant is unclear. We guess it is linked to imperfections in the deposition method since 200um are thin. It is clear that the $500\mu m$ electrodes offer a better stability than the $200\mu m$. However, since we only have 2 masks for $500\mu m$ and 7 masks for $200\mu m$, we keep working with the $200\mu m$ as well. This implies that all data results must be compared relatively to a previous state of the same electrode. Inter-electrode comparisons are not reliable given the large inter-electrode variation of the cell constant.

2 Qualitative trends in impedance variation

To get a better understanding of the simplified equivalent circuit in figure 3.2, we change each value separately by factors going up to ±100. The black (reference) case corresponds to the theoretical impedance seen by the IDE fingers when the nitrocellulose is humidified with a 0.5M NaCl solution.
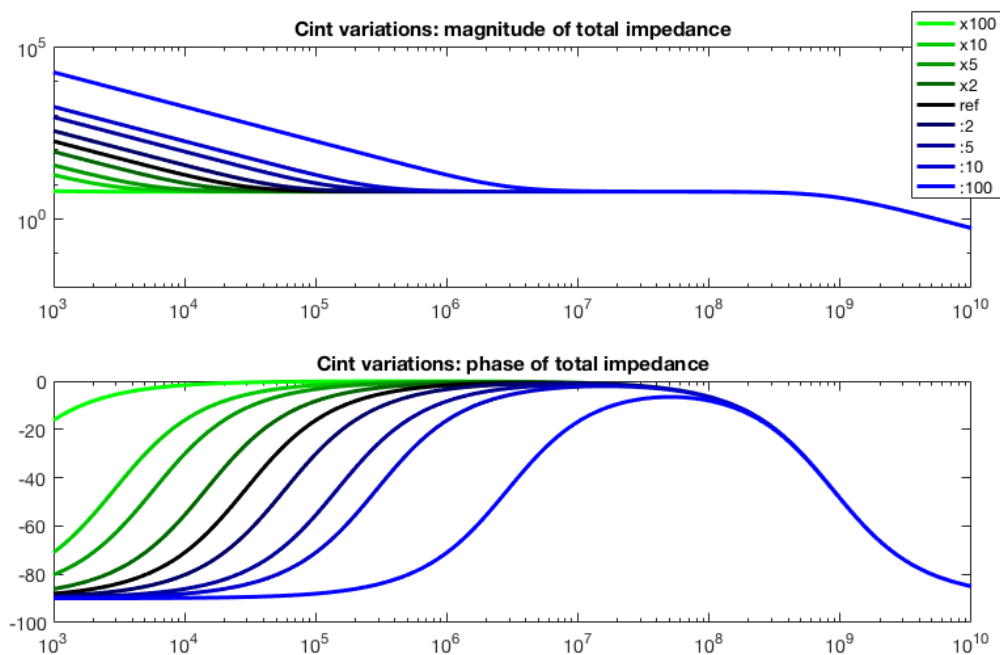

Figure C.2: Variation of the interfacial capacitance C_{int}
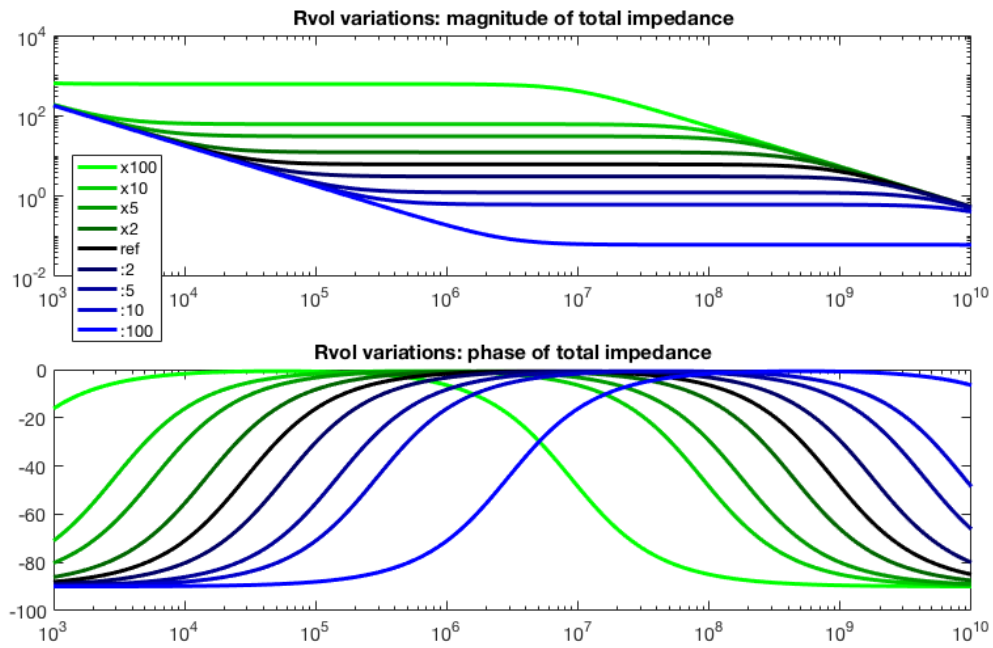
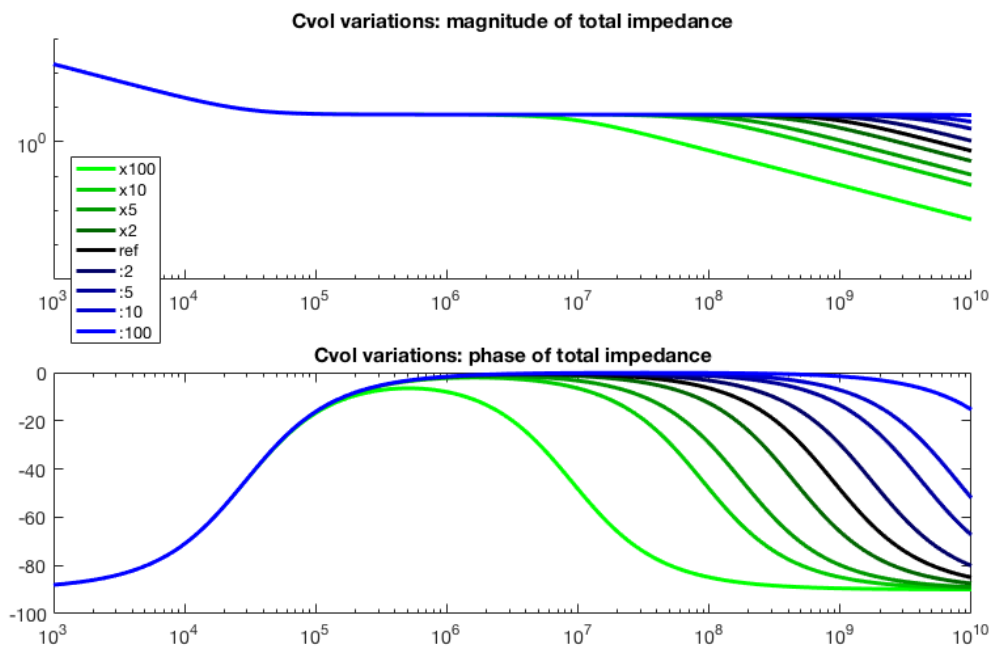Figure C.3: Variation of the volume resistance R_{vol}

Figure C.4: Variation of the volume capacitance C_{vol}

Appendix D

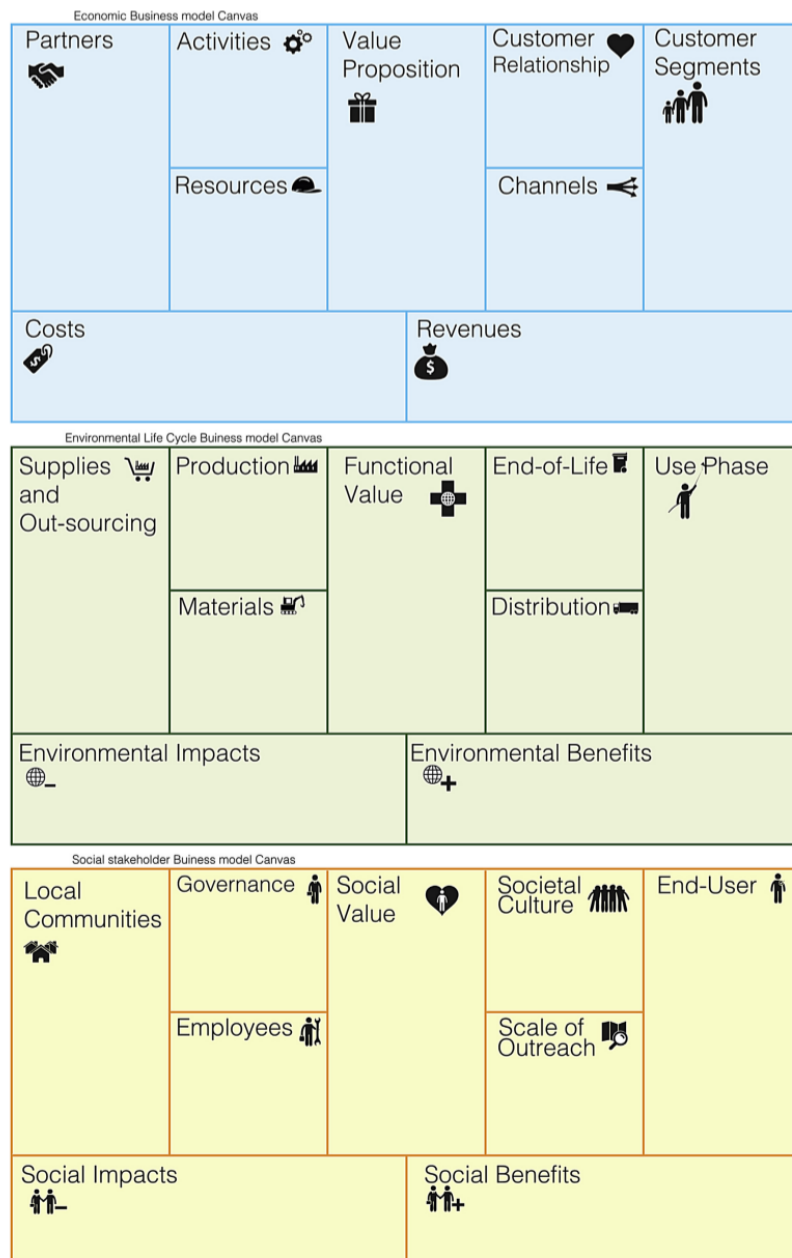# Triple Layer Business Model Canvas

Figure D.1: Triple layer business model canvas (TLBMC) [249]

Bibliography

[1] BBC Ideas: Universal wonders. Why water is one of the weirdest things in the universe. `https://www.bbc.co.uk/ideas/videos/why-water-is-one-of-the-weirdest-things-in-the-uni/p06y2c9k`.

[2] United Nations. Sustainable development goals: Goal 6: Ensure access to water and sanitation for all. `https://www.un.org/sustainabledevelopment/water-and-sanitation/`.

[3] G. Le Brun. Scientific section of the proposal. *FRIA CALL 2019 – FRIA-B1*. UCLouvain.

[4] C. S. Kosack, A-L Page, and P. R. Klatser. A guide to aid the selection of diagnostic tests. `https://www.who.int/bulletin/volumes/95/9/16-187468/en/`.

[5] Z. Yang K. Mao, H. Zhang. Can a paper-based device trace covid-19 sources with wastewater-based epidemiology. *Environmental Science & Technology*, 2020. Scientific opinion, non peer-reviewed.

[6] G. Le Brun. Disposable paper-based bacteria sensor for water quality monitoring. *Presentation of PhD project, UCLouvain*, 2019.

[7] O. Crahay. Towards the design of a paper-based microfluidic sensor for water quality monitoring and comparative life cycle assessment. *Master Thesis UCLouvain*, 2020.

[8] L Klappenbach. Prokaryotes and eukaryotes. `https://www.thoughtco.com/what-are-prokaryotes-and-eukaryotes-129478`.

[9] Schopf JW. Disparate rates, differing fates: tempo and mode of evolution changed from the precambrian to the phanerozoic. *Proceedings of the National Academy of Sciences of the United States of America. 91 (15)*, page 6735–6742, 1994.

[10] R. Sender, S. Fuchs, and R. Milo. Revised estimates for the number of human and bacteria cells in the body. *PLOS Biology 14 (8)*, 2016.

[11] N.Couniot. Highly-sensitive cmos capacitive biosensors towards detection of single bacterial cell in electrolyte solutions. *PhD thesis (UCLouvain)*, 2015.

[12] A.Liteanu. Fabrication of a high aspect ratio biosensor for bacteria detection. *Master thesis (UCLouvain)*, 2015.

[13] W. J. Peveler, M. Yazdani, and V. M. Rotello. Selectivity and specificity: Pros and cons in sensing. *ACS Sensors 1*, pages 1282–1285, 2016.

[14] Grace Wu and Muhammad H Zaman. Low-cost tools for diagnosing and monitoring hiv infection in low-resource settings, 2012.

[15] O. Lazcka, F. J. D. Campo, and F. X. Muñoz. Pathogen detection: A perspective of traditional methods and biosensors. *ACS Sensors 1 (22)*, pages 1205–1217, 2007.

[16] A.Yousef. Detection of bacterial pathogens in different matrices: Current practices and challenges. *Principles of Bacterial Detection: Biosensors*, 2008.

[17] J. Rameckers, S. Hummel, and B. Herrmann. How many cycles does a pcr need? determinations of cycle numbers depending on the number of targets and the reaction efficiency factor. *Naturwissenschaften 84*, pages 259–262, 1997.

[18] X. Muñoz-Berbel, N. Godino, O. Laczka, E. Baldrich, and F. Xavier Muñoz. Impedance-based biosensors for pathogen detection. *Principles of Bacterial detection: Biosensors, recognition receptors and microsystems*, 15:341–376, 2008.

[19] E. Engvall and P. Perlmann. Enzyme-linked immunosorbent assay. ii. quantitative assay of protein antigen, immunoglobulin g, by means of enzyme-labelled antigen and antibody-coated tubes. *Biochimica et Biophysica Acta (BBA) - Protein Structure*, 251:427–434, 1971.

[20] Medical and Biological Laboratories Japan. The principle and method of elisa. `https://ruo.mbl.co.jp/bio/e/support/method/elisa.html`.

[21] M. Karas and F. Hillenkamp. Laser desorption ionization of proteins with molecular masses exceeding 10,000 daltons. *Anal Chem*, 60:2299–2301, 1988.

[22] K. Tanaka, W. Hiroaki, S. Akita Y. Ido, Y. Yoshida, and T. Yoshida. Protein and polymer analyses up to m/z 100 000 by laser ionization time-of-flight mass spectrometry. *apid Commun Mass Spectrom*, 2:151–153, 1988.

[23] N. Singhal1, M. Kumar, P. K.Kanaujia, and J. S.Virdi1. Maldi-tof mass spectrometry; an emerging technology for microbial identification and diagnosis. *Frontiers in microbiology*, 6(791), 2015.

[24] R.Patel. Matrix-assisted laser desorption ionization–time of flight mass spectrometry in clinical microbiology. *Clinical infectious diseases*, 54(4):564–572, 2013.

[25] Jacob Fraden. *Handbook of modern sensors*. Springer-Verlag, 2004.

[26] Tim Shotter. Understanding accuracy and precision for mems pressure sensors. *All Sensors*, 2012.

[27] Keith Scott and Eileen Hao Yu. *Microbial Electrochemical and Fuel Cells. Fundamentals and applications*. Woodhead Publishing, 2016.

[28] P. A. Serra. *Biosensors*. Intech, Olajnica 19/2, 32000 Vukovar, Croatia, 2010.

[29] D. Grieshaber, B. MacKenzie, J. Vörös, and E. Reimhult. Electrochemical biosensors - sensor principles and architectures. *Sensors*, 8:1400–1458, 2008.

[30] Pavel Damborsky, Juraj Svitel, and Jaroslav Katrlik. Optical biosensors. *Essays in Biochemistry*, 60:91—-100, 2016.

[31] Zhi-Jun Kea, Dong-Lin Tanga, Xin Lai, Zhi-Yong Daib, and Qi Zhanga. Optical fiber evanescent-wave sensing technology of hydrogen sulfide gas concentration in oil and gas fields. *Optik*, 157:1094–1100, 2018.

[32] A. Taylor, J. Ladd, J. Homola, and S. Jiang. Surface plasmon resonance (spr) sensors for the detection of bacterial pathogens. *Principles of Bacterial Detection: Biosensors, Recognition Receptors and Microsystems*, page 83–108, 2008.

[33] A.Leung, P. Mohana Shankar, and R. Mutharasan. A review of fiber-optic biosensors. *Sensors and Actuators B 125*, pages 688–703, 2007.

[34] I. R. Matias, F. J. Arregui, J. M. Corres, and J. Bravo. Evanescent field fiber-optic sensors for humidity monitoring based on nanocoatings. *IEEE SENSORS JOURNAL*, 7(1):89–95, 2007.

[35] Notomi, H. Okayama, H. Masubuchi, T. Yonekawa, K. Watanabe, and N. Amino. Loop-mediated isothermal amplification of dna. *Nucleic Acids Res.*, 28, 2000.

[36] V. Xin-Ting Zhao, T. I. Wongb, X. T. Zheng, Y.N. Tan, and X. Zhou. Colorimetric biosensors for point-of-care virus detections. *Materials Science for Energy Technologies*, 3:237–249, 2020.

[37] Jun Ji, Xin Xu, Qianqian Wu, Xueyu Wang, Wanyu Li, Lunguang Yao, and Yunchao Kan. Simple and visible detection of duck hepatitis b virus in ducks and geese using loop-mediated isothermal amplification. *Poultry Science*, 99:791–796, 2020.

[38] Mori Y, Nagamine K, Tomita N, and Notomi T. Detection of loop-mediated isothermal amplification reaction by turbidity derived from magnesium pyrophosphate formation. *Biochem. Biophys. Res. Commun. 289 (1)*, pages 150—-154, 2001.

[39] P. Boullanger, D. Lafont, M.-N. Bouchu, L. Jiang, T. Liu, W. Lu, C.X. Guo, and J. Li. The use of glycolipids inserted in color-changeable polydiacetylene vesicles,as targets for biological recognition. *C. R. Chimie*, 11:43–60, 2008.

[40] J. Deng, Z. Sheng, K. Zhou, M. Duan, C. Yu, and L. Jiang. Construction of effective receptor for recognition of avian influenza h5n1 protein ha1 by assembly of monohead glycolipids on polydiacetylene vesicle surface. *Bioconjugate Chem*, 20:533–537, 2009.

[41] E. Karzbrun, A.M. Tayar, V. Noireaux, and R.H. Bar-Ziv. Programmable on-chip dna compartments as artificial cells. 2014.

[42] J.M. Callura, C.R. Cantor, and J.J. Collins. Genetic switchboard for synthetic biology applications. *Proc. Natl. Acad. Sci. U.S.A.*, 109:5850–5855, 2012.

[43] Buysschaert B., Vermijs L., and Naka A. Online flow cytometric monitoring of microbial water quality in a full-scale water treatment plant. *npj Clean Water 1, 16*, 2018.

[44] Favere J., Buysschaert B., Boon N., and De Gusseme B. Online microbial fingerprinting for quality management of drinking water: Full-scale event detection. 2020.

[45] Fulwyler MJ. Electronic separation of biological cells by volume. *Science*, 150:910–911, 1965.

[46] Miroslav Pohanka. Overview of piezoelectric biosensors, immunosensors and dna sensors and their applications. *Materials (Basel)*, 11(3):448, 2018.

[47] S.Tombelli. Piezoelectric biosensors for medical applications. *Biosensors for Medical Applications*, pages 41–64, 2012.

[48] Sauerbrey G. Use of quartz vibrator for weighing thin films on a microbalance. *Z PHYSIK*, 155:206–222, 1959.

[49] Shons A, Dorman F, and Najarian J. An immunospecific microbalance. *J Biomed Mater Res*, 6:565 – 570, 1972.

[50] M. Pohanka and P. Skladal. Piezoelectric immunosensor for the direct and rapid detection of francisella tularensis. *Folia Microbiol*, 52:325–330, 2007.

[51] Olsen E.V., Sorokulova I.B., Petrenko V.A., I.H. Chen, J.M. Brbaree, and V.J. Vodyanoy. Affinity-selected filamentous bacteriophage as a probe for acoustic wave biodetectors of salmonella typhimurium. *Biosens. Bioelectron.*, 21:1434–1442, 2006.

[52] F. Salam, Y. Uludag, and I.E. Tothill. Real-time and sensitive detection of salmonella typhimurium using an automated quartz crystal microbalance (qcm) instrument with nanoparticles amplification. *Talanta*, 115:761–767, 2013.

[53] X. Guo, C.S. Lin, S.H. Chen, R. Ye, and V.C. Wu. A piezoelectric immunosensor for specific capture and enrichment of viable pathogens by quartz crystal microbalance sensor, followed by detection with antibody-functionalized gold nanoparticles. *Biosens. Bioelectron.*, 38:177–183, 2012.

[54] M. Chaplin. Calorimetric biosensors. *Enzyme Technology*, 2014.

[55] Mehmet Ali Sen. Design and development of calorimetric biosensors using extraordinary optical transmission through nanohole arrays. *PhD B.S. Middle East Technical University*, 2005.

[56] David E. Gaddes and Srinivas Tadigadapa. Microcalorimetric detection of creatinine in urine. *IEEE SENSORS*, pages 1–3, 2016.

[57] Seung-Il Yoon, Mi-Hwa Lim, Se-Chul Park, Jeon-Soo Shin, and Yong-Jun Kim. Detection of neisseria meningitidis using a micromachined split-flow microcalorimeter. *IEEE 20th International Conference on Micro Electro Mechanical Systems (MEMS)*, pages 509–512, 2007.

[58] R. Koncki. Recent developments in potentiometric biosensors for biomedical analysis. *Analytica Chimica Acta*, 599:7–15, 2007.

[59] A. Touhami. Biosensors and nanobiosensors: Design and applications. *International journal of chemical studies*, pages 374–403, 2014.

[60] P. Bhattarai and S. Hameed. Basics of biosensors and nanobiosensors. *Nanobiosensors: From Design to Applications*, pages 374–403, 2014.

[61] K.Y. Chumbimuni-Torres, Z. Dai, and N. Rubinova. Potentiometric biosensing of proteins with ultrasensitive ion-selective microelectrodes and nanoparticle labels. *Journal of the American Chemical Society*, 128:13676–13677, 2006.

[62] O. Lazcka, F. Javier Del Campo, and F. X. Munoz. Pathogen detection: A perspective of traditional methods and biosensors. *Biosensors and Bioelectronics*, 22:1205–1217, 2007.

[63] S. Arora, N. Ahmed, and S. Siddiqui. Detecting food borne patogens using electrochemical biosensors: an overview. *International journal of chemical studies*, 6:1031–1039, 2018.

[64] I. Palchetti and M. Mascini. Amperometric biosensors for pathogenic bacteria detection. *Principles of bacterial detection: Biosensors, Recognition, Receptors and Microsystems*, 13:299–312, 2008.

[65] P.B. Luppa, L.J. Sokoll, and D.W. Chan. Immunosensors – principles and applications to clinical chemistry. *Clinica Chimica Acta*, 314:1–26, 2001.

[66] K. J. Aoki and J. Chen. Tips of voltammetry. *IntechOpen*, 2018.

[67] M.A. Alam. Amperometric sensors. *Purdue University*, 2013. Principles of electronic nanosensors, lecture 3.

[68] H. A. Abdulbari and E. A. M. Basheer. Electrochemical biosensors: electrode development, materials, designd and fabrication. *ChemBioEng*, 4:92–105, 2017.

[69] A. Wu and W. S. Khan. *Nanobiosensors: From Design to Applications*. Wiley-VCH, 2020.

[70] M. Zourob, S. Elwary, and A. Turner. *Principles of Bacterial Detection: Biosensors, recognition receptors and microsystems*. Springer, 2008.

[71] Abdel-Hamid I, Ivnitski D, Atanasov P, and Wilkins E. Flow-through immunofiltration assay system for rapid detection of e. coli o157:h7. *Biosens. Bioelectron.*, 14:309–316, 1999.

[72] D. Ivnitski, I. Abdel-Hamid, P. Atanasov, E. Wilkins, and S. Stricker. Application of electrochemical biosensors for detection of food pathogenic bacteria. *Electroanalysis*, 12:317–325, 2000.

[73] F. David, M. Hebeisen, G. Schade, E. Franco-Lara, and M. Di Berardino. Viability and membrane potential analysis of bacillus megaterium cells by impedance flow cytometry. *Biotechnol. Bioeng.*, 109:483–492, 2011.

[74] N. Haandbæk, S. C. Bürgel, F. Heer, and A. Hierlemann. Characterization of subcellular morphology of single yeast cells using high frequency microfluidic impedance cytometer. *Lab on a Chip*, 14:369–377, 2014.

[75] Amphasys AG. Impedance microflow cytometry - the technology. `https://amphasys.com/wp-content/uploads/2018/12/Amphasys_IFC_Impedance_Flow_Cytometry_for_Label_Free_Single_Cell_Analysis.pdf`.

[76] Y. Li M. Varshney. Interdigitated array microelectrodes based impedance biosensors for detection of bacterial cells. *Biosensors and Bioelectronics*, 24:2951–2960, 2009.

[77] Liju Yang, Yanbin Li, Carl Griffis, and Michael Johnson. Interdigitated microeletrode (ime) impedance sensor for the detection of viable salmonella typhimurium. *Biosensors and bioelectronics*, 19:1139– 1147, 2004.

[78] J. S. Daniels and N. Pourmanda. Label-free impedance biosensors: Opportunities and challenges. *Electroanalysis 19 (12)*, page 1239 – 1257, 2007.

[79] V. Perumal and U. Hashim. Advances in biosensors: principle, architecture and applications. *Manuscript of the University Malaysia Perlis*, 2019.

[80] R. A. Dorledo de Faria, L. G. Dias Heneine, T. Matencio, and Y. Messaddeq. Faradaic and non-faradaic electrochemical impedance spectroscopy as transduction techniques for sensing applications. *International Journal of Biosensors and Bioelectronics*, 5(1):136–144, 2019.

[81] E. Barsoukov and J. R. MacDonald. *Impedance spectroscopy: theory, experiment and applications*. Wiley, 2005.

[82] Cheng-Hsin Chuang and Muhammad Shaikh. *Label-free impedance biosensors for Point-of-Care diagnostics*, pages 171–201. 03 2017.

[83] G. Velve-Casquillas, M. Le Berre, M. Piel, and P. T Tran. Microfluidic tools for cell biological research. *Nano today*, 5:28–47, 2010.

[84] Adaris M. López-Marzo and Arben Merkoçi. Paper-based sensors and assays: a success of the engineering design and the convergence of knowledge areas. *Lab Chip*, 16:3150–3176, 2016.

[85] Yan Wang, Hong Guo, Jin ju Chen, Enrico Sowade, Yu Wang, Kun Liang, Kyle Marcus, Reinhard R. Baumann, and Zhe sheng Feng. Paper-based inkjet-printed flexible electronic circuits. *ACS Appl. Mater. Interfaces*, 2016.

[86] prof M. Lindström. Pulp and paper production. *KTH Royal Institute of Technology in Stockholm*, 2019. lecture ke2310 attended by O. Crahay.

[87] de Puig H., Bosch I., Gehrke L, and Hamad-Schifferli K. Challenges of the nano-bio interface in lateral flow and dipstick immunoassays. *Trends Biotechnol.*, 35:1169–1180, 2017.

[88] C. Zao, M.M. Thuo, and X. Liu. A microfluidic paper-based electrochemical biosensor array for multiplexed detection of metabolic biomarkers. *Lab Chip*, 14, 2013.

[89] R. P. Tortorich, H. Shamkhalichenar, and J-W Choi. Inkjet-printed and paper-based electrochemical sensors. *Applied sciences*, 288, 2018.

[90] EuroScientist. Paper biosensors: Towards eco-friendly diagnosis, 2018. `https://www.euroscientist.com/paper-biosensors/`.

[91] W.Nernst. Methode zur bestimmung von dielektrizitatskonstanten. *Zeitschrijt fur Elektrochemie*, 14:622–663, 1894.

[92] A. Guyader, F. Huet, and R. P. Nogueira. Polarization resistance measurements: Potentiostatically or galvanostatically? *Zeitschrijtfur Elektrochemie*, 65:136–144, 2009.

[93] M. Grossi and B. Riccò. Electrical impedance spectroscopy (eis) for biological analysis and food characterisation: a review. *Journal of Sensors and Sensor systems*, 6:303–325, 2017.

[94] G. Barbero, F. Batalioto, and A. M. Figueiredo Neto. Theory of small-signal ac response of a dielectric liquid containing two groups of ions. *Applied Physics Letters*, 92(17):172908, 2008.

[95] L. ALMQUIST. Nonlinear impedance spectroscopy: Using higher harmonics response and differential impedance for electrical characterization of dc insulation materials. *Master's thesis CHALMERS UNIVERSITY OF TECHNOLOGY*, 2015.

[96] Michael Faraday. Identity of electricities derived from different sources and relation by measure of common and voltaic electricity. *Experimental researches in Electricity - third series*, pages 23–54, 1833.

[97] J. S. Park, H. J. Kim, J. H. Lee, J.H. Park, and K. S. Hwang. Amyloid beta detection by faradaic electrochemical impedance spectroscopy using interdigitated microelectrodes. *SENSORS 18, 426*, 2018.

[98] Y. Song and P. Hung. Electrochemical impedance spectroscopy analysis on type iii anodized aluminum 6061-t6 with thermal cycling. *ANODIZING CONFERENCE, San Diego, California*, 2015.

[99] Tektronix. Utilisation of the dpo/mso/mdo4000 series oscilloscope. update 2020.

[100] K. M. Chew, R. Sudirman, N. Seman, and C. Y. Yong. Relaxation frequency and relaxation time estimation for phantom modeling by proposed fitting linear models. *IEEE International conference on biomedical Engineering and Sciences*, 2012.

[101] A. M. Namisnyk. Electrode/electrolyte interfaces: Structure and kinetics of charge transfer. *Fuel Cells. Springer, Boston, MA*, 2006.

[102] D. Rockstraw. Spring 2020 chme elective course: Electrochemistry- basics and applications. *New Mexico State University, Chemical & Materials engineering*, 2019. `https://web.nmsu.edu/~snsm/classes/chem435/Lab14/double_layer.html`.

[103] A. M. Namisnyk. A survey of electrochemical supercapacitor technology. *Bachelor Project University of Technology (Sydney)*, 2003.

[104] P. Pham, M. Howorth, A. Planat-Chrétien, and S. Tardu. Numerical simulation of the electrical double layer based on the poisson-boltzmann models for ac electroosmosis flows. *Excerpt from the Proceedings of the COMSOL Users Conference 2007*, 2007.

[105] J.O'M.Bockris, M.A.V.Devanathan, and K.Muller. On the structure of charged interfaces. *Proceedings of the royal society A*, 274, 1963.

[106] P. LICHVÁR, M. LISKA, and D. GALUSEK. What is the true kramers-kronig transform? *Ceramics − Silikáty 46 (1)*, pages 25–27, 2002.

[107] Shimadzu. Kramers-kronig transform and applications. *C103-E031 No. 228*.

[108] M. Lacey. Electrochemical impedance spectroscopy. `http://lacey.se/science/eis/`.

[109] F Heer, W Franks, A Blau, S Taschini, C Ziegler, A Hierlemann, and H Baltes. Cmos microelectrode array for the monitoring of electrogenic cells. *Biosensors and Bioelectronics*, 20(2):358 – 366, 2004.

[110] Mona Tolba, Minhaz Uddin Ahmed, Chaker Tlili, Fritz Eichenseher, Martin J. Loessner, and Mohammed Zourob. A bacteriophage endolysin-based electrochemical impedance biosensor for the rapid detection of listeria cells. *Analyst*, 137:5749–5756, 2012.

[111] Asif Ahmed, Jo V. Rushworth, John D. Wright, and Paul A. Millner. Novel impedimetric immunosensor for detection of pathogenic bacteria streptococcus pyogenes in human saliva. *Analytical chemistry*, 85:12118−12125, 2013.

[112] Rapid Quantitative Detection of Brucella melitensis by a Label-Free Impedance Immunosensor Based on a Gold Nanoparticle-Modified Screen-Printed Carbon Electrode. Novel impedimetric immunosensor for detection of pathogenic bacteria streptococcus pyogenes in human saliva. *Sensors (Basel)*, 13:8551–8563, 2013.

[113] Jae Ho Yoon, Yong Duk Han, and Pyung Cheon Lee. Rapid quantitative detection of brucella melitensis by a label-free impedance immunosensor based on a gold nanoparticle-modified screen-printed carbon electrode. *BioChip Journal*, 7:344–352, 2013.

[114] O. Laczka, E. Baldrich, F. X. Muñoz, and F. J. del Campo. Detection of eschericia coli and salmonella thyphimurium using interdigitated micro-electrode capacitive immunosensors: the importance of transducer geometry. *Anal Chem*, 80:7239–7247, 2008.

[115] J. Paredes, S. Becerro, F. Arizti, A. Aguinaga, J.L. Del Pozo, and S. Arana. Real time monitoring of the impedance characteristics of staphylococcal bacterial biofilm cultures with a modified cdc reactor system. *Biosensors and Bioelectronics*, 38:226–232, 2012.

[116] Yang L. Electrical impedance spectroscopy for detection of bacterial cells in suspensions using interdigitated microelectrodes. *Talanta*, 74:1621–1629, 2008.

[117] Varshney M and Li Y. Double interdigitated array microelectrode-based impedance biosensor for detection of viable escherichia coli o157:h7 in growth medium. *Talanta*, 74:518–525, 2008.

[118] C.J. Dias Rui Igreja. Analytical evaluation of the interdigital electrodes capacitance for a multi-layered structure. *ELSEVIER Sensors and Actuators A*, (112):281–301, 2004.

[119] Subhas Chandra Mukhopadhyay. *Next Generation Sensors and Systems*. Springer, 2016.

[120] S. Ali, A. Hassan, and G. Hassan. Disposable all-printed electronic biosensor for instantaneous detection and classification of pathogens. *Sci Rep*, 8:5920, 2018.

[121] Almudena Rivadeneyra, José Fernández-Salmerón, Jesús Banqueri, Juan A. López-Villanueva, Luis Fermín Capitan-Vallvey, and Alberto J. Palma. A novel electrode structure compared with interdigitated electrodes as capacitive sensor. *Sensors and Actuators B: Chemical*, 204:552 – 560, 2014.

[122] N. Mazlan, Muhammad Ramli, Mohd Mustafa Al Bakri Abdullah, Dewi Suriyani Che Halin, Siti Salwa Mat Isa, L. Talip, Nuaim Danial, and Sohiful Anuar Zainol Murad. Interdigitated electrodes as impedance and capacitance biosensors: A review. volume 1885, page 020276, 09 2017.

[123] A. C. Eloka-Eboka, F. Inambao, and K. Ukoba. Review of nanostructured nio thin film deposition using the spray pyrolysis technique. *Renewable and Sustainable Energy Reviews*, 82:2900–2915, 2018.

[124] Introduction. In G. Faraji, H. S. Kim, and H. T. Kashi, editors, *Severe Plastic Deformation*, pages 1 – 17. Elsevier, 2018.

[125] N. M. Jokerst, J. Cahoon, C. Donley, and J. Jones. Nanotechnology: A maker's course. In *Coursera online courses*. 2019.

[126] Denton Vacuum. E-beam evaporation solutions. `https://www.dentonvacuum.com/products-technologies/e-beam-evaporation/`.

[127] P. Arunkumar, Sushil Kumar Kuanr, and K. Suresh Babu. *Thin Film: Deposition, Growth Aspects and Characterization.* Springer, 2018.

[128] R. Luttge. Basic tehcnologies for microsystems. In *Microfabrication for Industrial Applications*, pages 13–54. William Andrew, 2011.

[129] J. Koskinen. Cathodic-arc and thermal-evaporation deposition. In *Reference module in Materials Science and Materials Engineering*, pages 3–55. ELSEVIER, 2014.

[130] F. Ejeian, S. Azadi, A. Razmjou, and Y. Orooji. Design and applications of mems flow sensors: a review. *Sensors and Actuators A: Physical*, 295:483–502, 2019.

[131] M. O. Mavukkandy, S. A. McBride, D. M. Warsinger, N. Dizge, and S. W. Hasan. Thin film deposition techniques for polymerci membranes: a review. *Journal of Membrane Science*, 610, 2020.

[132] ATL Advanced coating solutions. What is cvd? `https://www.cvd.co.uk/new-to-cvd`.

[133] M. Hakl. Study of properties of heterostructured thin silicon films in nanometer resolution. *Bachelor thesis at Charles University (Prague)*, 2012.

[134] Chemical vapor deposition. In Andrew R. Barron, editor, *Chemistry of Electronic Materials*. Rice University, 2013.

[135] R. P. Seisyan. Nanolithography in microelectronics: A review. *Technical physics*, 56, 2011.

[136] Nanolithography Techniques. Photolithography, 2018. `http://www.nanolithography.org/2018/07/18/photolithography/`.

[137] Z. Taleat, A. Khoshroo, and M. Mazloum-Ardakani. Screen-printed electrodes for biosensing: a review (2008-2013). *Microchim Acta*, 181:865– 891, 2014.

[138] H. Lee, Y. J. Hong, S. Baik, and T. Hyeon. Enzyme based glucose sensor: From invasive to wearable device. *Advanced Healthcare Materials*, 7, 2018.

[139] R. . Kadara, N. Jenkinson, and C. E. Banks. Characterization and fabrication of disposable screen printed micro-electrodes. *Electrochemistry communications*, 11:1377– 1380, 2009.

[140] V. Bhalla, S. Carrara, P. Sharmaa, Y. Nangiaa, and C. R. Suria. Gold nanoparticles mediated label-free capacitance detection of cardiac troponin i. *Sensors and Actuators B Chemical*, 7, 2011.

[141] T. Schüler, T. Asmus, W. Fritzsche, and R. Möller. Screen-printing as cost-efficient fabrication method for dna-chips with electrical readout for detection of viral dna. *Biosensors and bioelectronics*, 24:2077–2084, 2009.

[142] M. Wegener, D. Spiehl, F. Mikschl, and X. Liu. Printing of ultrathin nanoparticulate indium tin oxide structures. *Additional Conferences (Device Packaging, HiTEC, HiTEN & CICMT)*, pages 92–102, 2015.

[143] Poonam Sundriyal and Shantanu Bhattacharya. *Inkjet-Printed Sensors on Flexible Substrates.* 12 2017.

[144] Ma S, Ribeiro F, Powell K, Lutian J, Møller C, Large T, and Holbery J. Fabrication of novel transparent touch sensing device via drop-on-demand inkjet printing technique. *Mater Interfaces*, 7:21628–21633, 2015.

[145] MacDonald WA, Looney M, MacKerron D, Eveson R, Adam R, Hashimoto K, and Rakos K. Latest advances in substrates for flexible electronics. *J Soc Inform Display*, 15:1075–1083, 2007.

[146] Zardetto V, Brown TM, Reale A, and Di Carlo A. Substrates for flexible electronics: a practical investigation on the electrical, film flexibility, optical, temperature, and solvent resistance properties. *J Polym Sci Part B Polym Phys*, 49:638–648, 2011.

[147] Stempien Z, Kozicki M, Pawlak R, Korzeniewska E, Owczarek G, Poscik A, and Sajna D. Ammonia gas sensors ink-jet printed on textile substrates. *Sensors IEEE*, pages 1–3, 2016.

[148] Shawkat Ali, Arshad Hassan, Gul Hassan, Chang-Ho Eun andJinho Bae, Chong Hyun Lee, and In-Jung Kim. Disposable all-printed electronic biosensor for instantaneous detection and classification of pathogens. *Scientific reports*, 8:5920, 2018.

[149] Tongfen Lianga, Xiyue Zoua, and Aaron. D. Mazzeo. A flexible future for paper-based electronics. *Proc. of SPIE*, 9836.

[150] Poonam Sundriyal and Shantanu Bhattacharya. Inkjet printed electrodes on a4 paper substrates for low cost, disposable and flexible asymmetric supercapacitors. *ACS Appl. Mater. Interfaces*, 2017.

[151] C. Carrasquilla, J. R. L. Little, Y. Li, and J. D. Brennan. Patterned paper sensors printed with long-chain dna aptamers. *Chem. – Eur. J.*, 21:7369–7373, 2015.

[152] W. Dungchai, O. Chailapakul, and C. S. Henry. Electrochemical detection for paper-based microfluidics. *Anal Chem*, 81:5821–5826, 2009.

[153] E. W. Nery and L. T. Kubota. Sensing approaches on paper-based devices: a review. *Anal Bioanal Chem*, 405:7573–7595, 2013.

[154] A. Tribhuwan Singh, D. Lantigua, A. Meka, S. Taing, M. Pandher, and G. Camci-Unal. Paper-based sensors: Emerging themes and applications. *Sensors*, 51:2838, 2018.

[155] C. Silveira, T. Monteiro, and M. Almeida. Biosensing with paper-based miniaturized printed electrodes–a modern trend. *Biosensors*, 51, 2016.

[156] A low-cost paper-based inkjet-printed platform for electrochemical analyses. A. maattanen and u. vanamo and p. ihalainen and p. pulkkinen and h. tenhu and j. bobacka and j. peltonen. *Sens. Acuators B Chem*, 177:153–162, 2013.

[157] T.H. Da Costa, E. Song, R.¨. Tortorich, and R.P. Choi. A paper-based electrochemical sensor using inkjet-printed carbon nanotube electrodes. *ECS J. Solid State Sci Technol*, 4, 2015.

[158] H. Shamkhalichenar and J.W Choi. An inkjet-printed non-enzymatic hydrogen peroxide sensor on paper. *J. Electrochem. Soc.*, 164, 2017.

[159] P. Rattanarat, W. Dungchai, W. Siangproh, and W. Chailapakul. Sodium dodecyl sulfate-modified electrochemical paper-based analytical device for determination of dopamine levels in biological samples. *Anal Chim Acta*, 744:1–7, 2012.

[160] N. Ruecha, R. Rangkupan, N. Rodthongkum, O. Chailapakul, and O. Novel. Novel paper-based cholesterol biosensor using graphene plyvinylpyrrolidone polyaniline nanocomposite. *Biosens. Bioelectron*, 52:13–19, 2014.

[161] J. Yang, Y-G Nam, S-K Lee, C-S Kim, Y-M Koo, and W-J Chang. Paper-fluidic electrochemical biosensing platform with enzyme paper and enzymeles electrodes. *Sens. Actuators B Chem*, 203:44–53, 2014.

[162] Aaron D Mazzeo, William B Kalb, Lawrence Chan, Matthew G Killian, Jean-Francis Bloch, Brian A Mazzeo, and George M Whitesides. Paper-based, capacitive touch pads. *Advanced materials (Deerfield Beach, Fla.)*, 24(21), 2012.

[163] C. Lin, Z. Zhao, and J. Kim. Pencil drawn strain gauges and chemiresistors on paper. *Sci Rep*, 4:3812, 2015.

[164] Zhihong Nie, Frédérique Deiss, Xinyu Liu, Ozge Akbulut, and George M. Whitesides. Integration of paper-based microfluidic devices with commercial electrochemical readers. *Lab Chip*, 10:3163–3169, 2010.

[165] Bingwen Liu, Dan Du, Xin Hua, Xiao-Ying Yu, and Yuehe Lin. Paper-based electrochemical biosensors: From test strips to paper-based microfluidics. *Electroanalysis*, 26:1214 – 1223, 2014.

[166] Gura T. Citizen science: amateur experts. *Nature*, 496(7444):259–261, 2013.

[167] B. K. Wiederhold. *Cyberphsychology, Behavior and Social Networking*, 14(2), 2011.

[168] D. Brossard, B. Lewenstein, and R. Bonney. Scientific knowledge and attitude change: the impact of a citizen science project. *International Journal of Science Education*, 27:1099–21, 2005.

[169] C. T. Callaghan, J. J. L. Rowley ad W. K. Cornwell, A. G. B. Poore, and R. E. Major. Improving big citizen science data: Moving beyond haphazard sampling. *PLOS BIOLOGY*, 17(6), 2019.

[170] J.H. redmon, K.E. Levine, A.M. Aceituno, K. Litzenberger, and J. MacDonald Gibson. Lead in drinking water at north-carolina childcare centers: piloting a citizen science-based. *Environmental research*, 2019.

[171] Luftdaten. Reallabor für nachhaltige mobilitätskultur der universität stuttgart. `https://luftdaten.info`.

[172] Luftdaten. Sensor.community. `https://sensor.community/en/`.

[173] D. Renders (citizen involved in Over.Meten). Citizen-science monitoring of urban air quality in aalst, March 2020. personal communication.

[174] S. J. Park, T.A. Taton, and C.A. Mirkin. Array-based electrical detection of dna with nanoparticle probes. *Science*, 295:1503–1506, 2002.

[175] A. Leprince. Personal communication, July 2020. Earth and Life Institute, Applied Microbiology.

[176] Roger A. Freedman Hugh D. Young. *University physics with modern physics*. Addison-Wesley, Reading, Massachusetts, 2012.

[177] Robert Dorey. Chapter 53 - aluminum and aluminum alloys. In E. Ghali, editor, *Uhlig's corrosion handbook, third edition*, The electrochemical society series, pages 715–747. John Wiley & Sons, 2011.

[178] G.J.Luzzi. Gas pressure build-up in aluminium conductor cable. *IEEE Transactions on Power Apparatus and Systems*, PAS-101(6), 1982.

[179] T. I. Eltsov, V. N. Dorovsky, and D.N. Gapeev. Dielectric spectra of water-oil-saturated porous media for the khz range and determination of volume fractions of system components. *Russian geology and geophysics*, 55:1009–1018, 2014.

[180] Xing-Da Liu, Zhi-Ling Hou, Bao-Xun Zhang, Ke-Tao Zhan, Peng He, Kai-Lun Zhang, and Wei-Li Song. A general model of dielectric constant for porous materials. *Applied physics letters*, 108, 2016.

[181] D. zed Mezdour, S. Sahli, and M. Tabellout. Study of the electrical conductivity in fiber composites. *Int. journal of Multiphysics*, 4:141–150, 2010.

[182] B. Sareni, L. Krähenbühl, A. Beroual, and C. Brosseau. Effective dielectric constant of periodic composite materials. *Journal of Applied Physics*, 80:1688–1696, 1996.

[183] N. Couniot, A. Afzalian, N. Van Overstraeten, L. Francis, and D. Flandre. Capacitive biosensing of bacterial cells: Analytical model and numerical simulations. Sensors and Actuators B: Chemical : international journal devoted to research and development of physical and chemical transducers:428–438, 2015.

[184] L. Francis, D. Flandre, and N. Couniot. An integrated capacitive array biosensor for the selectrive and real-time detection of whole bacterial cells. *Presentation at the 4th International Symposium on Sensor Science*, 2015.

[185] N. Kamsali, B.S.N. Prasad, and J. Datta. Atmospheric electrical conductivity measurements and modeling for application to air pollution studies. *Advances in Space Research*, 44:1067–1078, 2009.

[186] Premier Farnell Limited. Fr-4 datasheet. `https://www.farnell.com/datasheets/1644697.pdf`.

[187] P. Sirviö, K. Backfolk, R. Maldzius, J. Sidaravicius, and E. Montrimas. Dependence of paper surface and volume resistivity on electric field strength. *Journal of Imaging Science and Technology*, 52, 2008.

[188] N. Gavish and K. Promislow. Dependence of the dielectric constant of electrolyte solutions on ionic concentration - a microfield approach. *Physical Review*, 94, 2016.

[189] S. Faniel. Personal communication, April 2020. DI water fabricated at WINFAB UCLouvain.

[190] H. Golnabi1, M. R. Matloob, M. Bahar, and M. Sharifian. Investigation of electrical conductivity of different water liquids and electrolyte solutions. *Iranian Physical Journal*, 3:24–28, 2009.

[191] Anil Koklu, Ahmet Sabuncu, and Ali Beskok. Rough gold electrodes for decreasing impedance at the electrolyte/electrode interface. *Electrochimica Acta*, 205, 04 2016.

[192] C. Chu, I. Sarangadharan, and A. Regmi. Beyond the debye length in high ionic strength solution: direct protein detection with field-effect transistors (fets) in human serum. *Sci Rep*, 7:5256, 2017.

[193] 6 - response of ti–ni alloys for dental biomaterials to conditions in the mouth. In Takayuki Yoneyama and Shuichi Miyazaki, editors, *Shape Memory Alloys for Biomedical Applications*, Woodhead Publishing Series in Biomaterials, pages 101 – 149. Woodhead Publishing, 2009.

[194] Diana El Khoury. *Towards the use of Electrostatic Force Microscopy to study interphases in nanodielectric materials*. PhD thesis, 11 2017.

[195] H. E. KUBITSCHEK. Cell volume increase in escherichia coli after shifts to richer media. *JOURNAL OF BACTERIOLOGY*, 172(1):94–101, 1990.

[196] Robert Dorey. Chapter 4 - microstructure–property relationships: How the microstructure of the film affects its properties. In Robert Dorey, editor, *Ceramic Thick Films for MEMS and Microdevices*, Micro and Nano Technologies, pages 85 – 112. William Andrew Publishing, Oxford, 2012.

[197] C.D. Hodgman. *Handbook of Chemistry and Physics, 44th Ed.* Chemical Rubber Publishing Co., 1962.

[198] N. Couniot, A. Afzalian, N. Van Overstraeten-Schlögel, L. A. Francis, and D. Flandre. Capacitive biosensing of bacterial cells: Sensitivity optimization. *IEEE Sensors Journal*, 16, 2015.

[199] A. Rogiest. Towards a wearable impedimetric sensor for emotional sweat monitoring. *Master Thesis UCLouvain*, 2019.

[200] I.A Stegun M.Abramawotiz. *Handbook of mathematical functions with Formulas, Graphs and Mathematical Tables.* Dover Publishers, 1965.

[201] S.Gevorian E.Carlsson. Conformal mapping of the field an charge distribution of multilayer substrate cpw's. *IEEE Trans. Microwave Theory Tech.*, (47):1544–1552, 1999.

[202] J.S. Joshi M.Gillick, I.D. Robertson. An analytical method for direct calculation of e- and h- field patterns of conductor-backed coplanar waveguides. *IEEE Trans. Microwave Theory Tech.*, (41):1606–1610, 1993.

[203] W. Olthius. Theoretical and experimental determination of cell constants of planar-interdigitated electrolyte conductivity sensors. *Sensors and actuators. B: Chemical*, 24:252–256, 1995.

[204] Cell constant of interdigitated electrodes. *Mosaic Documentation Web*, 2011. `http://www.mosaic-industries.com/embedded-systems/instrumentation/conductivity-meter/microfabricated-planar-interdigitated-electrodes-cell-constant`.

[205] Sartorius Stedim Biotech. Unisart® nitrocellulose membranes: The substrate of choice for protein assays. 2018. `https://www.sartorius.com/download/89574/4/broch-unisart-nitro-sl-1536-e-1--data.pdf`.

[206] Winfab UCLouvain. Thin-films deposition. `https://sites.uclouvain.be/winfab/NEW_website/Public/Facilities/Deposition.php`.

[207] AXON' CABLE SAS. Equipment: wires & cables for high temperatures. 2019. `https://www.axon-cable.com/publications/WIRES-CABLES.pdf`.

[208] Greg Amorese. Lcr/ impedance measurement basics. *Hewlett Packard: Back to Basics Seminar*, 1997.

[209] Agilent technologies. *Agilent Technologies Impedance Measurement Handbook*. 2003.

[210] Atika Arshad, Shahida Khan, A.H.M. Alam, and Rumana Tasnim. Automated person tracking using proximity capacitive sensors. *2014 IEEE International Conference on Smart Instrumentation, Measurement and Applications, ICSIMA 2014*, 02 2015.

[211] Hioki Corporation. *Impedance Measurement Handbook*. 2018.

[212] P. KanakaRaju and M. PurnaChandra Rao. Design and development of portable digital lcr meter by auto balancing bridge method. *International Journal of Innovations in Engineering and Technology*, 7, 2016.

[213] Test & measurements tips David Herres. Understanding and displaying the j operator. `https://www.testandmeasurementtips.com/understanding-displaying-j-operator/`.

[214] Hewlett Packard. Effective impedance measurement using open/short/load correction: Application note 346-3. `https://literature.cdn.keysight.com/litweb/pdf/5091-6553E.pdf?id=1000030303:epsg:dow`.

[215] National Instruments. Introduction to network analyzer measurements: fundamentals and background. `http://download.ni.com/evaluation/rf/Introduction_to_Network_Analyzer_Measurements.pdf`.

[216] Rohde & Schwarz. Fundamentals of vector network analysis. `https://www.signalintegrityjournal.com/ext/resources/White-papers-App-notes/Vector-Network-Analyzer-Fundamentals-Primer.pdf?1520951631`.

[217] J. Gruszynski D. Anderson, L. Smith. Application note 95-1: S-parameter techniques. *HP Hewlett Packard Company*, 2006.

[218] Agilent Technologies. De-embedding and embedding s-parameter networks using a vector network analyzer. *Application Note 1364-1*, 2004.

[219] F. Sischka. Non-s-parameter - twoport definitions: Interpretation and applications of the matrix elements. *Lecture SisConsult*, 2017.

[220] Hewlett Packard. *Dielectric Constant Measurement of Solid Materials.* 1989.

[221] A. Peyman, C. Gabriel, and E.H. Grant. Complex permittivity of sodium chloride solutions at microwave frequencies. *Bioelectromagnetics*, 28:264–274, 2007.

[222] Toomas Rang Georgios Giannoukos, Mart Min. Relative complex permittivity and its dependence on frequency. *Journal of Engineering*, 2017.

[223] Scribner. Zview for windows. `http://www.scribner.com/software/68-general-electrochemistr376-zview-for-windows/`.

[224] N. Couniot, T. Vanzieleghem, J. Rasson, N. Van Overstraeten, O. Poncelet, J. Mahillon, L. Francis, and D. Flandre. Lytic enzymes as selectivity means for label-free, microfluidic and impedimatric detection of whole-cell bacteria using ald-al2o3 passivated microelectrodes. *Biosensors and Bioelectronics*, 67:154–161, 2014.

[225] P. Mehrotra, B. Chatterjee, and S. Sen. Em-wave biosensors: a review of rf, microwave, mm-wave and optical-sensing. *Sensors*, 19:1013, 2019.

[226] Aaron A. Rowe, Andrew J. Bonham, Ryan J. White, Michael P. Zimmer, Ramsin J. Yadgar, Tony M. Hobza, Jim W. Honea, Ilan Ben-Yaacov, and Kevin W. Plaxco. Cheapstat: An open-source, "do-it-yourself" potentiostat for analytical and educational applications. *PLOS ONE*, 6:1–7, 09 2011.

[227] Cheng-Hsin Chuang, Yi-Chun Du, Ting-Feng Wu, Cheng-Ho Chen, Da-Huei Lee, Shih-Min Chen, Ting-Chi Huang, Hsun-Pei Wu, and Muhammad Shaikh. Immunosensor for the ultrasensitive and quantitative detection of bladder cancer in point of care testing. *Biosensors and Bioelectronics*, 84, 12 2015.

[228] E. Aydindogan, E. G. Celik, and S. Timur. Paper-based analytical methods for smartphone sensing with functional nanoparticles: Bridges from smart surfaces to global health. *Anal. Chim*, 90(21):12325–12333, 2018.

[229] D. Soleri, J. W. Long, M. D. Ramirez-Andreotta, R. Eitemiller, and R. Pandya. Finding pathways to more equitable and meaningful public-science partnerships. *Citizen Science: theory and practice*, 9:1–11, 2016.

[230] M. Minkler and N. Wallerstein. Community-based participatory research for health. 2008. San Francisco: Jossey-Bass.

[231] M. D. Ramirez-Andreotta, M.L. Brusseau, J.F. Maier, and A.J. Gandolfi. Environmental research translation: enhancing interactions with communities at contaminated sites. *Science of the Total Environment*, 497:651–664, 2014.

[232] P. Brown. Integrating medical and environental sociology with environmental health crossing boundaries and building connections through advocacy. *Journal of Health and Social Behavior*, 54:145–164, 2013.

[233] M. Conde. Acivism mobilizing science. *Ecological economics*, 105:67–77, 2014.

[234] G. Macey, R. Breech abd M. Chernaik, C Cox, D. Larson, D Thomas, and D. Carpenter. Air concentrations of volatile compounds near oil and gas production: a community-based exploratory research. *Environmental health*, 13(82), 2014.

[235] F. Berthoud, P. Balin, A. Bohas, C. Charbuillet, E. Drezet, J-D Dubois, C. Gossart, and M. Parry. *Impacts écologiques des technologies de l'information et de la communication: les faces cachées de l'immatérialité.* QuinteScience. edp Sciences, 2012.

[236] M. F. Ashby. *Materials and sustainable development.* Butterworth-Heinemann Publishing. Elsevier, 2016.

[237] William Baumol. On the proper cost tests for natural monopoly in a multiproduct industry. *American Economic Review*, 67(5):809–22, 1977.

[238] Vlaamse Milieu Maatschappij (VMM). Drinkwatervoorziening in vlaanderen: organisatie en een blik vooruit. 2017. `https://www.vmm.be/water/drinkwater/drinkwatervoorziening_in_vlaanderen_organisatie_en_een_blik_vooruit_tw.pdf/view`.

[239] B. Buysschaert (FARYS). The organisation of farys and their water quality monitoring., March 2020. personal communication.

[240] B. Ochoo, J. Valcour, and A. Sarkar. Association between perceptions of public drinking water quality and actual drinking water quality: a community-based exploratory study in newfoundland (canada). *Environmental Research*, 159:435–443, 2017.

[241] Stad Gent. Legionellabesmetting gentse kanaalzone. 2019. `https://stad.gent/nl/over-gent-en-het-stadsbestuur/nieuws-evenementen/legionellabesmetting-gentse-kanaalzone`.

[242] N. Boon (UGent). Potential industrial applications for point-of-care water monitoring, May 2020. personal communication.

[243] L. Wilmaerts (veterinary service of the Belgian army). The interest of point-of-care water sensors in the army, April 2020. personal communication.

[244] C. Furlong, J. Jegatheesan, M. Currell, U. Iyer-Raniga, T. Khan, and A.S. Ball. Is the global public willing to drink recycled water? *Utilities Policy*, 56:53–61, 2019.

[245] J. Kidd, P. Westerhoff, and A. D. Maynard. Public perceptions for the use of nanomaterials for in-home drinking water purification devices. *NanoImpact*, 18:100220, 2020.

[246] N. Herzberg and C. Hecketsweiler. L'analyse des eaux usées pour pister le sars-cov-2. *Le Monde*, 3/08/2020.

[247] Hilde van den Eynde (Universiteit Antwerpen). Rioolwater moet coronavirus verraden. *De Standaard*, 17/08/2020.

[248] World Health Organisation (WHO). Guidelines for environmental surveillance of poliovirus circulation. *Vaccine Assessment and Monitoring of the Department of Vaccines and Biologicals*, 2003.

[249] A. Joyce and R. L. Paquin. The triple layered business model canvas: A tool to design more sustainable business models. *Journal of Cleaner Production*, 135:1474–1486, 2016.